University of Warsaw
Institute of Theoretical Physics

Marek Lewicki

Aspects of electroweak symmetry breaking in light of new data from the LHC

Thesis advisor: Professor Zygmunt Lalak

July, 2016

Acknowledgements

I would like to thank Professor Zygmunt Lalak for his guidance and encouragement as well as for all for the incredible research opportunities.

I am also grateful to Professor James Wells for support, deep insights and granting me the opportunity to work in in CERN and at the University of Michigan.

Finally I would like to thank my Friends and Family for their constant support during the completion of this thesis.

This work was supported by the National Science Center under research grant 2014/13/N/ST2/02712 and doctoral scholarship 2015/16/T/ST2/00527 and by the Foundation for Polish Science International PhD Projects Programme co-financed by the EU European Regional Development Fund.

Abstract

Recent years mark a great success of the Standard Model. Discovery of the Higgs boson confirmed that electroweak symmetry is broken by a vacuum expectation value of a scalar field, thus finally proving the fifty year old theoretical idea. However a modification of the SM is required to accommodate many already observed phenomena such as the existence of dark matter or proper inclusion of gravitational interactions.

Discovery of the Higgs boson opened a new era of precision measurements which can guide us to the correct extension of the SM by the determination of the properties of new particle. Currently all the data is consistent with the SM prediction, however the accuracy of these measurements leaves open a possibility of significant modification of the SM. Due to lack of direct evidence of new physics at the LHC it is the new data about the Higgs boson properties that we will use as a guide towards its extension. We will begin by discussing the properties of the SM Higgs boson in the Standard Model and its supersymmetric extension which still is the best hope against the SM Hierarchy problem.

Next we will exhibit a more practical approach and address issues present in the Standard Model, namely the vacuum stability issue. While the SM does not require an extension to be consistent, having a vacuum which is not absolutely stable is not a comfortable situation. We will also discuss bounds on theories beyond the SM coming from requirement of not destabilizing the electroweak vacuum to much. Here we will use the very generic framework of higher dimensional operators provided by nonrenormalisable theories.

Lastly we will discuss baryogenesis, another necessary phenomenon, absent in the Standard Model. We will again use effective field theory approach and focus on the bounds on such extensions, that we can extract from requiring successful baryogenesis. Our main focus here will be the possible modification of such bounds coming from our lack of knowledge of the early universe cosmological history.

This thesis is mainly based on published papers [1, 2, 3, 4, 5, 6, 7, 8] .

Contents

Chapter 1

The Standard Model of elementary particle physics

1.1 Introduction

The Standard Model [9, 10, 11] is the renormalisable theory correctly describing all experiments at modern colliders. It succesfully predicts all known elementary particles particles and gauge interactions, excluding gravity. We will review some of its basic properties before proceeding to discuss its extensions.

1.2 SM Lagrangian

Standard Model is defined by the Lagrangian

$$\mathscr{L} = \mathscr{L}_G + \mathscr{L}_M + \mathscr{L}_H + \mathscr{L}_Y, \tag{1.1}$$

where $\mathscr{L}_G$ describes gauge interactions, $\mathscr{L}_M$ contains fermionic matter fields, $\mathscr{L}_H$ is the Higgs sector responsible for electroweak symmetry breaking and $\mathscr{L}_Y$ describes Yukawa interactions between the previous two.

SM is based on the $SU(3) \times SU(2) \times U(1)$ gauge group. The corresponding part of the Lagrangian reads

$$\mathscr{L}_G = -\frac{1}{4} G^{\alpha}_{\mu\nu} G^{\mu\nu}_{\alpha} - \frac{1}{4} W^{a}_{\mu\nu} W^{\mu\nu}_{a} - \frac{1}{4} B_{\mu\nu} B^{\mu\nu}, \tag{1.2}$$

where $G_{\mu\nu}$, $W_{\mu\nu}$ and $B_{\mu\nu}$ are field strength tensors associated with spin one fields of all the gauge groups.

The scalar sector of SM is described by

$$\mathscr{L}_H = |D_\mu H|^2 - V(H), \tag{1.3}$$

where

$$V(H) = -m^2 |H|^2 + \lambda |H|^4. \tag{1.4}$$

For $\mu^2 > 0$ the minimum of the potential corresponds to non zero value of the field, thus ground state of the theory is not symmetric under the gauge group. This is precisely the Brout-Englert-Higgs mechanism [12, 13, 14] responsible for masses of the gauge bosons and fermions. We can rewrite the scalar field as

$$H = \begin{pmatrix} \chi^- \\ (v + h + i\eta)/\sqrt{2}, \end{pmatrix} \tag{1.5}$$

where the vacuum expectation value is $v \simeq 246\,\text{GeV}$. The three Nambu-Goldstone bosons η and $\chi^\pm$ of the spontaneous breaking become longitudinal polarisations of the gauge bosons $W^\pm$ and Z as they acquire their masses.

$$m_W = \frac{g}{2} v \simeq 80.39\,\text{GeV}, \qquad m_Z = \frac{\sqrt{g^2 + g'^2}}{2} v \simeq 91.19\,\text{GeV}. \tag{1.6}$$

where $g = g_2$ and $g' = (5/3)g_1$ Thus electroweak symmetry $SU(2) \times U(1)$ is broken and only electromagnetic $U(1)_{\text{em}}$ symmetry remains, mediated by the photon which is the remaining massless combination of electroweak gauge fields. The last scalar degree of freedom h corresponds to the physical Higgs boson [12]. Only recently, with the discovery of the Higgs boson [15, 16] and measurement of its mass $m_h \simeq 125$GEV, the last free parameter of the SM was determined, namely at the tree level $\lambda = \frac{m_h^2}{2v^2} \simeq 0.13$.

Fermionic matter fields are minimally coupled to gauge fields,

$$\mathscr{L}_M = \sum_f i\bar{\psi}_f \gamma^\mu D_\mu^{(f)} \psi_f, \tag{1.7}$$

where the covariant derivative reads $D_\mu^f = \partial_\mu - ig_3 G_\mu^a \mathcal{T}_a^f - ig_2 W_\mu^i T_i^f - ig_1 Y^f B_\mu$, $\mathcal{T}_\alpha^{(f)}$, $T_a^{(f)}$ are the $SU(3)$ and $SU(2)$ generators in the representation of the gauge group corresponding to ψ_f and Y^f is the hypercharge of ψ_f. Standard Model is a chiral theory in which only the left-handed fermions are charged under $SU(2)$, while the right-handed fermions are $SU(2)$ singlets. Table 1.1 summarises the matter content of the Standard Model. In the quark sector we have one doublet and two singlets, corresponding to the

	q_L	u_R	d_R	l_L	e_R
$SU(3)$	**3**	$\bar{\mathbf{3}}$	$\bar{\mathbf{3}}$	**1**	**1**
$SU(2)$	**2**	**1**	**1**	**2**	**1**
Y	1/6	2/3	-1/3	-1/2	-1

Table 1.1: Matter content of the Standard Model.

left- and right-handed up and down quarks. In the lepton sector there is one left-handed doublet and one right-handed singlet. All the fermions come in three generation, which differ only in the Yukawa sector which describes their interactions with the Higgs field, and is defined by.

$$\mathscr{L}_Y = \frac{1}{\sqrt{2}} \sum_{i,j} y_u^{ij} \bar{q}_L^i H^c u_R^j + y_d^{ij} \bar{q}_L^i H d_R^j + y_\ell^{ij} \bar{\ell}_L^i H e_R^j, \tag{1.8}$$

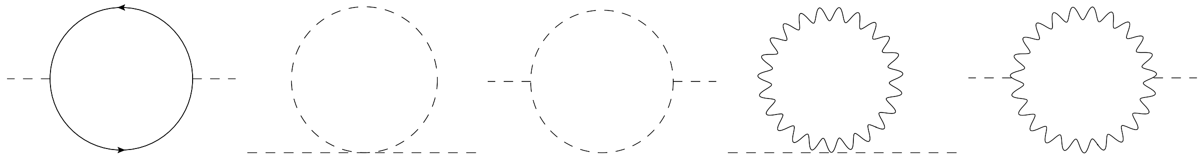

Figure 1.1: Feynman diagram contributing to m_h at one loop in the Standard Model.

where $H^c = i\sigma^2 H^*$ and i, j number the three generations. When H acquires a vev the above equation generates the masses of the fermions

$$m_f = \frac{y_f}{\sqrt{2}} v \tag{1.9}$$

which is crucial since the $SU(2) \times U(1)$ symmetry would not allow a gauge invariant mass term for them. Different families differ only in their Yukawa couplings and consequently in their masses.

1.3 Problems in the SM

Brout-Englert-Higgs mechanism made it possible to create a renormalisable theory explaining most of the existing collider experiments, however it could not do so without introducing additional theoretical problems. First of these is the long standing naturalness problem resulting from very high sensitivity of scalar mass terms to quantum corrections. The second one is more specific to SM and comes from large corrections to the Higgs potential coming from the top quark which render the electroweak minimum unstable.

1.3.1 Naturalness problem

In the Standard Model the $SU(2) \times U(1)$ gauge symmetry forbids mass terms for vectors and fermions. These masses have to vanish in the limit of unbroken symmetry and as we have seen they are consequently proportional to the Higgs vev. The point of vanishing mass would increase the symmetry of the theory and has to be stable under quantum corrections, since the renormalisation procedure preserves all symmetries. This holds to all orders in perturbation theory,which is a very important result because it implies that size of the quantum corrections is controlled by the tree level contribution. Consequently we say that fermion and vector masses are *protected* from quantum corrections.

Unfortunately the same is not true for bosons. In SM the mass of the Higgs boson is an arbitrary parameter not protected by any symmetry. Instead it is *additively* renormalized and receives corrections proportional to masses of all particles that couple to it. For example second diagram shown in Figure 1.1 generically predicts correction

$$\delta m_h^2 = \lambda \int^{\Lambda} \frac{d^4k}{(2\pi)^4} \frac{1}{k^2} \propto \frac{\lambda}{16\pi^2} \int^{\Lambda} dk^2 \propto \frac{\lambda}{16\pi^2} \Lambda^2 \tag{1.10}$$

which is quadratically divergent. Including this correction gives the physical mass

$$m_h^2 = m_{h0}^2 + \delta m_h^2 = m_{h0}^2 + \frac{\lambda}{16\pi^2}\Lambda^2, \tag{1.11}$$

where Λ is a mass scale above which SM does not describe physics any longer. Taking typical values m_h =125.09 GeV and $\Lambda \approx M_p \approx 10^{19}$ GeV, we can see that the tree level value m_0 and the correction have to be adjusted to cancel some 30 orders of magnitude. This is an incredible *fine-tuning* to most people.

Looking more closely at the whole Higgs mass correction in the SM given by diagrams in Figure 1.1 we get

$$\delta m_h^2 = \frac{3\Lambda^2}{8\pi^2 v^2}(4m_t^2 - m_h^2 - 2m_W^2 - m_Z^2), \tag{1.12}$$

where the corrections appear in the same order as in Figure 1.1. From left to right we get top quark correction proportional to its Yukawa coupling (corrections from other fermions are much smaller), Higgs correction proportional to λ and W and Z bosons corrections, where all couplings have been expressed through corresponding masses. We can define a measure of the needed cancellation (or fine-tuning)

$$\Delta = \frac{\delta m_h^2}{m_h^2} \approx 0.2\frac{\Lambda^2}{v^2}. \tag{1.13}$$

For example if $\Delta = 100$, right hand side of (1.11) has to be tuned to an order of a percent to cancel δm_h^2 and the tree level value m_{h0}^2.

If there would be no physics beyond the Standard Model there would be no naturalness problem, the above equations can be solved and do not pose a computational problem. However as soon as new physics appear, the scale Λ becomes a dynamical quantity connected with said physics and obtaining the correct Higgs mass would simply be very unlikely. This implies that the scale of new physics should not be higher than a few TeV to avoid large fine tuning. We will discuss the most motivated solution to the naturalness problem, supersymmetry in Chapter 2.

1.3.2 SM vacuum stability problem

Even if we chose to ignore the issue of naturalness, SM is not free of problems. Another one, connected with stability of the Higgs potential, arises when we try to extrapolate the theory to very high energies. To do so we need to properly incorporate quantum corrections, the first is the one-loop effective potential [17] which in SM takes the form [18]

$$V_{SM}(h)^{1-loop} = -\frac{m^2}{2}h^2 + \frac{\lambda}{4}h^4 + \sum_{i=W,Z,t,\chi,h} \frac{n_i}{64\pi^2} m_i^4 \left[\ln\left(\frac{m_i^2}{\mu^2}\right) - C_i\right] \tag{1.14}$$

with

$$
\begin{aligned}
n_W &= 6 & m_W^2 &= \frac{g^2}{4}h^2 & C_W &= \frac{5}{6} \\
n_Z &= 3 & m_Z^2 &= \frac{g^2+g'^2}{4}h^2 & C_Z &= \frac{5}{6} \\
n_t &= -12 & m_t^2 &= \frac{y_t^2}{2}h^2 & C_t &= \frac{3}{2} \\
n_\chi &= 3 & m_\chi^2 &= \frac{1}{2}\lambda h^2 - m^2 & C_\chi &= \frac{3}{2} \\
n_h &= 1 & m_h^2 &= \frac{3}{2}\lambda h^2 - m^2 & C_Z &= \frac{3}{2}
\end{aligned}
\tag{1.15}
$$

and all the couplings are calculated at the scale μ.

In order to improve the convergence of the perturbative series and thus ensure our one-loop potential is a good approximation we must choose an appropriate scale. To this end we could numerically minimize the one-loop correction for all values of the field, however in the SM one can simply set the scale equal to the value of the field $\mu =< h >$. Then the logarithms in the one-loop correction will remain small for all values of the field. In fact we can note that with this substitution the potential (1.14) simplifies significantly for very large values when we can neglect the explicit mass term $m \approx 0$. All the masses are simply proportional to h and the one-loop correction can be thought of as a modification of the quartic coupling

$$V(h) \approx \frac{\lambda_{eff}}{4}h^4. \tag{1.16}$$

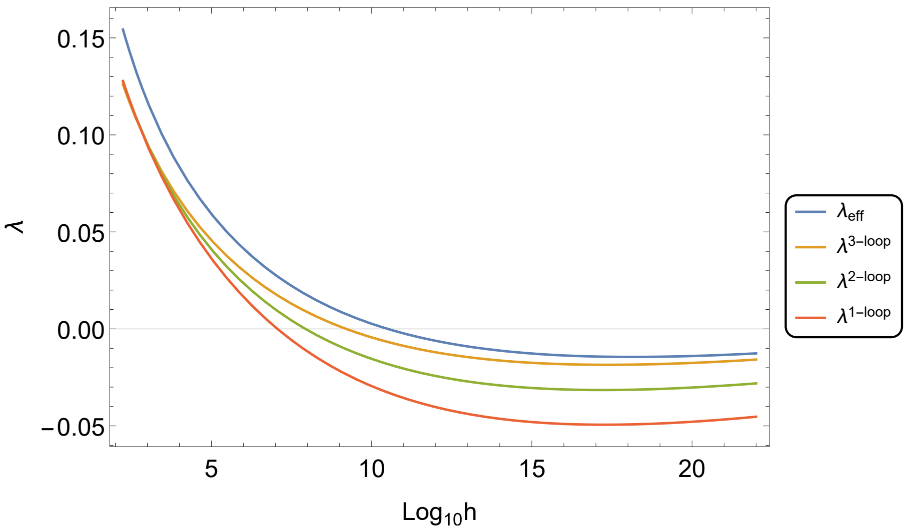

Figure 1.2: Runninf of λ_{eff} at different levels of accuracy together with λ_{eff} from (1.17) (using three-loop λ) in the Standard Model

To be able to compute all the couplings at the scale $\mu = h$ we use renormalisation group equations. The most important one is the running of λ, because the one loop correction is very small due to appropriate choice of the scale. At the one-loop order for λ we have [19]

$$\frac{d\lambda}{d\mu} = \frac{1}{16\pi^2}\left(24\lambda - 6y_t^4 + \lambda(12y_t^2 - 9g_2^2 - \frac{9}{5}g_1^2) + \frac{9}{8}g_2^4 + \frac{27}{200}g_1^4 + \frac{9}{20}g_1^2 g_2^2\right). \qquad (1.17)$$

The first two terms on the right hand side of the above equation are sufficient to roughly explain the problem. The measured Higgs mass predicts a rather small value $\lambda \approx 0.13$ while the large top quark mass means a large Yukawa coupling $y_t \approx 0.93$. This makes the Higgs quartic coupling run negative around $h = 10^{11}$ GeV, which means the potential bends back down and a very deep minimum appears at very large values of the field. Figure 1.2 depicts running of the λ coupling at various level of accuracy togehter with the effective coupling λ_{eff} including quantum corrections to the potential. We will discuss this issue and its implications in detail in Chapter 3.

1.3.3 Baryogenesis

We will discuss one of the most interesting scenarios of baryogenesis called electroweak baryogenesis [20, 21, 22, 23] that in principle does not require an extension of the Standard Model. In this scenario the observed baryon asymmetry of the Universe is created during the electroweak phase transition (EWPT). This requires [24]

- baryon number violation
- both C and CP violation
- departure from thermal equilibrium.

The last condition can be fulfilled if the phase transition is of the first order. However, in the Standard Model with a Higgs mass of 125 GeV it is of the second order and the field transitions smoothly into its new non-symmetric minimum which develops as the temperature drops. Thus, to realize electroweak baryogenesis (EWBG) we require new physics modifying SM near the electroweak scale in order to generate a barrier between the symmetric phase and the minimum which breaks the symmetry [25, 26]. Such exensions of SM gained renewed attention recently, since the experimental accuracy with which we measure the Higgs properties increases and all models predicting modification to its scalar potential can be probed with higher and higher accuracy [27, 28]. We will discuss how modified cosmological history of the universe can facilitate EWBG and make these experimental bounds less stringent.

Chapter 2

Supersymmetric solution to problems of SM

2.1 Introduction to SUSY

Supersymmetry remains the most promising extension of the Standard Model which can help to solve its naturalness problem.

The main advantage of supersymmetric theories is their theoretical robustness. Supersymmetry is the biggest possible extension of spacetime symmetries in quantum field theory [29, 30]. Even the minimal realisation of SUSY containing the minimal number of fields needed to extend SM into a supersymmetric theory (called MSSM) represents a very rich phenomenology which we will discuss in this chapter.

2.1.1 Supersymmetry algebra

We begin by summarising the extension of Poincare algebra to the Sypersymmetry algebra containing both commutators and anticommutators. In genera SUSY algebra can contain multiple generators. Algebras with more than one spinorial generator ($N > 1$) are called extended SUSY algebras. However, extended algebras are not very useful for phenomenological perspective, thus we will concentrate on the simplest example with $N = 1$, for which the algebra reads,

$$
\begin{aligned}
\{Q_\alpha, Q_\beta\} = \{\bar{Q}_{\dot{\alpha}}, \bar{Q}_{\dot{\beta}}\} = 0, \\
[P_\mu, Q_\alpha] = [P_\mu, \bar{Q}_\alpha] = 0, \\
\{Q_\alpha, \bar{Q}_{\dot{\alpha}}\} = 2\sigma^\mu_{\alpha\dot{\alpha}} P_\mu,
\end{aligned}
\tag{2.1}
$$

where σ are the Pauli matrices, P is the momentum and Q and $\bar{Q}$ are the SUSY generators forming Weyl spinors.

2.1.2 Supremultiplets

We will try to explain the meaning of SUSY algebra through a direct construction of the physical states. The first and the simplest case is the massless supermultiplet. We will consider a normalized state of a massless particle $|p,\lambda\rangle$ where p is an energy-momentum four-vector and λ is the chirality. We will use a frame in which $p_\mu = (E,0,0,E)$, which gives

$$\{Q_\alpha, \bar{Q}_{\dot{\alpha}}\} = \begin{pmatrix} 0 & 0 \\ 0 & 4E \end{pmatrix}. \tag{2.2}$$

We begin our construction with a state

$$|p,\lambda\rangle = Q_1 Q_2 |E,\lambda'\rangle \tag{2.3}$$

for which,

$$Q_\alpha |p,\lambda\rangle = 0, \tag{2.4}$$

because

$$Q_{\underline{\alpha}} Q_{\underline{\alpha}} = 0, \tag{2.5}$$

where underline means no sum, due to first line of the algebra (2.1). The state generated by $\bar{Q}_{\dot{1}}$ has zero norm, since

$$\langle p,\lambda|Q_1\bar{Q}_{\dot{1}}|p,\lambda\rangle + \langle p,\lambda|\bar{Q}_{\dot{1}}Q_1|p,\lambda\rangle = 0, \tag{2.6}$$

Thus the massless supermultiplet consists of only two states $|p,\lambda\rangle$ oraz $\bar{Q}_{\dot{2}}|p,\lambda\rangle$ with chiralities λ and $\lambda - \frac{1}{2}$. Via the CPT transformation we also obtain a supermultiplet containing states with chiralities $-\lambda$ oraz $-\lambda + \frac{1}{2}$.

We can now proceed to description of massive supermultiplets. In the rest frame of a particle with mass m we have $p_\mu = (m,0,0,0)$, which together with (2.1) gives

$$\{Q_\alpha, \bar{Q}_{\dot{\alpha}}\} = \begin{pmatrix} 2m & 0 \\ 0 & 2m \end{pmatrix}. \tag{2.7}$$

Similarly to the massless case we begin with a state for which

$$Q_\alpha |p,s,s'\rangle = 0. \tag{2.8}$$

Next by acting on that state with $\bar{Q}_{\dot{\alpha}}$ we create all the other possible states. Starting from the state with spin 0 we have

$$\begin{aligned} &|p,0,0\rangle, \\ \bar{Q}_{\dot{1}}&|p,0,0\rangle \propto |p,\tfrac{1}{2},\tfrac{1}{2}\rangle, \qquad (2.9) \\ \bar{Q}_{\dot{2}}&|p,0,0\rangle \propto |p,\tfrac{1}{2},-\tfrac{1}{2}\rangle, \\ \bar{Q}_{\dot{2}}\bar{Q}_{\dot{1}}&|p,0,0\rangle \propto |p,0,0\rangle'. \qquad (2.10) \end{aligned}$$

In genera starting from a state with the spin s we will obtain a multiplet with spins s,$s+\frac{1}{2}$ and $s-\frac{1}{2}$.

2.1.3 Superfields

We will proceed to discussion of the superspace formalism which is based on generalisation of spacetime by adding four additional anticommuting coordinates $\bar{Q}_{\dot{\alpha}}$,Q_α $(\alpha, \dot{\alpha} = 1, 2)$. In superspace we can define superfields $\Phi(x, \theta, \bar{\theta})$ which play the role of SUSY representation. Irreducible representations of SUSY, play a fundamental role in the superspace formalism. In the MSSM the most important ones are the chiral and vector superfields. Chiral superfield

$$\begin{aligned}\Phi(y) &= \phi(y) + \sqrt{2}\theta\psi(y) + \theta^2 F(y) \\ &= \phi(x) - i\theta\sigma^\mu\bar{\theta}\partial_\mu\phi(x) - \frac{1}{4}\theta^2\bar{\theta}^2\partial^2\phi(x) \\ &\quad + \sqrt{2}\theta\psi(x) + \frac{i}{\sqrt{2}}\theta^2\partial_\mu\psi(x)\sigma^\mu\bar{\theta} + \theta^2 F(x)\end{aligned} \tag{2.11}$$

where $y^\mu = x^\mu - i\theta\sigma^\mu\bar{\theta}$, contains a scalar field $\phi(x)$, and a spinor field $\psi(x)_\alpha$ together with a non-dynamical auxiliary field $F(x)$, which can be expressed in a given model through dynamical fields using the equations of motion. The vector superfield in Wess-Zumino gauge reads

$$V^a = \theta\bar{\sigma}^\mu\bar{\theta}v^a_\mu(x) + i\theta^2\bar{\theta}\bar{\lambda}^a(x) - i\bar{\theta}^2\theta\lambda^a(x) + \frac{1}{2}\theta^2\bar{\theta}^2 D^a(x), \tag{2.12}$$

and contains a vector field $A^a_\mu(x)$, a spinor field $\lambda^a_\alpha(x)$ and also a non-dynamical field $D^a(x)$.

2.1.4 Supersymmetric Lagrangians

We will start by discussing a simplest possible supersymmetric model containing only a few chiral superfields. Kinetic part of the Lagrangian reads

$$\mathcal{L}_0 = \partial^\mu\bar{\phi}_i\partial_\mu\phi_i + i\bar{\psi}_i\bar{\sigma}^\mu\partial_\mu\psi_i + \bar{F}_i F_i, \tag{2.13}$$

Which we can rewrite using (2.11), as

$$\mathcal{L}_0 = \Phi_i\bar{\Phi}_i|_{\theta\theta\bar{\theta}\bar{\theta}}. \tag{2.14}$$

The most general interaction part of the Lagrangian reads

$$W = \frac{1}{2}m_{ij}\Phi_i\Phi_j|_{\theta\theta}\frac{1}{3}g_{ijk}\Phi_i\Phi_j\Phi_k|_{\theta\theta} + \text{h.c.} \tag{2.15}$$

where m_{ij} and g_{ijk} are symmetric under the change of indexes. The W is the superpotential. Theory described by the Lagrangian, $\mathcal{L}_{WZ} = \mathcal{L}_0 + W$ was first described by Wess and Zumino [31].

The next step towards a supersymmetric version of SM is introducing gauge symmetries. We will start by considering a non-abelian gauge transformation

$$\begin{aligned}\Phi &\to e^{i\Lambda}\Phi \\ V &\to V + i(\Lambda - \Lambda^\dagger) + \dots \\ V &= T^a_{ij} V_a \\ \Lambda &= T^a_{ij}\Lambda_a\end{aligned} \tag{2.16}$$

where, Λ is a chiral superfield and T^a is a hermitian generator of the gauge group. The kinetic part of a gauge-invariant Lagrangian describing a vector superfield reads

$$\mathcal{L}_V = -\frac{1}{4}F^a_{\mu\nu}F^{a\mu\nu} + i\bar{\lambda}^a\bar{\sigma}^\mu D_\mu\lambda^a + \frac{1}{2}D^aD^a, \tag{2.17}$$

where the field strength tensor reads

$$F^a_{\mu\nu} = \partial_\mu v^a_\nu - \partial_\nu v^a_\mu - g f^{abc} v^b_\mu v^c_\nu, \tag{2.18}$$

and the covariant derivatives take the form

$$\begin{aligned}D_\mu\lambda^a &= \partial_\mu\lambda^a - g f^{abc} A^b_\mu \lambda^c \\ D_\mu\phi_i &= \partial_\mu\phi_i + igA^a_\mu T^a\phi_i \\ D_\mu\psi_i &= \partial_\mu\psi_i + igA^a_\mu T^a\psi_i.\end{aligned} \tag{2.19}$$

To obtain a gauge invariant Lagrangian describing interaction of chiral and vector fields, we rewrite the WZ lagrangian (2.1.4) replacing derivatives with their covariant versions and add an interaction term [32], obtaining

$$\mathcal{L} = \mathcal{L}_{WZ} + \mathcal{L}_V - \sqrt{2}g\left[(\bar{\phi}T^a\psi)\lambda^a + \bar{\lambda}^a(\bar{\psi}T^a\phi)\right] + g(\bar{\phi}T^a\phi)D^a. \tag{2.20}$$

Equations of motion for non-dynamical fields read

$$\begin{aligned}D^a &= -g\phi^* T^a\phi, \\ Fi &= -\bar{W}_i, \\ \bar{F}_i &= -W_i,\end{aligned} \tag{2.21}$$

where W is the superpotential (2.15), and

$$W_i = \frac{\partial W(\phi)}{\partial \phi^i}. \tag{2.22}$$

Using these EOMs we obtain the scalar potential

$$V(\phi,\bar{\phi}) = \bar{F}_iF_i + \frac{1}{2}D^aD^a = \bar{W}_iW_i + \frac{1}{2}g^2(\bar{\phi}T^a\phi)^2. \tag{2.23}$$

2.2 MSSM

Superpartners have identical quantum numbers. Thus in order to extend SM to a supersymmetric theory we need to at least double the number of fields to include superpartners of known particles. We do this by promoting SM quarks and leptons to chiral superfields. Gauge bosons become vector parts of vector superfields, which means adding so called bino, wino and gluino which are fermionic superpartners of the known W bosons Z bosons and gluons. We also promote the Higgs boson to a chiral supermultiplet which means adding its fermionic superpartner. Unfortunately adding a charged fermion introduces a chiral anomaly. This means that even in the minimal model we need an additional Higgs doublet with opposite charge in order to cancel the anomaly. Another reason is that the superpotential W is a holomorphic function of the fields. Thus to recreate SM Yukawa couplings which contained conjugate Higgs field, we need a new Higgs doublet with an opposite charge.

The MSSM superpotential reads

$$W_{MSSM} = U_R \boldsymbol{y_u} Q H_u + D_R \boldsymbol{y_d} Q H_d + E_R \boldsymbol{h_e} L H_d + \mu H_u H_d, \tag{2.24}$$

where U_R,D_R,Q,E_R,L,H_u,H_d are chiral superfields corresponding to supermultiplests fro Table 2.1, $\boldsymbol{h}$ are 3×3 matrices in the space of fermionic families.

	supermultiplet	fermions	bosons	$SU(3)$	$SU(2)$	$U(1)_Y$
quarks	$Q^i = \begin{pmatrix} U_L^i \\ D_L^i \end{pmatrix}$	q_L^i	$\tilde{q}_L^i$	3	2	$\frac{1}{6}$
	U_R^i	u_R^i	$\tilde{u}_R^i$	$\bar{3}$	1	$-\frac{2}{3}$
	D_R^i	d_R^i	$\tilde{d}_R^i$	$\bar{3}$	1	$\frac{1}{3}$
leptons	$L^i = \begin{pmatrix} \nu^i \\ E_L^i \end{pmatrix}$	l_L^i	$\tilde{l}_L^i$	1	2	$-\frac{1}{2}$
	E_R^i	e_R^i	$\tilde{e}_R^i$	1	1	1
Higgs bosons	$H_u = \begin{pmatrix} H_u^+ \\ H_u^0 \end{pmatrix}$	$\begin{pmatrix} \tilde{h}_u^+ \\ \tilde{h}_u^0 \end{pmatrix}$	$\begin{pmatrix} h_u^+ \\ h_u^0 \end{pmatrix}$	1	2	$\frac{1}{2}$
	$H_d = \begin{pmatrix} H_d^0 \\ H_d^- \end{pmatrix}$	$\begin{pmatrix} \tilde{h}_d^0 \\ \tilde{h}_d^- \end{pmatrix}$	$\begin{pmatrix} h_d^0 \\ h_d^- \end{pmatrix}$	1	2	$-\frac{1}{2}$
Gauge bosons	g	$\tilde{g}$	g	8	1	0
	W	$\tilde{W}$	W	1	3	0
	B	$\tilde{B}$	B	1	1	0

Table 2.1: Fields present in the MSSM. Index $i = 1, 2, 3$ numbers families.

2.2.1 R-parity

There are terms allowed by gauge symmetries and supersymmetry which we did not include in our superpotential (2.24) for example

$$H_u L, LQD, DDU, LLE. \tag{2.25}$$

Including them would violate baryon and lepton number conservation, which would go agains experimental results. To exclude those terms we postulate a new symmetry, R-parity. To all the fields we assign charges such that

$$P_M = (-1)^{3(B-L)}, \tag{2.26}$$

where B is the baryon number and L is the lepton number. The superpotential terms we did not include in MSSM (2.25) are excluded since products of their P_M are not equal to one, however all the terms present in (2.24) are allowed.

2.2.2 Soft SUSY Breaking

If supersymmetry was preserved superpartners of known particles would have the same mass as observed particles. However we did not observe any superpartners to the date, and so SUSY has to be violated. There are many known mechanisms of SUSY breaking. In order to investigate phenomenology of the models while remaining oblivious to the specific mechanism we can parametrise this breaking by adding so called soft terms to the Lagrangian. These are terms which preserve the gauge symmetries and explicitly break supersymmetry without reintroducing quadratic divergences present in the SM. In case of MSSM these terms take the form [33]

$$\begin{aligned}\mathcal{L}_{soft} = & - \frac{1}{2}\left(M_3\tilde{g}\tilde{g} + M_2\tilde{W}\tilde{W} + M_1\tilde{B}\tilde{B} + \text{h.c.}\right) \\ & - \left(\tilde{\bar{U}}\boldsymbol{a_u}\tilde{Q}H_u + \tilde{\bar{D}}\boldsymbol{a_d}\tilde{Q}H_d + \tilde{\bar{E}}\boldsymbol{a_e}\tilde{L}H_d + \text{h.c.}\right) \\ & - \tilde{Q}^\dagger\boldsymbol{m_Q^2}\tilde{Q} - \tilde{\bar{U}}\boldsymbol{m_U^2}\tilde{\bar{U}}^\dagger - \tilde{\bar{D}}\boldsymbol{m_D^2}\tilde{\bar{D}}^\dagger - \tilde{L}^\dagger\boldsymbol{m_L^2}\tilde{L} - \tilde{\bar{E}}\boldsymbol{m_E^2}\tilde{\bar{E}}^\dagger \\ & - m_{H_u}^2 H_u^\dagger H_u - m_{H_d}^2 H_d^\dagger H_d + (bH_uH_d + \text{h.c.})\end{aligned} \tag{2.27}$$

where, $\boldsymbol{m_Q^2}$,$\boldsymbol{m_U^2}$,$\boldsymbol{m_D^2}$, $\boldsymbol{m_L^2}$,$\boldsymbol{m_E^2}$ are 3×3 matrices in the family space, which generate the fermion masses, $\boldsymbol{a_u}$,$\boldsymbol{a_d}$,$\boldsymbol{a_e}$, are 3×3 matrices in the family space, representing triple scalar couplings. The terms M_3,M_2,M_1 are gluino, wino and bino masses, while $m_{H_u}^2$,$m_{H_d}^2$ and b are SUSY breaking corrections to the Higgs potential.

Off-diagonal elements in matrices $\boldsymbol{m_Q^2}$, $\boldsymbol{m_U^2}$,$\boldsymbol{m_D^2}$, $\boldsymbol{m_L^2}$,$\boldsymbol{m_E^2}$ would introduce additional flavour breaking. Hovewer experiments do not observe flavour breaking beyond the one present in SM. Thus it is natural to assume these marices are diagonal, say

$$\boldsymbol{m_U^2} = \begin{pmatrix} m_{U_1}^2 & & \\ & m_{U_2}^2 & \\ & & m_{U_3}^2 \end{pmatrix}. \tag{2.28}$$

To avoid new flavour breaking from the couplings $\boldsymbol{a_u}$,$\boldsymbol{a_d}$ and $\boldsymbol{a_e}$ we assume they are proportional to the Yukawa couplings $\boldsymbol{y}$,

$$\boldsymbol{a_u} = A_u\boldsymbol{y_u} \quad , \quad \boldsymbol{a_d} = A_d\boldsymbol{y_d} \quad , \quad \boldsymbol{a_e} = A_e\boldsymbol{y_e}. \tag{2.29}$$

We also assume all soft terms are real, thus limiting the flavour breaking to the one coming from SM. This setup is called minimal Flavour Violation (MFV) and it will be realized in all the models we will discuss in this thesis.

2.2.3 MSSM mass specrtum

Given the soft terms at a given energy scale we can compute the full mass spectrum of MSSM. We will now rewiew this procedure at the tree level.

We will begin with squarks and sleptons, by finding the appropriate part of the MSSM Lagrangian for each field $\tilde{f}$.

$$\mathcal{L}_{\text{mass }\tilde{f}} = -\begin{pmatrix}\tilde{f}_L^* & \tilde{f}_R^*\end{pmatrix} \boldsymbol{m}_{\tilde{f}}^2 \begin{pmatrix}\tilde{f}_L \\ \tilde{f}_R\end{pmatrix}, \tag{2.30}$$

For the third family this leads to the following mass matrices

$$\begin{aligned}
\boldsymbol{m}_{\tilde{t}}^2 &= \begin{pmatrix} m_{Q_3}^2 + m_t^2 + \left(\frac{1}{2} - \frac{2}{3}\sin^2\theta_W\right) m_Z^2 \cos 2\beta & m_t \left(A_t - \mu \cot\beta\right) \\ m_t \left(A_t - \mu\cot\beta\right) & m_{U_3}^2 + m_t^2 + \frac{2}{3}\sin^2\theta_W m_Z^2 \cos 2\beta \end{pmatrix}, \\
\boldsymbol{m}_{\tilde{b}}^2 &= \begin{pmatrix} m_{Q_3}^2 + m_b^2 - \left(\frac{1}{2} - \frac{1}{3}\sin^2\theta_W\right) m_Z^2 \cos 2\beta & m_b \left(A_b - \mu \tan\beta\right) \\ m_b \left(A_b - \mu\tan\beta\right) & m_{D_3}^2 + m_b^2 - \frac{1}{3}\sin^2\theta_W m_Z^2 \cos 2\beta \end{pmatrix}, \\
\boldsymbol{m}_{\tilde{\tau}}^2 &= \begin{pmatrix} m_{L_3}^2 + m_\tau^2 - \left(\frac{1}{2} - \sin^2\theta_W\right) m_Z^2 \cos 2\beta & m_\tau \left(A_\tau - \mu \tan\beta\right) \\ m_\tau \left(A_\tau - \mu\tan\beta\right) & m_{E_3}^2 + m_\tau^2 - \sin^2\theta_W m_Z^2 \cos 2\beta \end{pmatrix},
\end{aligned} \tag{2.31}$$

where $m_{Q_3}^2$,$m_{U_3}^2$,$m_{D_3}^2$,$m_{L_3}^2$,$m_{E_3}^2$, A_t,A_b,A_τ are the soft terms from (2.27) , m_t,m_b,m_τ are msses of the fermionic superpartners of discussed scalars and m_Z is the Z boson mass. The angle θ_W is the Weinberg angle known from SM and angle β is given by the ratio of vevs of the Higgs fields

$$\tan\beta = \frac{v_u}{v_d} = \frac{\langle H_u^0\rangle}{\langle H_d^0\rangle}. \tag{2.32}$$

The mass matrices $\boldsymbol{m}_{\tilde{f}}^2$ from (2.31) are diagonalized by a rotation by angle θ_f such that

$$\tan 2\theta_f = \frac{m_{f\,12}^{\,2} + m_{f\,21}^{\,2}}{m_{f\,11}^{\,2} - m_{f\,22}^{\,2}} \tag{2.33}$$

which gives the mass eigenstates

$$\begin{pmatrix}\tilde{f}_1 \\ \tilde{f}_2\end{pmatrix} = \boldsymbol{S}\begin{pmatrix}\tilde{f}_L \\ \tilde{f}_R\end{pmatrix} = \begin{pmatrix}\cos\theta_f & \sin\theta_f \\ -\sin\theta_f & \cos\theta_f\end{pmatrix}\begin{pmatrix}\tilde{f}_L \\ \tilde{f}_R\end{pmatrix} \tag{2.34}$$

with masses

$$\boldsymbol{S}\boldsymbol{m}_{\tilde{f}}^2\boldsymbol{S}^{-1} = \begin{pmatrix} m_{\tilde{f}_1}^2 & 0 \\ 0 & m_{\tilde{f}_2}^2\end{pmatrix}. \tag{2.35}$$

For other families the mass matrices can be approximated by diagonal ones because the mixing terms are proportional to their small Yukawa couplings which are negligible compared to the soft terms.

Chargino masses are defined by parts of the Lagrangian of the form

$$\mathcal{L}_{\text{mass }\chi^\pm} = -\frac{1}{2}(\psi^\pm)^T \boldsymbol{M}_\pm \psi^\pm, \tag{2.36}$$

where $\psi^{\pm} = \left(\tilde{W}^{+}, \tilde{h}_u^{+}, \tilde{W}^{-}, \tilde{h}_d^{-}\right)$ and $\boldsymbol{M}_{\pm}$ is in block diagonal form

$$\boldsymbol{M}_{\pm} = \begin{pmatrix} 0 & (\boldsymbol{M}_{\chi^{\pm}})^T \\ \boldsymbol{M}_{\chi^{\pm}} & 0 \end{pmatrix} \tag{2.37}$$

consisting of

$$\boldsymbol{M}_{\chi^{\pm}} = \begin{pmatrix} M_2 & \sqrt{2} m_W \sin\beta \\ \sqrt{2} m_W \cos\beta & \mu \end{pmatrix}, \tag{2.38}$$

containing the soft terms M_2,μ and W boson mass m_W. To find the physical masses we diagonalize the above matrix with two unitary matrices $\boldsymbol{U}$ i $\boldsymbol{V}$:

$$\boldsymbol{U}^* \boldsymbol{M}_{\chi^{\pm}} \boldsymbol{V}^{-1} = \begin{pmatrix} m_{\chi_1^{\pm}} & 0 \\ 0 & m_{\chi_2^{\pm}} \end{pmatrix}, \tag{2.39}$$

following a convention where $m_{\chi_1^{\pm}} \leq m_{\chi_2^{\pm}}$.

Part of the Lagrangian relevant for neutralino masses reads

$$\mathcal{L}_{\text{masa } \chi^0} = -\frac{1}{2} (\psi^0)^T \boldsymbol{M}_{\chi^0} \psi^0, \tag{2.40}$$

where $\psi^0 = \left(\tilde{B}, \tilde{W}^0, , \tilde{h}_d^0, \tilde{h}_u^0\right)$. The neurtalino mass matrix is given by

$$\boldsymbol{M}_{\chi^0} = \begin{pmatrix} M_1 & 0 & -m_Z \cos\beta \sin\theta_W & m_Z \sin\beta \sin\theta_W \\ 0 & M_2 & m_Z \cos\beta \cos\theta_W & -m_Z \sin\beta \cos\theta_W \\ -m_Z \cos\beta \sin\theta_W & m_Z \cos\beta \cos\theta_W & 0 & -\mu \\ m_Z \sin\beta \sin\theta_W & -m_Z \sin\beta \cos\theta_W & -\mu & 0 \end{pmatrix}. \tag{2.41}$$

We find the eigenvalues, diagonalising the above with a unitary matrix $\boldsymbol{N}$ such that

$$\boldsymbol{N}^* \boldsymbol{M}_{\chi^0} \boldsymbol{N}^{-1} = \begin{pmatrix} m_{\chi_1^0} & 0 & 0 & 0 \\ 0 & m_{\chi_2^0} & 0 & 0 \\ 0 & 0 & m_{\chi_3^0} & 0 \\ 0 & 0 & 0 & m_{\chi_4^0} \end{pmatrix}, \tag{2.42}$$

requiring that $|m_{\chi_1^0}| \leq |m_{\chi_2^0}| \leq |m_{\chi_3^0}| \leq |m_{\chi_4^0}|$.

2.2.4 Higgs sector and electroweak symmetry breaking

The Higgs potential in the MSSM takes the form

$$\begin{aligned} V &= (\mu^2 + m_{H_u}^2)(|H_u^0|^2 + |H_u^+|^2) + (\mu^2 + m_{H_d}^2)(|H_d^0|^2 + |H_d^-|^2) \\ &+ [b(H_u^+ H_d^- - H_u^0 H_d^0) + \text{h.c}] \\ &+ \frac{1}{2} g^2 |H_u^+ H_d^{0*} + H_u^0 H_d^{-*}|^2 \\ &+ \frac{1}{8}(g^2 + g'^2) \left(|H_u^0|^2 + |H_u^+|^2 - |H_d^0|^2 - |H_d^-|^2\right)^2. \end{aligned} \tag{2.43}$$

To minimize it we notice that $SU(2)$ invariance allows us to perform a transformation such that $H_u^+ = 0$. The the minimisation condition $\partial V/\partial H_d^- = 0$ gives $H_d^- = 0$, which allows us to use only neutral components $H_u^+ = 0$, $H_d^- = 0$, $H_d^0 = H_d$, $H_u^0 = H_u$. Now the potential reads

$$\begin{aligned} V &= (\mu^2 + m_{H_u}^2)|H_u|^2 + (\mu^2 + m_{H_d}^2)|H_d|^2 + (bH_u^0 H_d^0 + \text{h.c}) \\ &+ \frac{1}{8}(g^2 + g'^2)\left(|H_u|^2 - |H_d|^2\right)^2 . \end{aligned} \tag{2.44}$$

The Z boson mass takes the form

$$v_u^2 + v_d^2 = v^2 = \frac{4m_Z^2}{g^2 + g'^2}. \tag{2.45}$$

This allows us to rewrite the minimisation condition $\partial V/\partial H_d = \partial V/\partial H_u = 0$ as

$$\begin{aligned} \mu^2 &= \frac{1}{2}\left[\tan 2\beta \left(m_{H_u}^2 \tan\beta - m_{H_d}^2 \cot\beta\right) - m_Z^2\right] \\ b &= B\mu = \frac{1}{2}\sin 2\beta \left(m_{H_u}^2 + m_{H_d}^2 + 2\mu^2\right) , \end{aligned} \tag{2.46}$$

thus expressing μ and B parameters through the soft terms, β angle and Z mass.

Two Higgs doublets consist of four complex scalars from which three are used to give masses to Z and $W^\pm$ bosons. The remaining five are, a peusdoscalr A with mass

$$m_A^2 = 2\mu^2 + m_{H_u}^2 + m_{H_d}^2, \tag{2.47}$$

two charged bosons

$$m_{H^\pm}^2 = m_A^2 + m_W^2, \tag{2.48}$$

and two neutral ones h and H, whose masses are foun by diagonalising

$$\boldsymbol{M}_{h,H} = \begin{pmatrix} m_A^2 \sin^2\beta + m_Z^2 \cos^2\beta & -(m_Z^2 + m_A^2)\sin\beta\cos\beta \\ -(m_Z^2 + m_A^2)\sin\beta\cos\beta & m_A^2\cos^2\beta + m_Z^2\sin^2\beta \end{pmatrix}. \tag{2.49}$$

The eigenstates take the form

$$\begin{pmatrix} H \\ h \end{pmatrix} = \begin{pmatrix} \cos\alpha & \sin\alpha \\ -\sin\alpha & \cos\alpha \end{pmatrix} \begin{pmatrix} H_d \\ H_u \end{pmatrix}. \tag{2.50}$$

The lighter of neutral bosons plays the role of the SM Higgs boson, its mass in the MSSM reading

$$m_h^2 = \frac{2m_Z^2 m_A^2 \cos^2 2\beta}{m_A^2 + m_Z^2 + \sqrt{\left(m_A^2 + m_Z^2\right)^2 - 4m_Z^2 m_A^2 \cos^2 2\beta}}. \tag{2.51}$$

From this we get a tree level bound on the Higgs mass in the MSSM

$$m_h^2 \leq m_Z^2 \cos^2 2\beta \leq m_Z^2. \tag{2.52}$$

This bound is not fulfilled by observed masses and large loop corrections are required to reach agreement with the experiment. Later on we will see this reintroduces the naturalness problem in MSSM to certain extent.

2.2.5 Renormalisation group equations

In the previous section we discussed obtaining the spectrum of the theory, staring with the soft terms (2.27). To properly resum all corrections the soft terms should be computed at the scale near the masses of the superpartners, here we will assume this scale is a geometric average of the stop masses

$$M_{EWSB} = \sqrt{m_{\tilde{t}_1}(M_{EWSB}) m_{\tilde{t}_2}(M_{EWSB})}. \tag{2.53}$$

At this scale the one-loop correction to the effective potential is minimal [34]. This means that the perturbative series converges as fast as possible, and our results containing only one and two-loop corrections is as close as possible to the full result. Now we will discuss how to obtain the soft terms at the M_{EWSB} scale from their initial values given by a SUSY breaking mechanism that usually occurs at a much higher scale. The form of RGEs depends on on the renormalisation scheme. We will use values in the *Dimensional reduction* ($\overline{DR}$) scheme which is the most convenient for SUSY calculations since it preserves SUSY in radiative corrections [33] contrary to a usually more popular $\overline{MS}$ scheme.

In MSSM RGEs for the gauge couplings take the form

$$\frac{d}{dt} g_i = \frac{1}{16\pi^2} b_{\underline{i}} g_{\underline{i}}^3 \quad , \quad b_i = (\frac{33}{5}, 1, -3), \tag{2.54}$$

where $t = \ln(Q/Q_0)$, Q is the renormalisation scale and Q_0 is some reference scale. A very important feature of the MSSM is the fact that the gauge couplings unify at a certain energy scale, giving hope that we can embed MSSM in a theory which unifies all the forces.

RGEs of the gaugino masses read

$$\frac{d}{dt} M_i = \frac{2}{16\pi^2} M_{\underline{i}} b_{\underline{i}} g_{\underline{i}}^2 \quad , \quad b_i = (\frac{33}{5}, 1, -3). \tag{2.55}$$

Masses of quarks and leptons are generated by the Higgs mechanism and their values are proportional to elements of the matrices $\boldsymbol{h}$. Since the firs two families are much lighter than the third one, we can neglect their couplings and keep only diagonal elements generating masses of the third families

$$\boldsymbol{y_t} = \begin{pmatrix} 0 & 0 & 0 \\ 0 & 0 & 0 \\ 0 & 0 & y_t \end{pmatrix} \quad , \quad \boldsymbol{y_b} = \begin{pmatrix} 0 & 0 & 0 \\ 0 & 0 & 0 \\ 0 & 0 & y_b \end{pmatrix} \quad , \quad \boldsymbol{y_\tau} \begin{pmatrix} 0 & 0 & 0 \\ 0 & 0 & 0 \\ 0 & 0 & y_\tau \end{pmatrix}. \tag{2.56}$$

RGEs of those couplings read

$$\begin{aligned} \frac{d}{dt} y_t &= \frac{y_t}{16\pi^2} \left(6|y_t|^2 + |y_b|^2 - \frac{16}{3} g_3^2 - 3 g_2^2 - \frac{13}{15} g_1^2 \right), \\ \frac{d}{dt} y_b &= \frac{y_b}{16\pi^2} \left(6|y_b|^2 + |y_t|^2 + |y_\tau|^2 - \frac{16}{3} g_3^2 - 3 g_2^2 - \frac{7}{15} g_1^2 \right), \\ \frac{d}{dt} y_\tau &= \frac{y_b}{16\pi^2} \left(4|y_\tau|^2 + 3|y_b|^2 - 3 g_2^2 - \frac{9}{5} g_1^2 \right). \end{aligned} \tag{2.57}$$

Using the above simplification and keeping in mind the soft terms $\boldsymbol{a}$ are proportional to Yukawa couplings, we can replace them with A-terms A_t , A_b and A_τ from (2.29). Their RGEs read

$$\begin{aligned}
8\pi^2 \frac{d}{dt} A_t &= 6|y_t|^2 A_t + |y_b|^2 A_b + \frac{16}{3} g_3^2 M_3 + 3 g_2^2 M_2 + \frac{13}{15} g_1^2 M_1, \\
8\pi^2 \frac{d}{dt} A_b &= 6|y_b|^2 A_b + |y_t|^2 A_t + |y_\tau|^2 A_\tau + \frac{16}{3} g_3^2 M_3 + 3 g_2^2 M_2 + \frac{7}{15} g_1^2 M_1, \\
8\pi^2 \frac{d}{dt} A_\tau &= 4|y_\tau|^2 A_\tau + 3|y_b|^2 A_b + 3 g_2^2 M_2 + \frac{9}{5} g_1^2 M_1. \qquad (2.58)
\end{aligned}$$

RGEs of the scalars apart from gauge interactions, contain terms coming from interactions with scalar which are proportional to their masses (2.27), and a hypercharge contribution

$$X = m_{H_u}^2 - m_{H_d}^2 + \mathrm{Tr}[\boldsymbol{m_Q^2} + \boldsymbol{m_D^2} + \boldsymbol{m_E^2} - 2\boldsymbol{m_U^2} - \boldsymbol{m_L^2}], \qquad (2.59)$$

together with Yukawa coupling contributions

$$\begin{aligned}
X_t &= 2|y_t|^2 (m_{H_u}^2 + m_{Q_3}^2 + m_{U_3}^2 + A_t^2), \\
X_b &= 2|y_b|^2 (m_{H_d}^2 + m_{Q_3}^2 + m_{D_3}^2 + A_b^2), \qquad (2.60) \\
X_\tau &= 2|y_t|^2 (m_{H_d}^2 + m_{L_3}^2 + m_{E_3}^2 + A_\tau^2).
\end{aligned}$$

(2.61)

For the first two families the result is,

$$16\pi^2 \frac{d}{dt} m_f^2 = -8 \sum_{i=1}^{3} C_i(f) g_i^2 M_i^2 + \frac{6}{5} Y_f g_1^2 X, \qquad (2.62)$$

where Y_f is the hypercharge of the field from (2.1), and the constants C are

$$\begin{aligned}
C_1(f) &= \frac{3}{5} Y_f^2, \\
C_2(f) &= \begin{cases} \frac{3}{4} & \text{dla} \quad f = Q, L, H_u, H_d \\ 0 & \text{dla} \quad f = U, D, E \end{cases} \qquad (2.63) \\
C_3(f) &= \begin{cases} \frac{4}{3} & \text{dla} \quad f = Q, U, D \\ 0 & \text{dla} \quad f = E, L, H_u, H_d, \end{cases}
\end{aligned}$$

while for the third family

$$\begin{aligned}
16\pi^2 \frac{d}{dt} m_{Q_3}^2 &= -\frac{32}{3} g_3^2 M_3^2 - 3 g_2^2 M_2^2 - \frac{2}{15} g_1^2 M_1^2 + X_t + X_b + \frac{1}{5} g_1^2 X, \\
16\pi^2 \frac{d}{dt} m_{U_3}^2 &= -\frac{32}{3} g_3^2 M_3^2 - \frac{32}{15} g_1^2 M_1^2 + 2X_t - \frac{4}{5} g_1^2 X, \\
16\pi^2 \frac{d}{dt} m_{D_3}^2 &= -\frac{32}{3} g_3^2 M_3^2 - \frac{8}{15} g_1^2 M_1^2 + 2X_b + \frac{2}{5} g_1^2 X, \qquad (2.64) \\
16\pi^2 \frac{d}{dt} m_{L_3}^2 &= -6 g_2^2 M_2^2 - \frac{6}{5} g_1^2 M_1^2 + X_\tau - \frac{3}{5} g_1^2 X, \\
16\pi^2 \frac{d}{dt} m_{E_3}^2 &= -\frac{24}{5} g_1^2 M_1^2 + 2X_\tau + \frac{6}{5} g_1^2 X.
\end{aligned}$$

Large contributions from the gaugino masses quickly increase the masses so their electroweak scale value can be large even for very small high energy values.

RGEs of the parameters in the Higgs potential read

$$\begin{aligned}
16\pi^2 \frac{d}{dt} m_{H_u}^2 &= -6g_2^2 M_2^2 - \frac{6}{5} g_1^2 M_1^2 + 3X_t + \frac{3}{5} g_1^2 X, \\
16\pi^2 \frac{d}{dt} m_{H_d}^2 &= -6g_2^2 M_2^2 - \frac{6}{5} g_1^2 M_1^2 + 3X_b + X_\tau - \frac{3}{5} g_1^2 X, \\
16\pi^2 \frac{d}{dt} \mu &= \mu \left(3|y_t|^2 + 3|y_b|^2 + |y_\tau|^2 - 3g_2^2 - \frac{3}{5} g_1^2 \right), \\
16\pi^2 \frac{d}{dt} B &= 6|y_t|^2 A_t + 6|y_b|^2 A_b + 2|y_\tau|^2 A_\tau + 6g_2^2 M_2 + \frac{6}{5} g_1^2 M_1.
\end{aligned} \tag{2.65}$$

It will be very important for our future discussion that the biggest contribution here usually comes from X_t. This happens because X_b and X_τ are proportional to their smaller Yukawa couplings ($y_b, y_\tau < y_t$). The X does not play a role if the soft masses of all the scalars are similar and cancel out in X (2.59). The fastest decreasing mass (as we decreases the renormalisation scale) is $m_{H_u}^2$. This is an important fact since this is the mass which usually changes its sign, thus triggering electroweak symmetry breaking.

2.2.6 Fine-tuning

While supersymmetry ameliorates hierarchy problem of the SM it can introduce a different hierarchy between heavy superpartners and the elecroweak scale. This is often called the little hierarchy problem of MSSM. To see the *fine-tuning*, that is an unacceptable sensitivity of observables with respect to high energy SUSY braking parameters. We start by inverting the equation for finding the minimum of the potential (2.46)

$$m_Z^2 = \tan 2\beta \left[\left(m_{H_u}^2 + \frac{t_u}{v_u} \right) \tan\beta - \left(m_{H_d}^2 + \frac{t_d}{v_d} \right) \cot\beta \right] - 2\mu^2, \tag{2.66}$$

thus expressing the Z boson mass through the soft terms. As we discussed in Section 2.2.4 the Higgs mass is bounded from above by m_Z at the tree level and pushing it to the observed value of 125GeV requires large radiative corrections. The biggest one comes from top-stop loop [35]

$$\delta m_h^2 = \frac{3g^2 m_t^4}{8\pi^2 m_W^2} \left[\log\left(\frac{M_S^2}{m_t^2} \right) + \frac{X_t^2}{M_S^2} \left(1 - \frac{X_t^2}{12 M_S^2} \right) \right], \tag{2.67}$$

where $M_S^2 = \sqrt{m_{\tilde{t}_1} m_{\tilde{t}_2}}$ is the average of stop masses, and $X_t = m_t(A_t - \mu\cot\beta)$ is an off diagonal element of stop mass matrix. Parameters in (2.66) also receive top-stop loop corrections, which in the simplest approximation read

$$\delta m_{H_u}^2|_{stop} = -\frac{3Y_t^2}{8\pi^2} \left(m_{Q_3}^2 + m_{U_3}^2 + |A_t|^2 \right) \log\left(\frac{M_u}{\mathrm{TeV}} \right), \tag{2.68}$$

where $m^2_{Q_3}$ $m^2_{U_3}$ and A_t are the high scale SUSY breaking soft terms, and M_u is the scale of SUSY breaking. Thus requiring correct Higgs mass gives large corrections that have to cancel out in the right hand side of (2.66) to predict the correct value of M_Z.

Now we can define fine-tuning with respect to parameter a as [36]

$$\Delta_a = \left| \frac{\partial \ln M_Z}{\partial \ln a} \right|. \tag{2.69}$$

To find a specific value we vary parameter a then solve RGEs from M_u to M_{EWSB} scale and use (2.66) to numerically calculate the derivative. After doing so for all the free parameters we calculate

$$\Delta = \max_{a_i} \Delta_{a_i}, \tag{2.70}$$

to find our final value for the whole set.

2.3 Numerical implementation

We will outline the implementation of the RG-solver and spectrum generator we developed to implement the results from previous section. The numerical procedure we use is similar to the ones used in existing codes [37, 38, 39]. We work with quantities renormalized in $\overline{DR}$ and use renormalization group equations (RGE), to iteratively find low energy parameters for a given set of high energy soft terms.

2.3.1 M_Z Scale

At the scale M_Z we include radiative corrections to couplings. We set Yukawa couplings using the tree-level relations

$$y_t = \frac{m_t\sqrt{2}}{v \sin\beta} \quad , \quad y_b = \frac{m_b\sqrt{2}}{v \cos\beta} \quad , \quad y_\tau = \frac{m_\tau\sqrt{2}}{v \cos\beta}, \tag{2.71}$$

where m_t, m_b, m_τ are fermion masses and v is the Higgs vev. At the first iteration we use physical masses and SM Higgs vev $v \approx 246,22\,\text{GeV}$. During subsequent iterations above quantities are renormalized in $\overline{DR}$ scheme and one-loop SUSY corrections are included. To calculate the top mass we use 2-loop QCD corrections [40] and 1-loop corrections from super-partners from the appendix of [41]. While calculating the bottom mass we follow *Les Houches Accord* [42], starting from running mass in $\overline{MS}$ scheme in SM $m_{b\,SM}^{\overline{MS}}$. Next applying the procedure described in [43] we find $\overline{DR}$ mass at M_Z, from which we get MSSM value by including corrections described in appendix D of [41]. While calculating the tau mass we include only leading corrections approximated in [41]. We calculate the Higgs vev in the MSSM using

$$v^2 = 4\frac{M_Z^2 + \mathrm{Re}\,\Pi^T_{ZZ}(M_Z)}{g_2^2 + 3g_1^2/5}, \tag{2.72}$$

where we include Z self interactions described in appendix D of [41]. To calculate g_1 , g_2, g_3 in $\overline{DR}$ in the MSSM we use the procedure described in appendix C of [41].

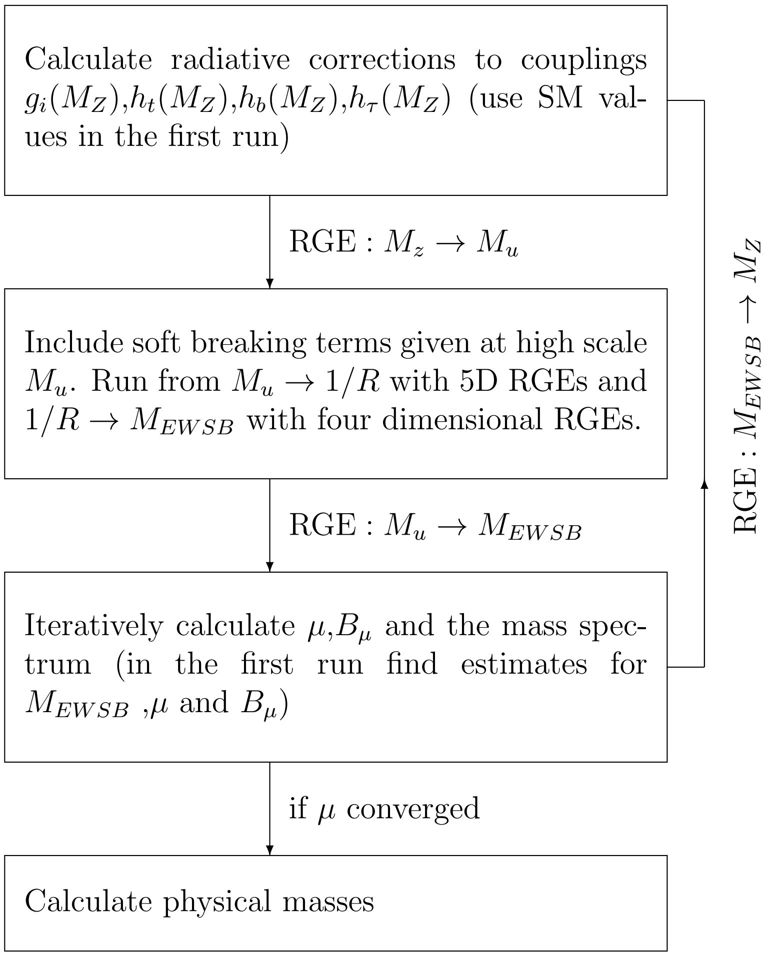

Figure 2.1: Schematic of the numerical algorithm. Subsequent steps are described in the appendix.

2.3.2 RGE and M_u scale

After calculating coupling constants at the scale M_Z we numerically solve RGEs [33],[44], to find their values at the scale M_u, at which we include the soft breaking terms. Then we solve RGEs again to find soft terms, coupling constants, $\tan\beta$ and Higgs vev v at the scale $M_{EWSB} = \sqrt{m_{\tilde{t}_1}(M_{EWSB}) m_{\tilde{t}_2}(M_{EWSB})}$. At first iteration we take $\mu = \mathrm{sgn}(\mu)$ GeV and $B_\mu = 0$ and run to the scale at which the above equation is fulfilled.

2.3.3 Electroweak symmetry breaking

In order to obtain correct electroweak symmetry breaking we use minimization conditions for the scalar potential to find new values of μ and B_μ. We include radiative corrections in these equations by the substitution

$$m_{H_u} \to m_{H_u} + \frac{t_u}{v_u} \quad , \quad m_{H_d} \to m_{H_d} + \frac{t_d}{v_d}. \tag{2.73}$$

We include full one-loop corrections to t_u and t_d presented in appendix E of [41] and leading two-loop corrections [45, 46, 47, 48, 49]. Since these corrections depend on sparticle masses which in turn depend on the μ parameter that we aim to calculate, an iterative calculation is performed to obtain new values of μ and B_μ.

If the new values differ significantly from the ones obtained in previous repetition of the whole algorithm described above, we run back to the M_Z scale and repeat the whole calculation once again. If however the values of μ and B_μ converged, we can move on to the calculation of physical masses.

2.3.4 Calculation of physical masses

To calculate physical masses we use only leading corrections described in [41] everywhere but the Higgs sector. In the Higgs masses calculation we use full one-loop corrections from [41] and leading two-loop corrections described in [45, 46, 47, 48, 49].

2.3.5 Constraints imposed on the scalar potential

To chceck if a given set of soft terms describes a realistic physical situation we check if the scalar potential is not unbounded from below (UFB). And if the potential dose not have minimums deeper than the one breaking electroweak symmetry, which would break $SU(3)$ or $U(1)_{em}$ (CCB). [50, 51, 52, 53, 54] . We include simple tree level bounds:

- for UFB
$$|\mu B_\mu| \leq m_{H_u}^2 + m_{H_d}^2 \quad \text{at scale} \quad M_x \in [M_{EWSB}, M_u], \tag{2.74}$$
- and CCB
$$A_f^2 \leq 3(m_{f_L}^2 + m_{f_R}^2 + \mu^2 + m_{H_u}^2) \quad \text{at scale} \quad M_x \in [M_{EWSB}, M_u]. \tag{2.75}$$

2.3.6 Fine-tuning

After the calculation of the spectrum is finished, one has a whole set of parameters and couplings that predict correct electroweak symmetry breaking. In order to calculate fine-tuning we solve the RGEs from M_u scale down to M_{EWSB} with one of the fundamental parameters a_i changed slightly at the high scale M_u . Then at the scale M_{EWSB} we recalculate the spectrum and use minimization conditions to calculate a new value of $\tan\beta$ and to obtain our new prediction for m_Z^2, which means that we calculate numerically the derivative in the definition of fine-tuning (2.69). We repeat that procedure for all parameters a_i and obtain our final result as a maximum of results obtained for each of those parameters (as in (2.70)).

2.4 Naturalness of gravity and gauge mediation

Gravity mediation is a generic concept in which SUSY breaking is mediated to the visible sector through gravitational interactions. The simplest and most popular of such models called minimal supergravity (mSUGRA) predicts parameters which are unified at the scale of SUSY breaking M_u, so the soft terms (2.27) take the form

$$\begin{gathered} M_1 = M_2 = M_3 = M_{\frac{1}{2}} \\ A_t = A_b = A_\tau = A \\ m_{H_u} = m_{H_d} = m_{Q_i} = m_{U_i} = m_{D_i} = m_{L_i} = m_{L_i} = m_0 \quad i = 1,2,3 \end{gathered} \tag{2.76}$$

In this section we will compare this model with a theoretically more promising class of models where SUSY breaking is mediated through gauge interactions.

Meade, Shih and Seiberg [55] defined gauge mediation models as those in which visible and hidden sectors completely decouple when gauge couplings vanish. Their most important result was that, in general, in such models there can be only six parameters determining the low energy sparticle spectrum. We parametrise the high energy soft terms with three parameters corresponding to gaugino masses

$$M_1 = \frac{\alpha_1}{4\pi} m_Y, \quad M_2 = \frac{\alpha_2}{4\pi} m_w, \quad M_3 = \frac{\alpha_3}{4\pi} m_c, \tag{2.77}$$

and three parameters determining masses of scalars Λ_c^2 , Λ_w^2 , Λ_Y^2. Scalar superpartner soft masses are given by

$$m_{\tilde{f}}^2 = 2\left[C_3(f)\left(\frac{\alpha_3}{4\pi}\right)^2 \Lambda_c^2 + C_2(f)\left(\frac{\alpha_2}{4\pi}\right)^2 \Lambda_w^2 + C_1(f)\left(\frac{\alpha_1}{4\pi}\right)^2 \Lambda_Y^2\right], \tag{2.78}$$

where $\alpha_i = g_i^2/4\pi^2$ and

$$\begin{aligned} C_1(f) &= \frac{3}{5} Y_f^2 \\ C_2(f) &= \begin{cases} \frac{3}{4} & \text{for} \quad f = Q, L, H_u, H_d \\ 0 & \text{for} \quad f = U, D, E \end{cases} \\ C_3(f) &= \begin{cases} \frac{4}{3} & \text{for} \quad f = Q, U, D \\ 0 & \text{for} \quad f = E, L, H_u, H_d. \end{cases} \end{aligned} \tag{2.79}$$

These parameters above are assumed do be independent of each other at the high scale so the whole set of parameters used in fine-tuning calculation contains

$$a_i = \{m_Y, m_w, m_c, \Lambda_Y, \Lambda_w, \Lambda_c, \mu, B_\mu\}. \tag{2.80}$$

A specific model of gauge mediation predicts the above quantities in terms of physical parameters. We will use two particular examples from [56]. The first one (GGM1) is defined by the superpotential

$$W_1 = X_i(y^i \bar{Q} Q + r^i \bar{U} U + s^i \bar{E} E), \tag{2.81}$$

with three independent parameters predicting the scalar mass parameters

$$\Lambda_Q = \frac{y^i F_i}{y^j X_j} \quad \Lambda_U = \frac{r^i F_i}{r^j X_j} \quad \Lambda_E = \frac{s^i F_i}{s^j X_j}, \tag{2.82}$$

and consequently

$$m_c = 2\Lambda_Q + \Lambda_U, \qquad m_w = 3\Lambda_Q, \qquad m_Y = \frac{4}{3}\Lambda_Q + \frac{8}{3}\Lambda_U + 2\Lambda_E,$$
$$\Lambda_c^2 = 2\Lambda_Q^2 + \Lambda_U^2, \qquad \Lambda_w^2 = 3\Lambda_Q^2, \qquad \Lambda_Y^2 = \frac{4}{3}\Lambda_Q^2 + \frac{8}{3}\Lambda_U^2 + 2\Lambda_E^2. \tag{2.83}$$
$$\tag{2.84}$$

the full set of free parameters used while calculating fine-tuning reads

$$a_i^{GGM1} = \{\Lambda_Q, \Lambda_U, \Lambda_E, \mu, B_\mu\}. \tag{2.85}$$

Superpotential of the second model (GGM2) reads

$$W_2 = X_i(y^i\bar{Q}Q + r^i\bar{U}U + s^i\bar{E}E + \lambda_q^i q\tilde{q} + \lambda_l^i l\tilde{l}) + F^i X_i. \tag{2.86}$$

Now we have five independent parameters predicting soft masses

$$\Lambda_Q = \frac{y^i F_i}{y^j X_j} \quad \Lambda_U = \frac{r^i F_i}{r^j X_j} \quad \Lambda_E = \frac{s^i F_i}{s^j X_j} \quad \Lambda_q = \frac{\lambda_q^i F_i}{\lambda_q^j X_j} \quad \Lambda_l = \frac{\lambda_l^i F_i}{\lambda_l^j X_j}. \tag{2.87}$$

Resulting soft masses are given by

$$m_c = \Lambda_q + 2\Lambda_Q + \Lambda_U, \qquad m_w = \Lambda_l + 3\Lambda_Q, \quad m_Y = \frac{2}{3}\Lambda_q + \Lambda_l + \frac{4}{3}\Lambda_Q + \frac{8}{3}\Lambda_U + 2\Lambda_E, \tag{2.88}$$
$$\Lambda_c^2 = \Lambda_q^2 + 2\Lambda_Q^2 + \Lambda_U^2, \qquad \Lambda_w^2 = \Lambda_l^2 + 3\Lambda_Q^2, \quad \Lambda_Y^2 = \frac{2}{3}\Lambda_q^2 + \Lambda_l^2 + \frac{4}{3}\Lambda_Q^2 + \frac{8}{3}\Lambda_U^2 + 2\Lambda_E^2.$$

The full set of parameters of GGM2 parameters used in fine-tuning calculation is

$$a_i^{GGM2} = \{\Lambda_Q, \Lambda_U, \Lambda_E, \Lambda_q, \Lambda_l, \mu, B_\mu\}. \tag{2.89}$$

Gauge mediation models have been known to struggle with fine-tuning issues because only negligible A-terms are generated. Large mixing in the sfermion mass matrices would increase their contribution to Higgs mass as in (2.67), making it easier to push the Higgs boson mass to 125 GeV. On the other nonuniversal gaugino masses make it easier to avoid the most severe experimental bounds coming from gluino mass. The nonuniversal scalar masses help avoiding severe bounds on masses of the squraks of the first and second generation. In our numerical calculations we used the following bounds on sparticle masses

$$\begin{aligned} m_{\tilde{g}} &\geq 1500\text{GeV}, \\ m_{\tilde{u}_i}, m_{\tilde{d}_i}, m_{\tilde{c}_i}, m_{\tilde{s}_i} &\geq 1500\text{GeV} \quad i = 1, 2, \\ m_{\tilde{t}_i} &\geq 560\text{GeV} \quad i = 1, 2, \\ m_{\tilde{b}_i} &\geq 620\text{GeV} \quad i = 1, 2, \\ m_{\tilde{\chi}_1} &\geq 250\text{GeV}. \end{aligned} \tag{2.90}$$

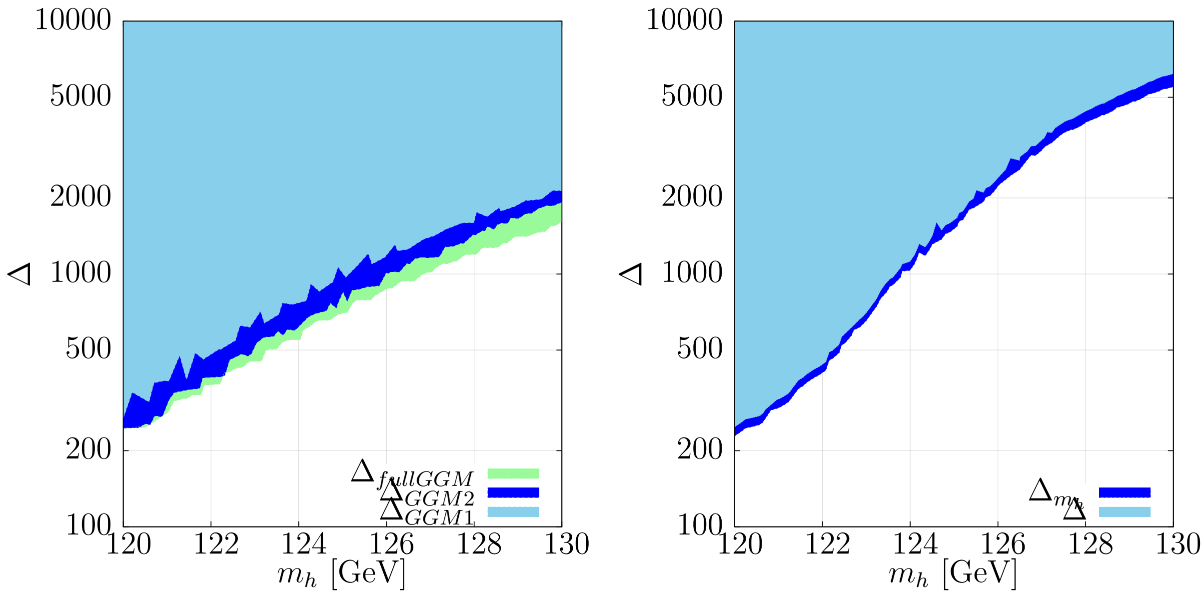

Figure 2.2: Fine-tuning in models GGM1 and GGM2 as well as in the general six parameter model (left panel). Fine-tuning in mSUGRA model calculated using standard definition (2.69) as well as using derivative of the Higgs mass instead of the Z boson mass (right panel).

We also fix the values $M_u = 10^8$ GeV and $\tan\beta = 40$.

Figure 2.2 shows minimal amount of fine-tuning predicted by the above models (including mSUGRA) as a function of the Higgs mass. As we can see generally models with larger number of free parameters predict smaller amount of fine-tuning. This is possible because they allow us to increasing the Higgs boson mass with subdominant corrections. We also verified that varying the SUSY breaking scale M_u between 10^6 GeV and 10^{12} GeV does not change the shape of the result, while thelowest possible fine-tuning changes by about thirty percent (with lower scales predicting less fine-tuning).

In the general model with 6 parameters, the biggest sources of fine-tuning are colored contributions. Namely the gluon mass parameter m_c or contributions to scalar masses Λ_c^2. The contribution from μ parameter is small in solutions which minimize fine-tuning (lower border of allowed fine-tuning regions in our plots), because it can be decreased by increasing Λ_Y^2 and Λ_w^2 and decreasing Λ_c^2 which in turn increases high scale $m_{H_u}^2$ without affecting masses of coloured particles. The value of $m_{H_u}^2$ decreases with decreasing energy scale and eventually runs negative to break electro-weak symmetry. As we can see from large $\tan\beta$ approximation of (2.66)

$$\frac{m_Z^2}{2} \approx -m_{H_u}^2 - |\mu|^2. \tag{2.91}$$

increasing high scale $m_{H_u}^2$ makes it run down towards less negative value and so decreases required μ. Since coloured particle masses which would affect fine-tuning the most, do not changed, we obtain a smaller μ parameter and similar fine-tuning. Meanwhile, increased

Λ_Y^2 and Λ_w^2 result in larger subdominant corrections to Higgs mass. The contribution from B_μ parameter is usually small because it enters the calculation only through potential minimization condition, and so the result is suppressed by a factor coming from (2.66)

$$\frac{\partial}{\partial \tan\beta} \tan 2\beta \tan\beta = \frac{\partial}{\partial \tan\beta} \frac{\tan^2\beta}{1-\tan^2\beta} = \frac{2\tan\beta}{(1-\tan^2\beta)^2} \propto \frac{1}{\tan^3\beta} \tag{2.92}$$

which is very small for large $\tan\beta$.

In model GGM2 squark and gluino masses have contributions from all parameters connected with color interactions $\Lambda_Q, \Lambda_U, \Lambda_q$. Consequently fine-tuning coming from coloured particle masses is distributed among these fundamental parameters. The worst fine-tuning contribution comes typically from the μ parameter. The same can be said about GGM1 model. The biggest source of fine-tuning is usually μ parameter.

The key result of this section is that fine-tuning in gauge mediated supersymmetry models is not higher than in a more standard gravity mediated case. This is surprising because A-terms which vanish in GGM are considered to be crucial for obtaining the correct Higgs mass within MSSM. The only other source of corrections are loop effects which require heavy superpartners which in turn, generically lead to higher fine tuning.

2.5 Constraints from muon anomalous magnetic moment

Muon anomalous magnetic moment is one of the few observables which do not agree with their SM predictions. The discrepancy between the experimental result from BNL [57] and the SM prediction is more than 3σ. SM predictions have been independently evaluated by several different groups [58, 59, 60] and their results are in a very good agreement. Currently this discrepancy between the SM prediction and the experiment is

$$\Delta a_\mu \equiv a_\mu^{\rm exp} - a_\mu^{\rm th} = (28.7 \pm 8.0) \times 10^{-10}. \tag{2.93}$$

This discrepancy is similar in size to the SM electroweak contribution and MSSM contribution from sleptons can accommodate it.

2.5.1 MSSM $(g-2)_\mu$ contribution

The bulk of the MSSM contribution to $(g-2)_\mu$ is given by [61, 62] chargino-sneutrino contribution which approximately reads

$$\delta a_\mu^\chi = \frac{\alpha\, m_\mu^2\, \mu\, M_2 \tan\beta}{4\pi \sin^2\theta_W\, m_{\tilde\nu_\mu}^2} \left(\frac{f_\chi(M_2^2/m_{\tilde\nu_\mu}^2) - f_\chi(\mu^2/m_{\tilde\nu_\mu}^2)}{M_2^2-\mu^2} \right), \tag{2.94}$$

and the bino-smuon contribution approximated by

$$\delta a_\mu^N = \frac{\alpha\, m_\mu^2\; M_1(\mu\tan\beta - A_\mu)}{4\pi\cos^2\theta_W\,(m_{\tilde\mu_R}^2 - m_{\tilde\mu_L}^2)} \left(\frac{f_N(M_1^2/m_{\tilde\mu_R}^2)}{m_{\tilde\mu_R}^2} - \frac{f_N(M_1^2/m_{\tilde\mu_L}^2)}{m_{\tilde\mu_L}^2} \right), \tag{2.95}$$

where $m_{\tilde{\mu}_L}$ and $m_{\tilde{\mu}_R}$ are the smuon masses, and the loop functions read

$$\begin{aligned} f_\chi(x) &= \frac{x^2-4x+3+2\ln x}{(1-x)^3}\,, \qquad f_\chi(1)=-2/3\,, \\ f_N(x) &= \frac{x^2-1-2x\ln x}{(1-x)^3}\,, \qquad f_N(1)=-1/3\,. \end{aligned} \tag{2.96}$$

In most of the MSSM parameter space the SUSY contribution is dominated by the chargino-sneutrino contribution (2.94). This contribution decouples when chargino or muon sneutrino masses are big. However this contribution can still be of the order of the SM EW one, even if these masses are many times larger than the W boson mass. This happens because the suppresion can be compensated by large values of $\tan\beta$.

2.5.2 Muon anomalous magnetic moment vs. naturalness

First let us note that accommodating the $(g-2)_\mu$ discrepancy (2.93) is impossible in the mSUGRA model. The reason is that all scalar masses have to be unified at the high scale, and severe experimental constraints push this unified mass towards high values. As a result slepton masses are also very heavy and the SUSY contribution (see (2.94) and (2.95)) is heavily suppressed.

General gauge mediation models allow different masses for coloured squarks and colorless sleptons (2.78). This means we can still accommodate the $(g-2)_\mu$ discrepancy (2.93) in GGM models. Figure 2.3 shows the SUSY contribution in GGM models discussed in Section 2.4. We can see that only the general case (with 6 free parameters) predicts δa_μ within 1σ bound for $m_h = 125\,\mathrm{GeV}$, while model 2 falls near 2σ bounds and model 1 is far beyond 2σ. Even the most general case makes it hard to increase δa_μ further, since all slepton generations have unified mass at the high scale. Unlike the first two generations the 3rd generation gets negative contribution from its large Yukawa coupling

$$16\pi^2\frac{d}{dt}m^2_{L_3} \supset 2|h_\tau|^2(m^2_{H_d}+m^2_{L_3}+m^2_{E_3}+A^2_\tau). \tag{2.97}$$

This makes stau tachionic before smuon is light enough to reproduce the required value of δa_μ.

Another important point is that small masses required in the slepton sector leave us with large squark corrections, needed to increase the Higgs mass, and those have severe impact on fine-tuning. This means all solutions with large $(g-2)_\mu$ contribution will be quite fine-tuned. This is shown in the right panel of Figure 2.3, where all the reagions predict fine-tuning roughly four times higher than the minimal one shown in Figure 2.2.

2.5.3 Maximal chargino and smuon masses from $(g-2)_\mu$

From the previous two section it is clear that a sufficiently light smuon and chargino are required to accommodate the $(g-2)_\mu$ discrepancy with MSSM contribution. There is actually one loophole since there is a contribution proportional to the μ term which does

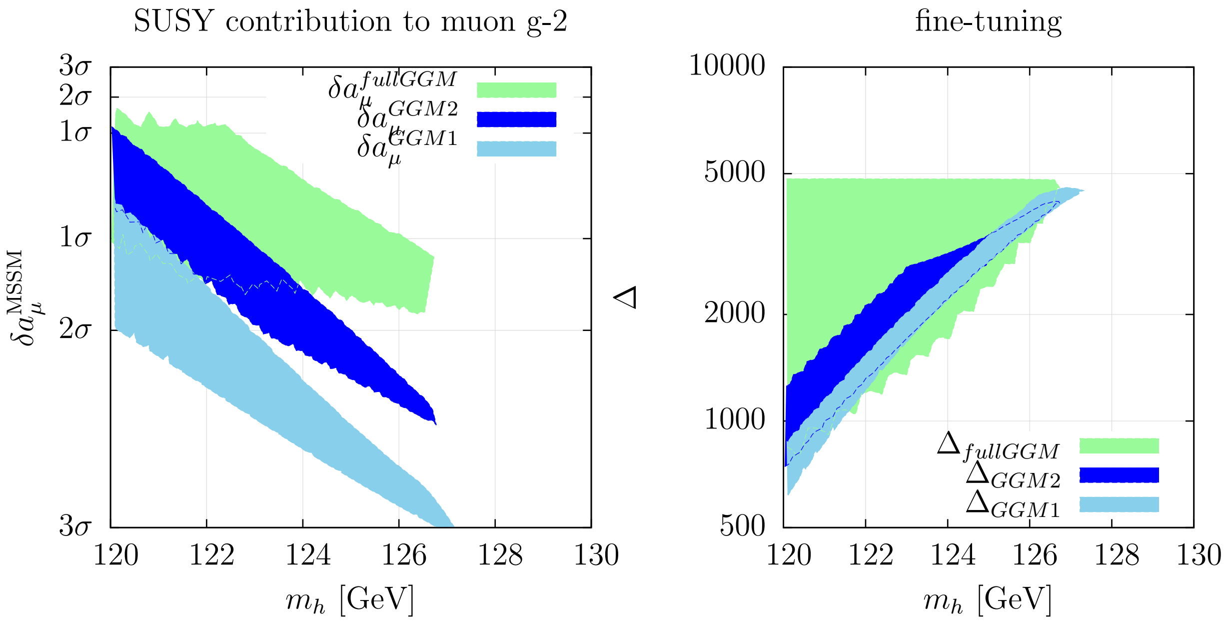

Figure 2.3: Regions of largest possible SUSY contribution to muon $(g-2)_\mu$ and corresponding fine-tuning

not decouple when these masses are large, however it requires μ to be in the multi TeV region to accomodate the discrepancy, and thus predicts a highly unnatural scenario. We will not discuss this possibility further.

Now we proceed to we calculate the upper bounds on the smuon and chargino masses as a function of $\tan\beta$. We perform a scan over the relevant parameters. As discussed in the previous sections, the MSSM contribution to $(g-2)_\mu$ depends mostly on $\tan\beta$, gaugino masses M_1, M_2, smuon and sneutrino soft terms, $m_{E_1} = m_{E_2}$ and $m_{L_1} = m_{L_2}$, and the μ parameter. We vary these parameters in the following ranges:

$$\begin{aligned} 1.5 \leq\ & \tan\beta && \leq 50\,, \\ 0\ \text{GeV} \leq\ & |M_1| && \leq 1500\ \text{GeV}\,, \\ 40\ \text{GeV} \leq\ & |M_2| && \leq 1500\ \text{GeV}\,, \\ 90\ \text{GeV} \leq\ & m_{L_2}, m_{R_2} && \leq 1500\ \text{GeV}\,, \\ 50\ \text{GeV} \leq\ & |\mu| && \leq 1500\ \text{GeV}\,. \end{aligned} \tag{2.98}$$

We calculated the full one loop and the leading two-loop supersymmetric contributions to the muon anomalous magnetic moment, given in [62]. In the two-loop contribution we set $M_{\rm SUSY}$ (defined in [62]) to be equal to either the bino or smuon mass, whichever is lighter. The largest positive MSSM contribution to $(g-2)_\mu$ is obtained when μ, M_1 and M_2 have positive signs because then both the chargino-sneutrino (2.94) and bino-smuon (2.95) contributions are positive. We have checked this by scanning over all possible sign assignments of μ, M_1 and M_2.

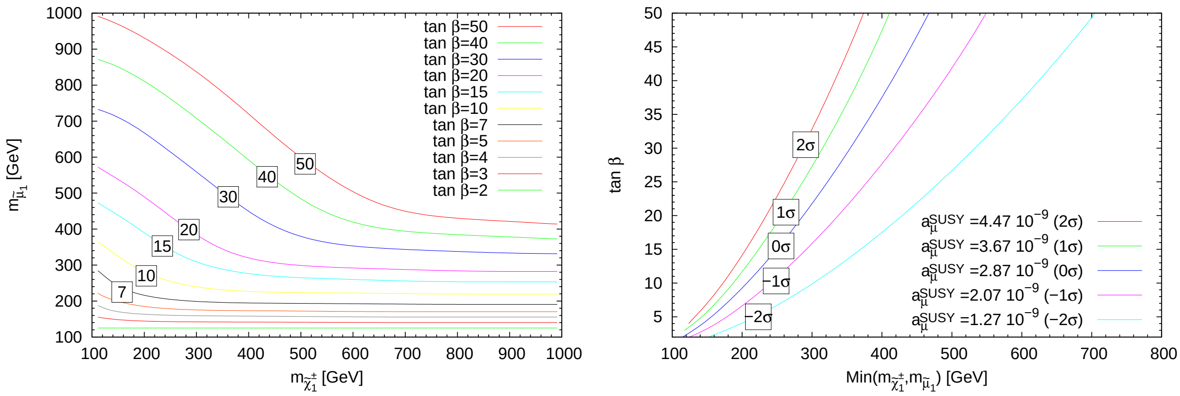

Figure 2.4: Left panel: Upper bound on the lightest chargino and smuon masses for several values of $\tan\beta$ obtained by requiring that the $(g-2)_\mu$ accommodate the experimental result with 1σ accuracy. Right panel: Lower bound on $\tan\beta$ as a function of a common experimental lower bound on the smuon and chargino masses resulting in the indicated a_μ^{SUSY}.

Left panel of Figure 2.4 shows the upper bounds on the masses of the lighter smuon and chargino consistent with the $(g-2)_\mu$ experimental result at 1σ level. The bounds come from requirement that the SUSY contribution to a_μ pushes the result to differ from the experimental central value by at most one standard deviation. For very large $\tan\beta \sim 50$, smuon masses up to a TeV are sufficient to explain the $(g-2)_\mu$ anomaly. With the lowest values allowed by LEP [63], namely 103.5 and 100 GeV for chargino and smuon mass respectively $\tan\beta \gtrsim 2$ is required to explain the $(g-2)_\mu$ anomaly. The right panel of Figure 2.4 shows a lower bound on $\tan\beta$ as a function of a common (hypothetical) experimental lower bound on the masses required to obtain a given value of $\Delta a_\mu^{\mathrm{SUSY}}$. The more recent LHC limits on the smuon and chargino masses are not as generic as the LEP ones. For example with mass-degeneracies smaller than about 10%, the LHC does not set any constraints.

2.5.4 Upper bounds on the stop masses

In the previous section we described how the lower limit on the smuon and chargino masses results in a lower bound on $\tan\beta$, if the $(g-2)_\mu$ anomaly is to be explained by supersymmetric contributions. Now we will discuss how such a bound can be translated into an upper bound on the stop masses [64, 65].

We will begin by recalculating the upper bound on the stop masses as a function of $\tan\beta$. The simple one-loop formula for the Higgs mass in the MSSM reads:

$$m_h^2 \approx m_Z^2 \cos^2 2\beta + \frac{3g^2 m_t^4}{8\pi^2 m_W^2}\left[\ln\left(\frac{m_{\tilde t}^2}{m_t^2}\right) + \frac{X_t^2}{m_{\tilde t}^2}\left(1 - \frac{X_t^2}{12 m_{\tilde t}^2}\right)\right], \tag{2.99}$$

where $m_{\tilde t} \equiv \sqrt{m_{\tilde t_1} m_{\tilde t_2}}$, $m_{\tilde t_i}$ are the eigenvalues of the stop mass matrix (2.31) and $X_t \equiv A_t - \mu/\tan\beta$ with A_t being the SUSY breaking top trilinear coupling. Once we set the stop masses, the Higgs mass is minimized for vanishing stop-mixing parameter X_t. Thus, we will consider $X_t = 0$ since we are interested in the upper bound on the stop masses.

We calculated the Higgs mass using FeynHiggs 2.10.0 [66, 67] which combines the existing fixed-order results for the radiative corrections up to two loops with a resummation of the leading and subleading logarithmic contributions from stops to all orders. The inclusion of the latter allows for a reliable prediction of the Higgs mass also for stops much heavier than the TeV scale.

The Higgs mass measurement at the LHC has reached a very good experimental precision [68, 69]

$$m_h = 125.09 \pm 0.21(\mathrm{stat}) \pm 0.11(\mathrm{syst})\mathrm{GeV}\,, \tag{2.100}$$

with which the dependence of the Higgs mass on other than stops sparticle masses (mainly gauginos and higgsinos) has to be taken into account. In order to explain the $(g-2)_\mu$ anomaly we need rather light charginos. On the other hand, we try to find a conservative upper bound on the stop masses. Thus in the following analysis we fix $M_2 = \mu = 1$ TeV. Lighter charginos would result in a larger Higgs mass, hence, a more stringent upper bound on the stop masses. For example, we find that for $M_2 = \mu = 200$ GeV the Higgs mass is typically bigger by about 1.5 GeV than in the case $M_2 = \mu = 1$ TeV. We also fix $M_3 = 2.5$ TeV to be on the safe side from the LHC gluino mass bounds. We checked that increasing M_3 up to $m_{\tilde{t}}$ decreases the prediction for the Higgs mass only by several hundreds of MeV.

The last parameter whose value has a non-negligible impact on the Higgs mass is the pseudoscalar Higgs mass, m_A. It controls the mixing between the SM-like and the heavy MSSM Higgs. Smaller values of m_A result in a smaller Higgs mass so, in order to be conservative, we use the values of m_A equal to the current experimental lower limits. For $\tan\beta \gtrsim 15$, the best limit comes from the Higgs searches in the $\tau\tau$ channel performed by ATLAS and CMS [70, 71]. It varies from about 400 GeV for $\tan\beta = 15$ up to 950 GeV for $\tan\beta = 50$. For a smaller $\tan\beta$, the main constraint comes from the LHC Higgs coupling measurements which sets the limit $m_A \gtrsim 400$ GeV almost independently of $\tan\beta$ for $\tan\beta \gtrsim 2$ [72] required to explain the $(g-2)_\mu$ anomaly. We found that for $m_A = 400$ GeV the Higgs mass is smaller by about 2 GeV than in the case of decoupled A.

In Figure 2.5 we plot the Higgs mass versus $m_{\tilde{t}}$ for several values of $\tan\beta$ with the remaining MSSM parameters set to the values described above. In the calculation we use the top mass from the recent combination of the LHC and Tevatron results which yields $m_t = 173.34 \pm 0.76$ GeV [73]. The upper bound on $m_{\tilde{t}}$ is below 25 TeV even for $\tan\beta = 5$. For $\tan\beta = 10$, the upper bound is about 6 TeV using the central values of the FeynHiggs prediction and the measured values of the Higgs and top masses. After taking into account the theoretical uncertainty reported by FeynHiggs (about 1 GeV for $m_{\tilde{t}} \approx 10$ TeV), using the top mass 1σ below the central value (which reduces the Higgs mass by about 0.7 GeV) and imposing the Higgs mass of 125.7 GeV (which is 2σ above the central value) the upper bound on the stop masses for $\tan\beta = 10$ is relaxed to about 9 TeV. We can combine now the results shown in Figure 2.4 with the Higgs mass dependence on $\tan\beta$ and the stop masses, for the vanishing stop mixing. In the left panel of Figure 2.6 we plot the contours of the upper bounds on the stop masses in the plane of

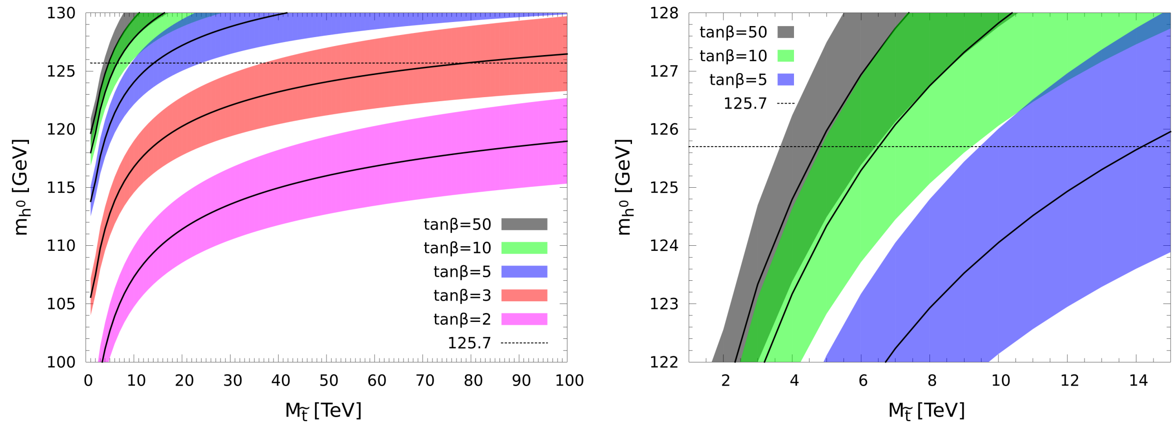

Figure 2.5: Left: The Higgs mass versus $m_{\tilde{t}}$ for several values of $\tan\beta$. Other relevant MSSM parameters are: $X_t = 0$, $M_3 = 2.5$ TeV, $M_2 = \mu = 1$ TeV and m_A is set to the current lower experimental limit, see the text for more details. The width of the bands corresponds to the theoretical uncertainty, as calculated by FeynHiggs, added linearly to the uncertainty from varying the top mass within 1σ from the experimental central value. Right: Zoom of the plot on the left.

the hypothetical experimental lower bounds on the lightest chargino and smuon masses, if one requires consistency with the $(g-2)_\mu$ measurement at 1σ level. In this plot we take the experimental upper bound on the Higgs mass at 95 % C.L. which is, according to eq. (2.100), about 125.7 GeV. In the theoretical prediction for the Higgs mass we use $\mu = M_2 = 1$ TeV, m_A equal to current experimental lower limit and take into account the theoretical uncertainties reported by FeynHiggs (in order to get conservative upper bound we assume that FeynHiggs overestimate the Higgs mass). Moreover, we use the value of the top mass, $m_t = 172.58$ GeV, which is 1σ below the current experimental central value. With these conservative numbers we find that the LEP constraints set the upper bound on the stop masses of about 7000 TeV. The left panel of Figure 2.6 demonstrates that relatively mild improvements of the limits on the chargino and smuon masses would have a strong impact on the upper bound on the stop masses. The reason is that the tree-level contribution to the Higgs mass strongly depends on $\tan\beta$ as long as $\tan\beta$ is not large. While the LHC limits are not generic, for typical spectra the smuon and chargino masses are excluded at least up to 300 GeV [74]. This is enough to bring down the upper bound on the stop masses to about 8 TeV.

An electron-positron collider with center-of-mass energy $\sqrt{s} = 500$ GeV, such as the planned ILC [75] or upgraded TLEP [76] could probe chargino and slepton masses up to 250 GeV, thus bringing the robust upper bound on the stop masses down to 10 TeV. Tree-level Higgs mass is saturated for large $\tan\beta$ and so, it is difficult to move the upper bound on the stop masses far below 10 TeV, as it as we can see in the left panel of Figure 2.6. In addition to the improvement in the stop mass bound from better limits on the smuon and chargino masses, a slightly better precision may come from stronger

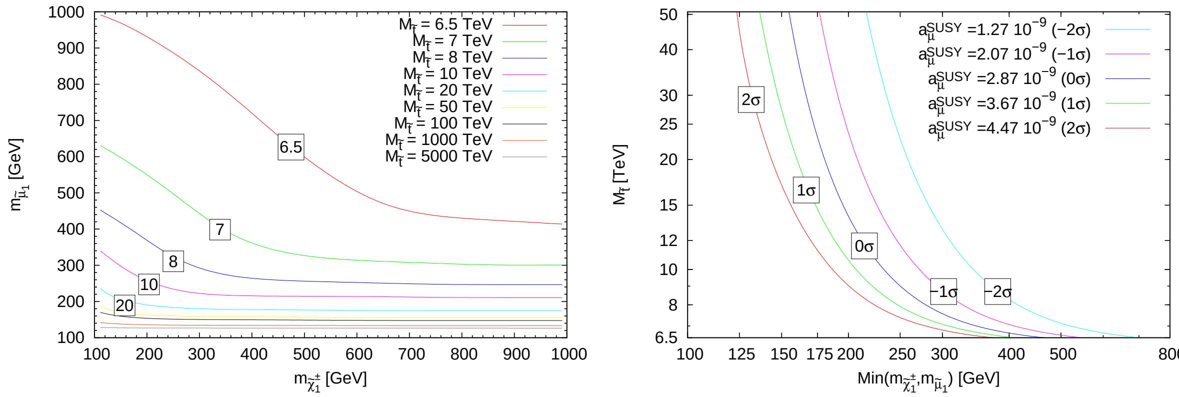

Figure 2.6: Left panel: The contours of the upper bounds on the stop masses in the plane of hypothetical experimental lower bounds on the lightest chargino and smuon masses and requiring the prediction for $(g-2)_\mu$ to be within 1σ from its experimental value. Right panel: The upper bound on the stop masses as a function of a common (hypothetical) experimental lower bound on the chargino and smuon masses for several values of $a_\mu^{\rm SUSY}$. The values of $a_\mu^{\rm SUSY}$ are as in Fig.1.

limits on m_A and from improvements in the top mass measurement. Similarly as in Figure 2.4, for a broader qualitative picture of the upper bounds on the stop masses, it is interesting to see how the results change if different experimental values of $(g-2)_\mu$ are taken. In the right panel of Figure 2.6 we plot the upper bound on the stop masses as a function of common hypothetical experimental limits on the smuon and chargino masses for several values of $a_\mu^{\rm SUSY}$. This plot is especially interesting since future lepton colliders are expected to set similar experimental lower limits on both masses. These bounds are roughly equal to a half of the center of mass energy of the colliding leptons. Assuming that the theoretical $(g-2)_\mu$ is consistent with the current measurement at 2σ, the upper bound on the stop masses is somewhat relaxed. However, if the lower experimental limit on the chargino and smuon masses was set around 300 GeV even the 2σ agreement with the current $(g-2)_\mu$ measurement would imply the upper bound on the stop masses around 10 TeV. The stops with masses around 10 TeV are beyond the LHC reach. While precise studies of the discovery potential of the 100 TeV hadron collider are still missing, preliminary simulations indicate that such masses could be probed at that collider provided that gluinos and other squarks are in a similar mass range [77]. A direct production of 10 TeV stops is, of course, more challenging. Nevertheless, in the recent article [78] it is argued that directly produced stops decaying to a top and a neutralino could be discovered (excluded) up to 6.5 (8) TeV with 3000 fb^{-1} of integrated luminosity at a 100 TeV collider.

To sum up, if SUSY is responsible for the $(g-2)_\mu$ anomaly, the chargino and smuon masses are strongly constrained from above. In consequence, experimental lower limits on the chargino and smuon masses lead to lower bounds on $\tan\beta$. We have translated the bounds on $\tan\beta$ into upper bounds on the stop masses from the requirement that the predicted Higgs mass does not overshoot the experimental value. The main results are presented in Figure 2.6. The LEP limits on the smuon and chargino masses result in an upper bound on the stop masses exceeding 10^3 TeV. However, even mild improvement of the LEP limits results in a significant improvement of this upper bound. Current LHC limits on smuon and chargino masses obtained for not too compressed gaugino and higgsino spectra reduce the upper bound on the stop masses to about 10 TeV. Electron-positron colliders operating at $\sqrt{s} = 500$ (1000) GeV would allow to set the upper bound on the stop masses to about 10 (5) TeV. Such stops could be discovered at the 100 TeV hadron collider.

The main conclusion of this section is that, with the help of the discussed future colliders, SUSY should be discovered, if superpartners are responsible for the explanation of the $(g-2)_\mu$ anomaly.

2.5.5 Possible loophole

There exists a contribution to $(g-2)_\mu$ that does not decouple in the limit of very heavy higgsino, hierarchically heavier than gauginos and sleptons even if the latter are very heavy. This effect comes from the Feynman diagram with the loop involving bino and smuon with a chirality flip occurring on the smuon line and it is approximately given by (2.95). This diagram is obviously suppressed by the smuon masses but it is proportional to the smuon mixing which, in turn, is proportional to $A_\mu - \mu\tan\beta$. This means that, contrary to other contributions, it grows with the higgsino mass rather than decouples. It is most effective when bino and smuon masses are close to each other (for $M_1 \ll m_{\tilde{\mu}}$ it is suppressed by M_1 in the numerator of (2.95) while for $M_1 \gg m_{\tilde{\mu}}$ it is suppressed by the loop function f_{χ^0} defined in (2.96)). This means that in principle the $(g-2)_\mu$ anomaly can be explained for any value of $\tan\beta$ and the smuon and bino masses by taking appropriately large μ. This is demonstrated in Figure 2.7. We can see that agreement with the $(g-2)_\mu$ measurement at 1σ is possible for heavier sleptons than discussed in the previous subsection but at the cost of highly unnatural values of μ. For example for $\tan\beta = 10$ and smuon masses of 500 GeV $(g-2)_\mu$ can be within 1σ from the experimental value for $\mu \approx 20$ TeV (for light charginos satisfying the LEP limits such smuon masses would not allow for $(g-2)_\mu$ within 1σ).

A large bino contribution due to such a spectrum is disfavoured by the naturalness arguments. However, it turns out that this possibility can be constrained also in a more objective way. A detailed study of that case was performed in Ref. [79]. Too large values of $\mu\tan\beta$ lead to instability of the EW vacuum due to large trilinear coupling of sleptons to the Higgs. It was shown in [79] that for universal slepton masses the vacuum stability implies that $(g-2)_\mu$ consistent with the measurement at 1σ can be obtained only for the lightest smuon mass below about 300 GeV (we reproduce this result, using the formula (14) from [79], in Figure 2.7). This upper bound is independent of $\tan\beta$ because the relevant quantity is $\mu\tan\beta$ (of course the saturation of this bound requires heavier higgsinos for smaller $\tan\beta$). Moreover, it was shown in Ref. [79] that most of that region

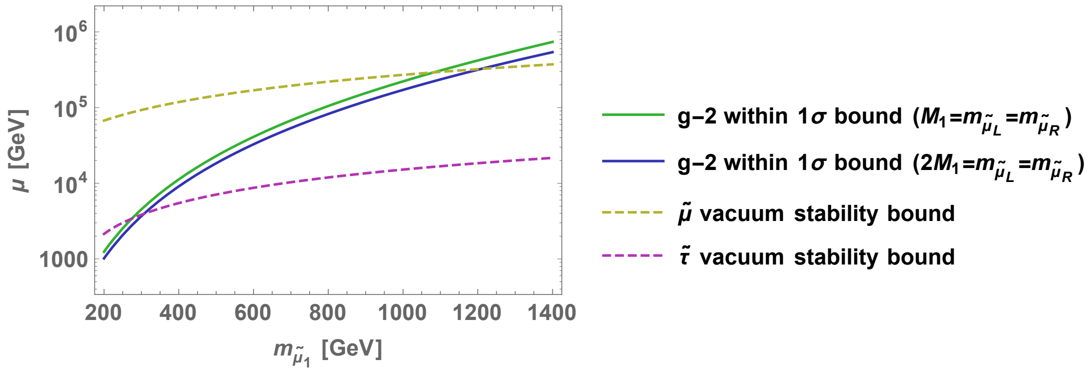

Figure 2.7: Minimal value of μ for $\tan\beta = 10$ required for the bino contribution to be consistent with the $(g-2)_\mu$ measurement at 1σ level as a function of the lightest smuon mass (solid lines). Upper bounds on μ from the EW vacuum stability in the smuon and stau directions, calculated using the formula (14) of Ref. [79], are also shown (dashed lines).

of the parameter space is already excluded by the LHC searches. Only a small window of the lightest smuon masses between about 290 and 300 GeV for a very restricted range of bino masses remains allowed. This window can be extended to about 400 GeV assuming that the $(g-2)_\mu$ is brought in agreement with the measurement only at 2σ. In any case, this window will be probed at the LHC with $\sqrt{s} = 13$ TeV.

The vacuum stability constraint can be relaxed if the stau masses are larger than the smuon masses because then larger values of $\mu\tan\beta$ (which control the size of the off-diagonal entry of the stau mass matrix that tends to destabilize the vacuum) are allowed. In consequence, for a given value of $a_\mu^{\rm SUSY}$ smuons can be heavier. However, if the stau masses are larger than the smuon masses by a factor bigger than about 15 (which roughly corresponds to the ratio of the tau to muon masses) the vacuum stability constraint in the muon direction becomes more stringent than that in the stau direction. In that case $(g-2)_\mu$ can be within the 1σ experimental bound for the lightest smuon mass up to about 1.2 TeV (for so heavy smuons μ would have to be above 300 TeV for $\tan\beta = 10$). For a heavier smuon the electroweak vacuum is unstable in the smuon direction. Neither the LHC nor future lepton colliders, such as the ILC or TLEP, will be able to probe 1.2 TeV smuons. However, they could be within the reach of CLIC which aims to operate at the center-of-mass energy of 3 TeV [80]. It is also possible that such smuon masses could be probed at a future 100 TeV collider.

It was also noted in [79] that a large non-universality between smuon and stau masses leads to a strong tension with $\mu \to e\gamma$ unless lepton flavor violation is extremely small (the mass-insertion parameters should be below 10^{-6}). Therefore, the bino contribution can be efficiently probed also by looking for rare decays. Similarly, the CP phase of the μ parameter has to be strongly suppressed in order to avoid constraints from the electric dipole moments.

2.6 Extnesion of MSSM with vectorlike top pratner

As we discussed in previous sections, in the minimal realization of supersymmetry, the Higgs boson mass at tree level is bounded by the Z boson mass and needs to be lifted up by radiative corrections from superpartners. This calls for large superpartner masses that introduce a new hierarchy between the weak scale and the scale of supersymmetry. This is often called the little hierarchy problem of the MSSM. In this section we will consider an extension of the MSSM with an added vectorlike top partner.

We will focus on an extension of MSSM with a vectorlike top quark partner. This is the simplest of vectorlike matter extensions [81, 82, 83, 84, 85, 86, 87, 88, 89, 90] that can effectively reduce the little hierarchy due to large new contributions it induces to the Higgs mass. Our aim is to revisit to what extent such an extension can raise the Higgs boson mass through radiative corrections and help ameliorate the MSSM hierarchy problem, and to specify what experimental probes at the LHC will find or exclude this possibility during the high-luminosity phase.

2.6.1 The Model

To illustrate the impact of adding a vectorlike quark we use the simplest possible supersymmetry spectrum with all soft terms at the scale M_{SUSY}. The only exceptions are the A terms equal to $-M_{SUSY}$. Also, the Higgs boson soft masses and B parameters are chosen to accommodate correct electroweak symmetry breaking. To this very simple spectrum we add a vectorlike top multiplet, t' and $\bar{t}'$, where t' has the quantum numbers of the right-handed top quark t_R^c and $\bar{t}'$ is its conjugate. The soft masses of the scalar components of t' and $\bar{t}'$ are also equal to M_{SUSY}.

The superpotential of the MSSM with an additional vectorlike top partner (omitting small Yukawa couplings of the first two families), reads

$$W = Y_t Q H_u \bar{t} + Y_{t'} Q H_u \bar{t}' + m t' \bar{t} + M t' \bar{t}' + Y_b Q H_d \bar{b} + Y_\tau L H_d \bar{\tau} + \mu H_u H_d. \tag{2.101}$$

The above superpotential leads to the following mass matrix in the basis $\Psi = (Q, t', \bar{t}^\dagger, \bar{t}'^\dagger)$:

$$\mathbf{M}_t = \begin{pmatrix} 0 & \mathbf{m}_t \\ \mathbf{m}_t^\dagger & 0 \end{pmatrix}, \quad \mathbf{m}_t = \begin{pmatrix} Y_t v_2 & Y_{t'} v_2 \\ m & M \end{pmatrix}, \tag{2.102}$$

where $v = \sqrt{v_1^2 + v_2^2} \approx 246$, $\tan\beta = v_2/v_1$ and $v_2 = v \sin\beta/\sqrt{2}$.

In order to obtain masses of the fermions we diagonalize the mass matrix by unitary L and R matrices:

$$L \mathbf{m}_t R^\dagger = \mathrm{diag}(m_{t_1}, m_{t_2}). \tag{2.103}$$

We always set the first eigenvalue equal to the top quark mass, while the second is the mass of the new vectorlike quark. The mass matrix of the scalars takes the following form:

$$\mathbf{M}_S^2 = \mathbf{M}_t^2 + \begin{pmatrix} m_{Q_3}^2 + D_{\frac{1}{2},\frac{2}{3}} & 0 & \frac{v_u}{\sqrt{2}}A_t - \frac{v_d}{\sqrt{2}}\mu Y_t & \frac{v_u}{\sqrt{2}}A_{t'} - \frac{v_d}{\sqrt{2}}\mu Y_{t'} \\ 0 & m_{\tilde{t}'}^2 + D_{0,\frac{2}{3}} & B_m & B_M \\ \frac{v_u}{\sqrt{2}}A_t - \frac{v_d}{\sqrt{2}}\mu Y_t & B_m & m_{U_3}^2 + D_{-\frac{1}{2},-\frac{2}{3}} & 0 \\ \frac{v_u}{\sqrt{2}}A_{t'} - \frac{v_d}{\sqrt{2}}\mu Y_{t'} & B_M & 0 & m_{\tilde{t}'}^2 + D_{0,-\frac{2}{3}} \end{pmatrix}, \tag{2.104}$$

in the basis $\Phi = (\tilde{t}, \tilde{t}', \tilde{\bar{t}}, \tilde{\bar{t}}')$, where $D_{T_3,q} = (T_3 - q\sin\theta_W)\cos(2\beta)M_Z^2$ is the electroweak D term contribution, and A and B are soft breaking terms corresponding to the appropriate couplings in the superpotential. Due to mixing with the vectorlike quark, the top Yukawa coupling can now be very different from its MSSM value while still keeping the predicted top mass unchanged. There are always two values of the top Yukawa that predict the correct top mass, and we always chose the larger one. The smaller value is a modification of the fermiophobic Higgs coupling approach, and generally is more constrained by the data.

In what follows we focus on two sets of new parameters. One set incorporates the small mixing example with $m = 0$, and the other incorporates the large mixing case with $m = M_{SUSY}$. In both cases the superpotential vectorlike mass term M is also equal to M_{SUSY}. New scalar soft masses are $m_{\tilde{t}'}^2 = m_{\tilde{t}'}^2 = M_{SUSY}^2$ and all other mass parameters which were not present in the MSSM are set to $B_m = B_M = A_{t'} = 0$. For simplicity we set the pseudoscalar mass m_A and all MSSM soft breaking terms to M_{SUSY} except m_{H_1}, m_{H_2} and B which we vary in order to achieve correct electroweak symmetry breaking for each value of M_{SUSY}. A-terms are all set to $-M_{SUSY}$. As mentioned above Y_t is always fixed by requiring that at the tree level $m_{t_1} = m_t^{MSSM}$ which corresponds to the physical top mass $m_t = 173.35\,\text{GeV}$ when one-loop corrections are included. The only free parameters left are M_{SUSY} and $\tan\beta$.

2.6.2 Higgs mass correction

We calculate the contribution to the mass of the light neutral Higgs boson using effective potential approximation in the decoupling regime [85]. The contribution to the effective potential from tops and stops and the new vectorlike states reads

$$\Delta V = \frac{6}{64\pi^2}\sum_{i=1}^{4}\left[F(m_{\tilde{t}_i}^2) - 2F(M_{t_i}^2)\right] \tag{2.105}$$

where $F(x) = x^2\ln(x/Q^2)$ while $M_{t_i}^2$ and $m_{\tilde{t}_i}^2$ are eigenvalues of the fermion mass matrix (2.102) and scalar mass matrix (2.104) respectively. The correction to the light Higgs boson squared mass is equal to

$$\Delta m_h^2 = \left[\frac{\sin^2\beta}{2}\left(\frac{\partial^2}{\partial v_u^2} - \frac{1}{v_u}\frac{\partial}{\partial v_u}\right) + \frac{\cos^2\beta}{2}\left(\frac{\partial^2}{\partial v_d^2} - \frac{1}{v_d}\frac{\partial}{\partial v_d}\right) + \sin\beta\cos\beta\left(\frac{\partial^2}{\partial v_d \partial v_u}\right)\right]\Delta V. \tag{2.106}$$

Since the above correction already includes the top and stop contribution, we subtract the MSSM top and stop correction $\Delta {m_h}^{\text{MSSM}}$ which was already included in our MSSM value m_h^{MSSM}. We calculate the $\Delta m_h{}^{\mathrm{MSSM}}$ correction using eigenvalues of the MSSM mass matrices in equation (2.105) and then using an equation similar to (2.106), with only MSSM masses. Our final computation of the corrected Higgs mass reads

$$m_h^2 = (m_h^{MSSM})^2 + \Delta m_h^2 - (\Delta m_h^{MSSM})^2. \tag{2.107}$$

Figure 2.8 shows the value of M_{SUSY} needed to obtain $m_h = 125.09\,\mathrm{GeV}$ as a function of $Y_{t'}$ together with various constraints explained in the following section. Figure 2.9 shows the minimal value of M_{SUSY} achievable without violating any of the experimental constraints. The smaller the value of M_{SUSY} the more the vectorlike extension of the MSSM helps to ameliorate the little hierarchy problem. The MSSM values of M_{SUSY} corresponding to $\tan\beta = 5, 7, 10$ and 30 are $M_{SUSY} = 11.4, 7.4, 5.7$ and 4.4 TeV, which means that in all presented cases we are able to achieve much lower M_{SUSY} than required in the MSSM, without violating any of the constraints.

Since the additional contribution to the Higgs mass from the vectorlike quark sector lowers the value of M_{SUSY} needed to achieve the observed Higgs mass, it also increases the prospects of finding the correspondingly lower superpartner masses at subsequent runs of the LHC .

2.6.3 RGE corrections

The introduction of additional states and additional Yukawa couplings to the MSSM causes the renormalization group flow trajectories of the couplings to be altered as the scale increases. In this section we discuss these effects and specify the implications and constraints they have on the unification of couplings and the possible development of Landau poles.

In this analysis we have calculated two-loop renormalization group equations using SARAH [91, 92, 93], and confirmed the results analytically using known results [94]. Very significant changes in the renormalization group trajectories come from new coefficients in the one-loop running of the gauge couplings,

$$\frac{d}{dt} g_i = \frac{1}{4\pi^2}\, b_i g_i^3 \qquad b_i = \left(\frac{41}{5}, 1, -2\right). \tag{2.108}$$

These new equations predict the unification scale M_U (defined here by $g_1(M_U) = g_2(M_U)$) to be significantly lower than in the MSSM. The new unification scale is not far above 10^{13} GeV.

It is important to point out that unification at a scale around 10^{16} GeV can still easily be achieved by positing appropriate high-scale threshold corrections [95] or by adding vectorlike quarks so that together all vectorlike superfields form a complete representation of $SU(5)$. This can reestablish coupling constant unification without significant modifications to other bounds discussed in the following sections.

However a more stringent constraint comes from the running of $Y_{t'}$ and its contribution to the running of Y_t. At one-loop order these contributions induce Landau poles in the Yukawa couplings' running when $Y_{t'}$ is sufficiently large, at two-loop order Y_t and $Y_{t'}$

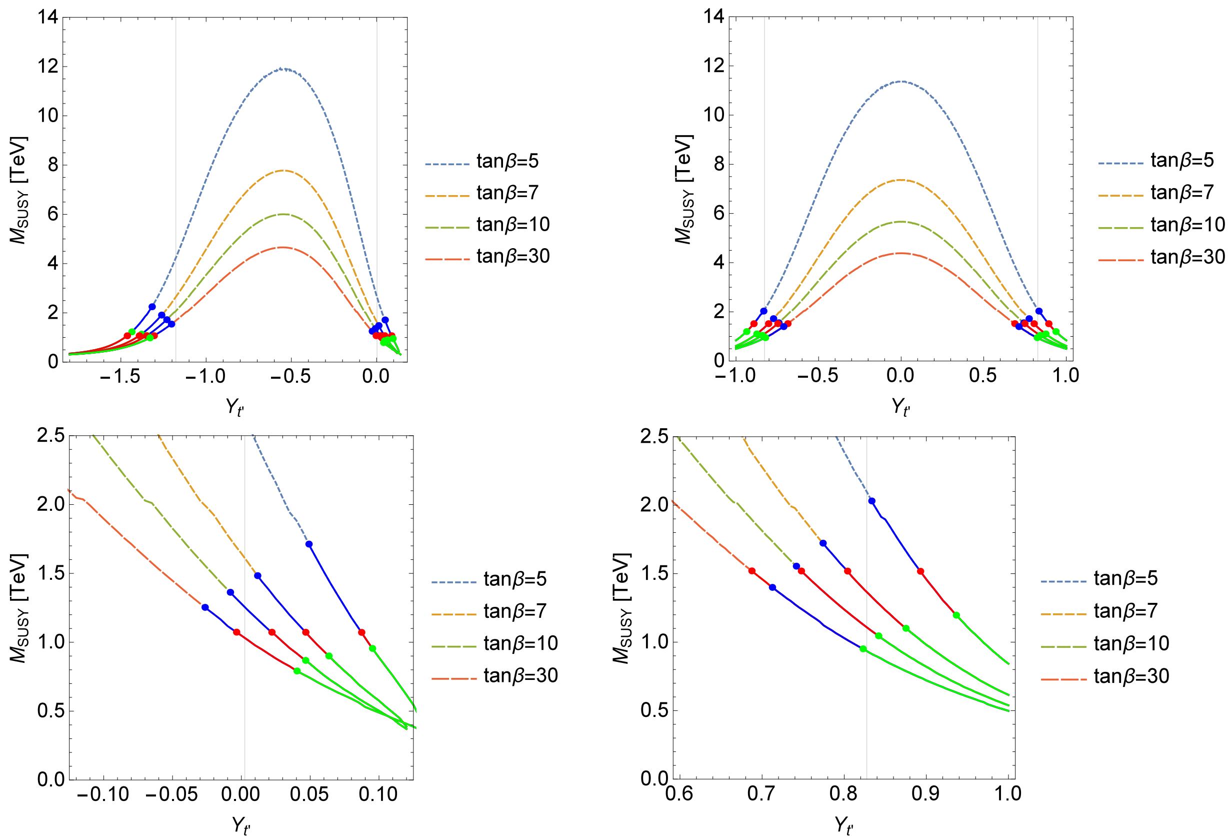

Figure 2.8: Common superpartner mass M_{SUSY} required to obtain $m_h = 125.09\,\mathrm{GeV}$ as a function of $Y_{t'}$ for $m = M$ (left panel) and $m = 0$ (right panel). Bottom row shows a zoom of the top row plots‘ lower right corners. MSSM values of M_{SUSY} required to obtain $m_h = 125.09\,\mathrm{GeV}$ corresponding to $\tan\beta = 5, 7, 10$ and 30 are $M_{SUSY} = 11.4, 7.4, 5.7$ and 4.4TeV. Dashed lines are allowed by all considered constraints, while solid lines correspond to different exclusions which will be achievable in HL-LHC. The calculation of these bounds is explained in the next subsection. Dark blue regions may be excluded by measurement of the Higgs boson signal strength at 2σ significance. Dark green regions predict corrections to oblique parameters that may be excluded by future HL-LHC measurements at 2σ significance, and red regions may be excluded in the second LHC run by direct detection of the top partner. Vertical lines show maximal $Y_{t'}$ allowing gauge coupling unification before the quasifixed point sets in. All parameters except $\tan\beta$ are fixed by assuming a single supersymmetry scale M_{SUSY} and requiring correct top and Higgs physical masses $m_t = 173.35\,\mathrm{GeV}$, $m_h = 125.09\,\mathrm{GeV}$.

develop a strongly coupled UV quasifixed point. The range of values of $Y_{t'}$ that allow gauge coupling unification before the UV quasifixed point sets in are $Y_{t'} \in (-1.775, 0.002)$ for $m = M_{SUSY}$ and $Y_{t'} \in (-0.8275, 0.8275)$ for $m = 0$. These values are marked on the plots showing our results. However, since we do not consider a specific UV completion, it is not necessary to treat them as constraints.

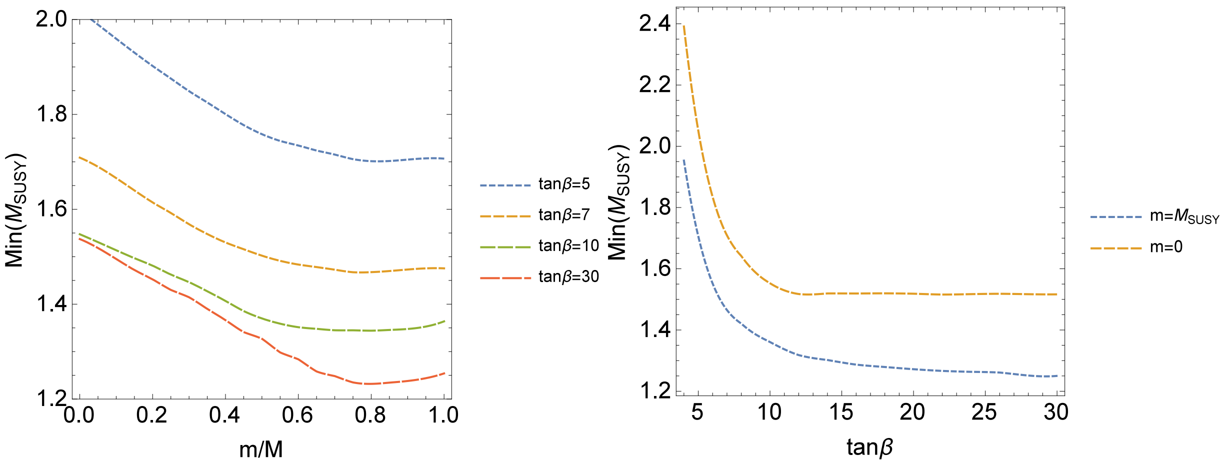

Figure 2.9: Minimal value of M_{SUSY} achievable without violating any of the above constraints as a function of $\frac{m}{M_{SUSY}}$ (left panel) and $\tan\beta$ (right panel). All other parameters are fixed by assuming a single supersymmetry scale M_{SUSY} and requiring correct top and Higgs masses $m_t = 173.35\,\text{GeV}$, $m_h = 125.09\,\text{GeV}$.

2.6.4 Oblique parameters

The Peskin-Takeuchi precision electroweak parameters [96] S and T are defined in terms of electroweak vector boson self-energies as

$$\begin{aligned} \frac{\alpha S}{4 s_W^2 c_W^2} &= \left[\Pi_{ZZ}(M_Z^2) - \Pi_{ZZ}(0) - \frac{c_{2W}}{c_W s_W}\Pi_{Z\gamma}(M_Z^2) - \Pi_{\gamma\gamma}(M_Z^2)\right]/M_Z^2, &(2.109)\\ \alpha T &= \Pi_{WW}(0)/M_W^2 - \Pi_{ZZ}(0)/M_Z^2. &(2.110)\end{aligned}$$

We calculate the S and T parameter contributions from the vectorlike quarks and their scalar superpartners using results from [85]. The one-loop functions $G(x)$, $H(x,y)$, $B(x,y)$, and $F(x,y)$ have been defined in ref. [97] and particle names stand for the squared mass of the particles when they appear as an argument of these functions.

Contributions from t' to the electroweak vector boson self-energies are:

$$\begin{aligned} \Delta\Pi_{\gamma\gamma} &= -\frac{N_c}{16\pi^2} 2 g^2 s_W^2 \left[e_u^2 G(M_{t_2})\right], \\ \Delta\Pi_{Z\gamma} &= -\frac{N_c}{16\pi^2} g s_W \left[e_u \sum_{i=1,2} (g^Z_{t_i t_i^\dagger} - g^Z_{\tilde{t}_i \tilde{t}_i^\dagger}) G(t_i)\right] - \Delta\Pi^{\rm SM}_{Z\gamma}, &(2.111)\\ \Delta\Pi_{ZZ} &= -\frac{N_c}{16\pi^2}\left[\sum_{i,j=1}^{2} (|g^Z_{t_i t_j^\dagger}|^2 + |g^Z_{\tilde{t}_i \tilde{t}_j^\dagger}|^2) H(t_i,t_j) - 4\mathrm{Re}(g^Z_{t_i t_j^\dagger} g^Z_{\tilde{t}_i \tilde{t}_j^\dagger}) m_{t_i} m_{t_j} B(t_i,t_j)\right] - \Delta\Pi^{\rm SM}_{ZZ}, \\ \Delta\Pi_{WW} &= -\frac{N_c}{16\pi^2}\sum_{i=1}^{2}\left[(|g^W_{t_i b^\dagger}|^2) H(b,t_i)\right] - \Delta\Pi^{\rm SM}_{WW}, \end{aligned}$$

where $N_c = 3$, $e_u = 2/3$, $e_d = -1/3$ and SM contributions are similar to those above with couplings in which $L_{11} = 1$ is the only nonzero element of the mixing matrix. The massive vector boson couplings with quarks are

$$
\begin{aligned}
g^Z_{t_i t_j^\dagger} &= \frac{g}{c_W}\left(\frac{1}{2}L^*_{i1}L_{j1} - e_u s_W^2 \delta_{ij}\right), \qquad g^Z_{\tilde{t}_i \tilde{t}_j^\dagger} = \frac{g}{c_W}\left(e_u s_W^2 \delta_{ij}\right), \\
g^W_{t_i b^\dagger} &= \frac{g}{\sqrt{2}} L^*_{i1},
\end{aligned} \tag{2.112}
$$

where L is the fermion mixing matrix defined in (2.103).

The up-type scalar mass matrix (2.104) is diagonalized by the unitary matrix U:

$$
U\mathbf{M}_S^2 U^\dagger = \mathrm{diag}(m^2_{\tilde{t}_1}, m^2_{\tilde{t}_2}, m^2_{\tilde{t}_3}, m^2_{\tilde{t}_4}), \tag{2.113}
$$

while the MSSM sbottom mass matrix $\mathbf{M}_D^2$ is diagonalized by the unitary matrix D

$$
D\mathbf{M}_D^2 D^\dagger = \mathrm{diag}(m^2_{\tilde{b}_1}, m^2_{\tilde{b}_2}). \tag{2.114}
$$

Contributions from third family squarks to the electroweak vector boson self-energies are

$$
\begin{aligned}
\Delta\Pi_{\gamma\gamma} &= \frac{N_c}{16\pi^2} g^2 s_W^2 \left[e_u^2 \sum_{i=1}^{4} F(\tilde{t}_i, \tilde{t}_i) + e_d^2 \sum_{i=1}^{2} F(\tilde{b}_i, \tilde{b}_i)\right], \\
\Delta\Pi_{Z\gamma} &= \frac{N_c}{16\pi^2} g s_W \left[e_u \sum_{i=1}^{4} g^Z_{\tilde{t}_i \tilde{t}_i^*} F(\tilde{t}_i, \tilde{t}_i) + e_d \sum_{i=1}^{2} g^Z_{\tilde{b}_i \tilde{b}_i^*} F(\tilde{b}_i, \tilde{b}_i)\right], \\
\Delta\Pi_{ZZ} &= \frac{N_c}{16\pi^2} \left[\sum_{i,j=1}^{4} |g^Z_{\tilde{t}_i \tilde{t}_j^*}|^2 F(\tilde{t}_i, \tilde{t}_j) + \sum_{i,j=1}^{2} |g^Z_{\tilde{b}_i \tilde{b}_j^*}|^2 F(\tilde{b}_i, \tilde{b}_j)\right], \\
\Delta\Pi_{WW} &= \frac{N_c}{16\pi^2} \sum_{i=1}^{2}\sum_{j=1}^{4} |g^W_{\tilde{b}_i \tilde{t}_j^*}|^2 F(\tilde{b}_i, \tilde{t}_j),
\end{aligned} \tag{2.115}
$$

where the vector boson couplings with the squarks are:

$$
\begin{aligned}
g^Z_{\tilde{t}_i \tilde{t}_j^*} &= \frac{g}{c_W}\left(\frac{1}{2}(U^*_{i1}U_{j1}) - e_u s_W^2 \delta_{ij}\right), \\
g^Z_{\tilde{b}_i \tilde{b}_j^*} &= \frac{g}{c_W}\left(-\frac{1}{2}(D^*_{i1}D_{j1}) - e_d s_W^2 \delta_{ij}\right), \\
g^W_{\tilde{b}_i \tilde{t}_j^*} &= \frac{g}{\sqrt{2}}(D^*_{i1}U_{j1}).
\end{aligned} \tag{2.116}
$$

To calculate MSSM contributions we use expressions from [97] excluding corrections from stops and sbottoms which were already included in the vectorlike contribution calculation. We also verified dominant corrections coming from new fermions with similar results from [98].

The currently allowed experimental values are $S = 0.06 \pm 0.09$ and $T = 0.1 \pm 0.07$ (assuming $U = 0$) with correlation 0.91 [99] (the correlation parameter is the tilt in the ellipse in the S-T plane). Only minimally more stringent constraints can be achieved from

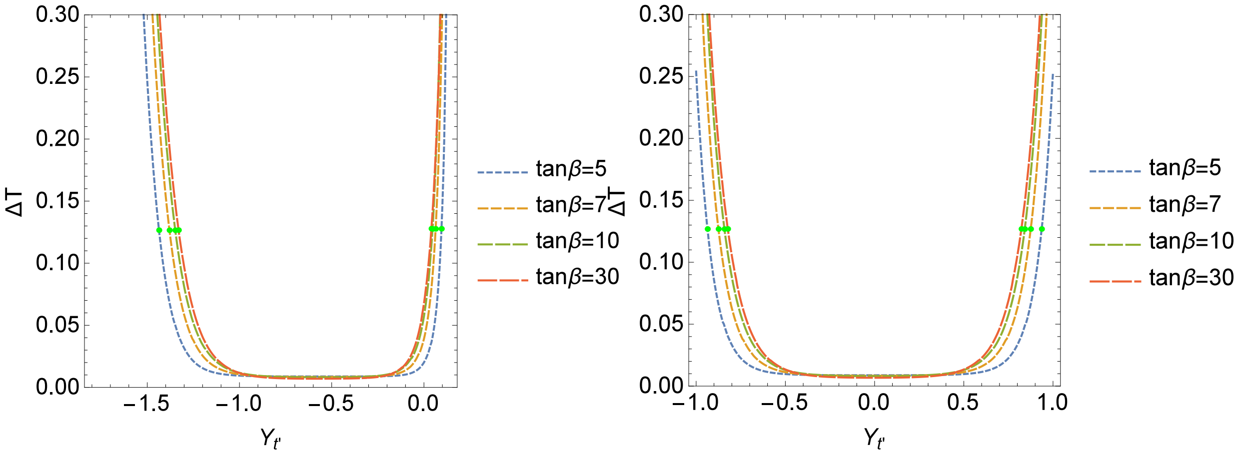

Figure 2.10: Correction to the T parameter as a function of $Y_{t'}$ for $m = M$ (left panel) and $m = 0$ (right panel). All values satisfy $m_h = 125.09\,\text{GeV}$. Green points show values above which the results can be excluded at 2σ by future experimental constraints.

LHC running at $\sqrt{s} = 14\,\text{TeV}$ with high integrated luminosity $300\,\text{fb}^{-1}$. Predicted future sensitivity values of $S = 0.06 \pm 0.09$ and $T = 0.1 \pm 0.06$ are taken from [100].

Figure 2.10 shows resulting corrections to the T parameter as a function of $Y_{t'}$ together with points showing values above which the results can be excluded at 2σ by future experimental constraints. These points are very close to forming a vertical line because corrections to the S parameter are very small for all interesting values of $Y_{t'}$. This is also the reason for which we do not include a plot of vectorlike corrections in the S- T plane.

Corrections from other superpartners are very small due to the simplified spectrum we chose. Figure 2.11 shows corrections coming from MSSM with and without the stops contribution from $100,000$ randomized spectra of masses up to $3\,\text{TeV}$. A more randomized spectrum is unlikely to produce points outside the the S and T exclusion ellipse. Most of the points would bring our results closer to the central values due to negative T competing against large positive vectorlike quark corrections and positive S contributions, which push our results towards the experimentally allowed ellipsis.

Superpartner corrections to electroweak precision observables are generally small because superpartners are largely decoupled even with current direct detection exclusions. However inclusion of a new quark can introduce unacceptably large corrections to the T parameter if its mixing with the SM top is substantial. Nevertheless, it is important to note that with currently available bounds, electroweak corrections are the most important constraints on our model. However, as the energy and luminosity increase for HL-LHC the observables at play in the electroweak precision analysis do not improve substantially. Therefore, precision electroweak analysis constraints become relatively less important in time compared to direct detection probes of new states and especially compared to precision Higgs analysis, which is discussed in the next subsection.

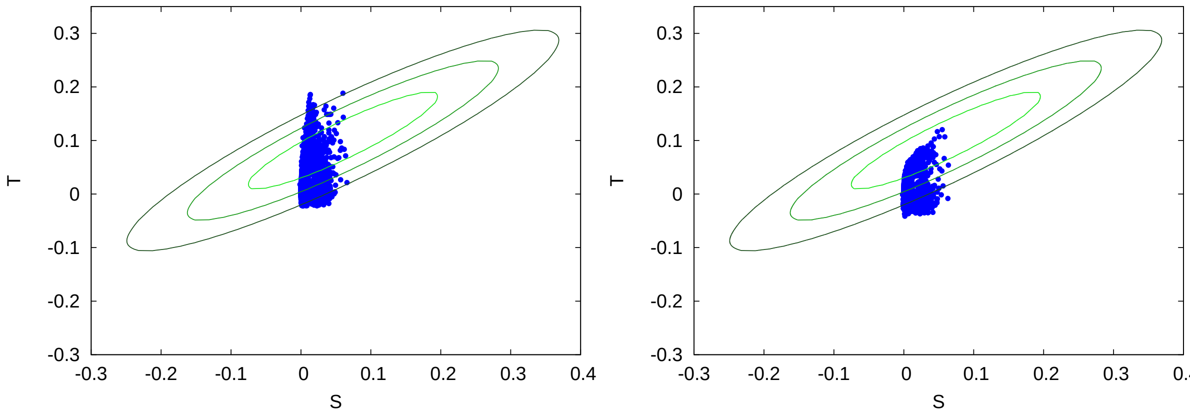

Figure 2.11: Oblique parameter corrections in $S-T$ plane coming from the MSSM (left panel) and the same results without stop and sbottom contribution (right panel), with a randomized spectrum of superpartner masses up to 3 TeV.

2.6.5 Higgs boson coupling corrections

Next we turn to calculation of Higgs boson branching ratios including the above modifications and new couplings to the top quark and its vectorlike partner. We start by discussing the shifts in couplings of the MSSM compared to the SM and then compare with the case with extra vectorlike top states. In the MSSM, the Higgs couplings to up and down type quarks and vector bosons take the form [101, 102]:

$$\begin{aligned} c_u = \frac{g_u}{g_u^{\rm SM}} &= \frac{\cos\alpha}{\sin\beta} \\ c_d = \frac{g_d}{g_d^{\rm SM}} &= \frac{-\sin\alpha}{\cos\beta} \\ c_V = \frac{g_V}{g_V^{\rm SM}} &= \sin(\beta-\alpha), \end{aligned} \tag{2.117}$$

where α is the Higgs mixing angle and $\tan\beta = v_u/v_d$.

Most experimentally important branching ratios have the same values as in the MSSM, which are obtained by multiplying the appropriate c_i coefficients in front of the SM partial width exprressoins

$$\begin{aligned} \Gamma(h\to b\bar{b}) &= c_d^2\Gamma^{\rm SM}(h\to b\bar{b}), \quad \Gamma(h\to\tau\bar{\tau}) = c_d^2\Gamma^{\rm SM}(h\to\tau\bar{\tau}), \\ \Gamma(h\to\mu\bar{\mu}) &= c_d^2\Gamma^{\rm SM}(h\to\mu\bar{\mu}), \quad \Gamma(h\to c\bar{c}) = c_u^2\Gamma^{\rm SM}(h\to c\bar{c}), \\ \Gamma(h\to WW) &= c_V^2\Gamma^{\rm SM}(h\to WW), \quad \Gamma(h\to ZZ) = c_V^2\Gamma^{\rm SM}(h\to ZZ). \end{aligned} \tag{2.118}$$

The remaining important branching ratios are loop induced and are modified due to modified top couplings and new particles in the loops. We will express these branching ratios as

$$\Gamma(h\to X) = \frac{|\mathcal{A}_X|^2}{|\mathcal{A}_X^{\rm SM}|^2}\Gamma(h\to X)^{\rm SM}. \tag{2.119}$$

In the following $N_c = 3$ and loop functions F, I and A, as well as coefficients τ, are defined in [101]. Charges and third components of isospin for fields used in the following equations are shown in Table 2.2, while modifications of the top and top prime couplings to the Higgs bosons are given by

$$g_{ht_i\bar{t}_i} = \frac{Y_t L_{i1} R_{i1} + Y_{t'} L_{i1} R_{i2}}{Y_t^{\mathrm{MSSM}}}, \tag{2.120}$$

where L and R are fermion mixing matrices defined in (2.103). $\mathcal{A}_X^{SUSY}$ are sums of the contributions of superpartners which we neglect since they have very small couplings $g \approx \frac{m_Z^2}{M_{SUSY}^2}$.

For branching ratio to two gluons we have,

$$\begin{aligned} \mathcal{A}_{gg} &= c_d \sum_{i=d,s,b} F_{\frac{1}{2}}(\tau_i) + c_u \sum_{i=u,c} F_{\frac{1}{2}}(\tau_i) + c_u \sum_{i=1}^{2} g_{ht_i\bar{t}_i} F_{\frac{1}{2}}(\tau_{t_i}) + \mathcal{A}_{gg}^{SUSY}, \qquad (2.121)\\ \mathcal{A}_{gg}^{\mathrm{SM}} &= \sum_{i=d,s,b} F_{\frac{1}{2}}(\tau_i) + \sum_{i=u,c,t} F_{\frac{1}{2}}(\tau_i). \end{aligned}$$

Similarly for the branching ratio to two photons we have,

$$\begin{aligned} \mathcal{A}_{\gamma\gamma} &= c_V F_1(\tau_W) + c_d e_e^2 \sum_{i=e,\mu,\tau} F_{\frac{1}{2}}(\tau_i) + c_d N_c e_d^2 \sum_{i=d,s,b} F_{\frac{1}{2}}(\tau_i) + c_u N_c e_u^2 \sum_{i=u,c} F_{\frac{1}{2}}(\tau_i) \\ &+ c_u N_c e_u^2 \sum_{i=1}^{2} g_{ht_i\bar{t}_i} F_{\frac{1}{2}}(\tau_{t_i}) + \mathcal{A}_{\gamma\gamma}^{\mathrm{SUSY}} \qquad (2.122)\\ \mathcal{A}_{\gamma\gamma}^{\mathrm{SM}} &= F_1(\tau_W) + e_e^2 \sum_{i=e,\mu,\tau} F_{\frac{1}{2}}(\tau_i) + N_c e_d^2 \sum_{i=d,s,b} F_{\frac{1}{2}}(\tau_i) + N_c e_u^2 \sum_{i=u,c,t} F_{\frac{1}{2}}(\tau_i). \end{aligned}$$

Lastly for branching ratio of Higgs to a photon and Z boson we obtain

$$\begin{aligned} \mathcal{A}_{Z\gamma} &= c_d e_e v_e \sum_{i=e,\mu,\tau} A_{\frac{1}{2}}(\tau_i, \lambda_i) + c_d N_c e_d v_d \sum_{i=d,s,b} A_{\frac{1}{2}}(\tau_i, \lambda_i) + c_u N_c e_u v_u \sum_{i=u,c} A_{\frac{1}{2}}(\tau_i, \lambda_i) \\ &+ c_u N_c e_u \sum_{i=1}^{2} v_{t_i} g_{ht_i\bar{t}_i} A_{\frac{1}{2}}(\tau_{t_i}, \lambda_{t_i}) + c_V A_1(\tau_W, \lambda_W) + \mathcal{A}_{Z\gamma}^{SUSY} \qquad (2.123)\\ \mathcal{A}_{Z\gamma}^{\mathrm{SM}} &= e_e v_e \sum_{i=e,\mu,\tau} A_{\frac{1}{2}}(\tau_i, \lambda_i) + N_c e_d^2 \sum_{i=d,s,b} A_{\frac{1}{2}}(\tau_i, \lambda_i) + N_c e_u^2 \sum_{i=u,c,t} A_{\frac{1}{2}}(\tau_i, \lambda_i) + A_1(\tau_W, \lambda_W), \end{aligned}$$

where $v_f = (2T_3^f - 4e_f s_W^2)/(s_W c_W)$, $s_W = \sin\theta_W$ and $c_W = \cos\theta_W$.

The branching ratios are given by

$$B(h \to X) = \frac{\Gamma_X}{\sum_i \Gamma_i} \tag{2.124}$$

f	t_i	u	d	e
e_f	$\frac{2}{3}$	$\frac{2}{3}$	$-\frac{1}{3}$	-1
T_3^f	$\frac{1}{2}L_{i1}$	$\frac{1}{2}$	$-\frac{1}{2}$	$-\frac{1}{2}$

Table 2.2: Charges and effective third isospin components. The mixing matrix L is defined in (2.103).

$\Delta\mu_{\gamma\gamma}$	$\Delta\mu_{bb}$	$\Delta\mu_{\tau\tau}$	$\Delta\mu_{WW}$	$\Delta\mu_{ZZ}$
0.06	0.11	0.08	0.06	0.07

Table 2.3: Higgs signal strength future experimental sensitivities at 1σ significance from CMS [103]

with the sum running over all decay channels computed in this section. We approximate the resulting signal strength modification by including only the gluon fusion production channel, which at leading order gives

$$\begin{aligned}\Delta\mu_X &= \frac{\sigma B(h\to X)-\sigma^{\text{SM}}B^{\text{SM}}(h\to X)}{\sigma^{\text{SM}}B^{\text{SM}}(h\to X)} = \frac{\sigma B(h\to X)}{\sigma^{\text{SM}}B^{\text{SM}}(h\to X)} - 1 \\ &\approx \frac{\sigma(gg\to h)}{\sigma^{\text{SM}}(gg\to h)}\frac{Br(h\to X)}{B^{\text{SM}}(h\to X)} - 1 \approx \frac{\Gamma(h\to gg)}{\Gamma^{\text{SM}}(h\to gg)}\frac{B(h\to X)}{B^{\text{SM}}(h\to X)} - 1.\end{aligned} \tag{2.125}$$

We confront these results with future experimental bounds as predicted by the CMS Collaboration [103] shown in Table 2.3. SM values of the branching ratios were taken from [104]. The resulting signal strength modifications are dominated by the increased $gg \to H$ production cross section compared to the SM and even MSSM. In our model all signal strengths grow rapidly when the mixing with the vectorlike state is increased. The most important exclusion limit comes from the $H \to WW$ signal. The high sensitivity in this channel is due to the onset of high statistics and high accuracy in the measurement of this channel at the HL-LHC. This can be compared to $H \to \gamma\gamma$ which is not as useful due to smaller modifications of its total $\sigma \cdot \mathrm{B}$ rate. There is a partial cancellation of vectorlike top contribution in the $\sigma \cdot \mathrm{B}$ product. The second best exclusion channel is $H \to ZZ$ with slightly worse experimental accuracy. The increased experimental sensitivities at HL-LHC leads to the conclusion that the first evidence for vectorlike quarks in this context of natural supersymmetry would likely come from deviations found in precision Higgs observables.

2.6.6 Direct detection

The best source for the direct mass bound for the new vectorlike states are dedicated analyses by the ATLAS and CMS collaborations at LHC. In particular, the recent CMS analysis [105] of t' decaying in three channels $t' \to bW, tZ, tH$ without assumptions on the branching ratios, has current mass limits between 687 GeV and 782 GeV.

A similar analysis of decay to the same final states in future colliders was performed in [106]. The authors predict mass ranges in which t' could be discovered or excluded for

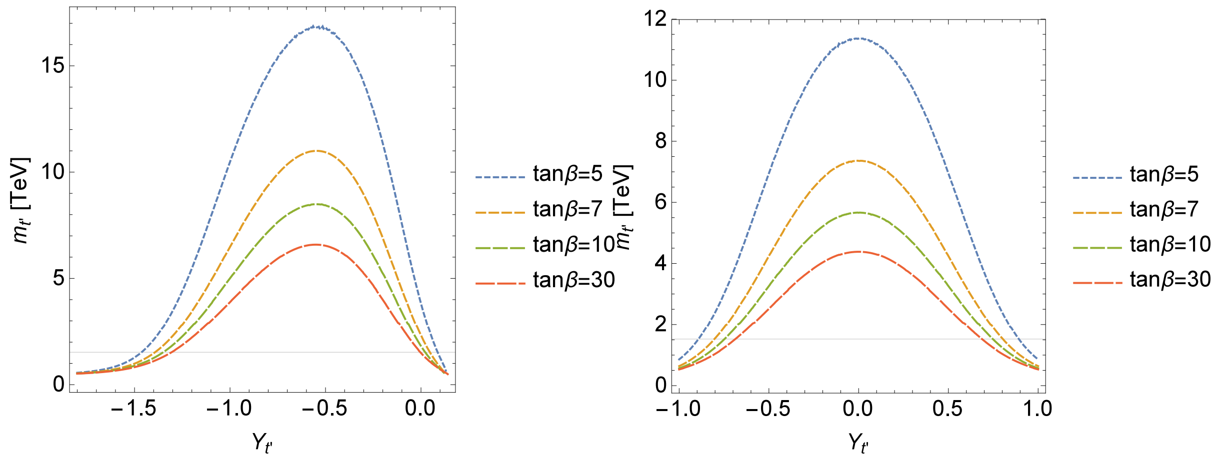

Figure 2.12: Vectorlike top partner mass for which $m_h = 125.09\,\text{GeV}$ as a function of $Y_{t'}$ for $m = M$ (left panel) and $m = 0$ (right panel). Horizontal line corresponds to the future experimental bound.

different energies and integrated luminosities. We use their exclusion limit (at 95% C.L.) for vectorlike top partner achievable in LHC at $\sqrt{s} = 14\,\text{TeV}$ with integrated luminosity $300\,\text{fb}^{-1}$, namely $m_{t'} < 1525\,\text{GeV}$.

Figure 2.12 shows the vectorlike top partner mass needed to achieve $m_h = 125.09\,\text{GeV}$ as a function of $Y_{t'}$. The right-hand side plot is very similar to Figure 2.8 because, as expected, the mass of the vectorlike top is close to M_{SUSY}, while in the left-hand side plot the mass is significantly enhanced due to large mixing.

It is important to point out here that direct detection is crucially dependent on the mass of the additional quark, while all previously discussed constraints were more dependent on its mixing with already observed states. Consequently the interplay between constraints described in this section and those of the previous two depends on the mixing, which is a consequence of our choice of spectrum parameters. This is why we include both small ($m = 0$) and maximal ($m = M_{SUSY}$) mixing scenarios in our analysis. Direct detection bounds turn out to be very important for our model. And in fact this probe proves to be the strongest for the part of parameter space corresponding to large $\tan\beta$, unless the mixing is sufficiently large ($m \approx M_{SUSY}$). Otherwise precision Higgs analysis will be a more powerful probe as shown in Figure 2.13.

2.6.7 Summary and comparison of bounds

To summarise, in this section we analyzed a single vectorlike top partner model, which is the simplest vectorlike extension of the MSSM that can significantly help with the little hierarchy problem. We calculated and compared different experimental constraints the model will face after $300\,\text{fb}^{-1}$ of data are gathered at the HL-LHC. Our key result is that the most constraining of the discussed bounds is modification of the Higgs boson properties. An exception to that is the case of large $\tan\beta$ and small mixing where the

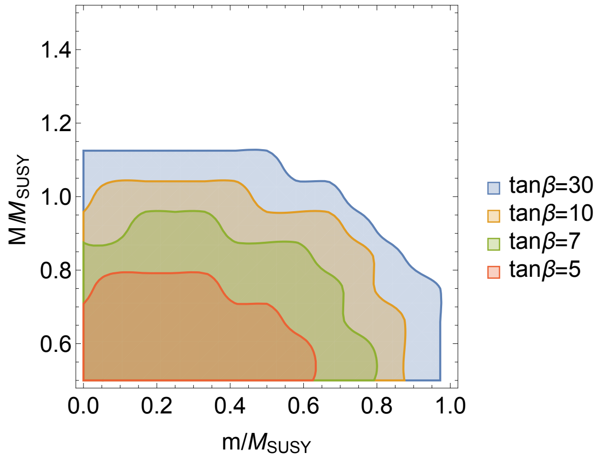

Figure 2.13: Region of vectorlike mass and mixing parameter space, where direct detection is the strongest constraint. The unmarked regions corresponds to precision Higgs measurements being the strongest constraint.

direct detection probes of the heavy vectorlike states at the collider are slightly more stringent, a sdiscussed at the ednd of previous subsection.

After including all the constraints achievable at the HL-LHC, the resulting M_{SUSY} can still be as low as 1.2 to 2.4 TeV for the simplest possible supersymmetry spectrum. These results are 3 to 5 times smaller compared to what otherwise would be allowed in the MSSM. Thus even a very simple vectorlike quark extension can greatly reduce the little hierarchy problem of the MSSM, and careful measurements of Higgs boson observables would likely give first evidence of this scenario.

2.7 Five dimensional SUSY models

In this section we turn to a very different extension of MSSM which can help in solving the hierarchy problem. Namely we explore the phenomenological predictions of a supersymmetric standard model, with a large extra dimension and unifying gauge couplings. The modified five dimensional renormalisation group equations make it possible to obtain light, maximally mixed stops, with a low scale of supersymmetry breaking and a low unification scale. This allows the fine-tuning to be lowered right down to the barrier coming directly from experimental lower limits on the stop masses. We also show that modifying the SUSY breaking pattern to obtain lighter stops at the high scale does not result in fine-tuning relaxation, and only RGE effects turn out to be effective in generating a lower fine-tuning.

In our analysis we used renormalisation group equations outlined in [107, 108] and adapted a C++ based spectrum generator originally intended for the (four dimensional) MSSM [1]. A similar modification may be carried out with any publicly available spectrum generator [37, 38, 39] [1]. The RGEs used in this paper may be found in [108] and further conventions in [107] and [111, 112, 113, 114, 115]. For earlier phenomenological studies of five dimensional theories see for example [116].

2.7.1 The 5D-SSM+($F^{\pm}$) Model

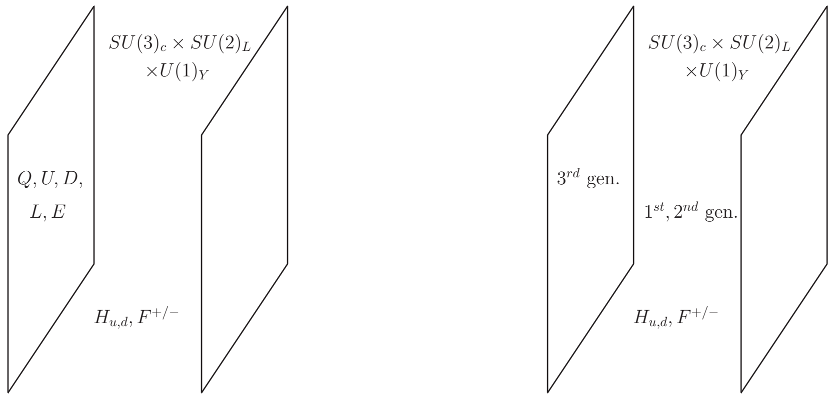

Figure 2.14: *Pictorials to represent the location of matter in the five dimensional model. In Model 1 (left), all generations of matter live on a brane. In Model 2 (right), only the 3rd generation lives on a brane*

The first model that we wish to explore is a five dimensional supersymmetric theory with the field content outlined in table 2.4 and is pictured in figure 2.14 (left). In this model the Higgs fields (H_u, H_d), gauge fields and additionally $F^{\pm}$ are bulk fields [117]. This matter content is necessary for the gauge couplings unification, as we shall explore further later. All five dimensional bulk matter fields are supersymmetric Hypermultiplets which due to even and odd boundary conditions lead to a four dimensional Chiral multiplet as a zero mode of the Kaluza-Klein expansion: such details are well documented, for instance in [111, 112, 113, 114, 115]. The second model we wish to explore is outlined in table 2.5 and pictured in figure 2.14 (right). In model 2 only the third generation is located on a brane and the first and second generation are in the bulk along with the Higgs multiplets and $F^{\pm}$ fields.

The superpotential for both models is given by

$$W = Y_u\, \hat{u}\, \epsilon_{ij} \hat{q}^i\, \hat{H}_u^j - Y_d\, \hat{d}\, \epsilon_{ij} \hat{q}^i\, \hat{H}_d^j - Y_e\, \hat{e}\, \epsilon_{ij} \hat{l}^i\, \hat{H}_d^j + \mu H_u H_d + \acute{\mu} F^- F^+ \; . \qquad (2.126)$$

It would be very worthwhile to consider the generation of the term $\acute{\mu} F^- F^+$ in the superpotential, although for this analysis we will not need to consider it, and postpone that to later work. We will now explore the running parameters of these two theories as one changes the scale of the extra dimension.

[1] To date, five dimensional theories are one such class of models that cannot yet be explored using `SARAH` [109, 91, 110, 92] although it can still be a powerful tool to determine the RGEs of the low energy four dimensional effective theory that the five dimensional theory runs to [108].

Superfields	Brane	Bulk	$U(1)_Y \times SU(2)_L \times SU(3)_c$
$\hat{q}^f$	✓	-	$(\frac{1}{6}, \mathbf{2}, \mathbf{3})$
$\hat{d}^f$	✓	-	$(\frac{1}{3}, \mathbf{1}, \overline{\mathbf{3}})$
$\hat{u}^f$	✓	-	$(-\frac{2}{3}, \mathbf{1}, \overline{\mathbf{3}})$
$\hat{l}^f$	✓	-	$(-\frac{1}{2}, \mathbf{2}, \mathbf{1})$
$\hat{e}^f$	✓	-	$(1, \mathbf{1}, \mathbf{1})$
$\hat{H}_d$	-	✓	$(-\frac{1}{2}, \mathbf{2}, \mathbf{1})$
$\hat{H}_u$	-	✓	$(\frac{1}{2}, \mathbf{2}, \mathbf{1})$
$\hat{F}_-$	-	✓	$(-1, \mathbf{1}, \mathbf{1})$
$\hat{F}_+$	-	✓	$(1, \mathbf{1}, \mathbf{1})$
$\hat{B}_V$	-	✓	$(0, \mathbf{1}, \mathbf{1})$
$\hat{W}_V$	-	✓	$(0, \mathbf{3}, \mathbf{1})$
$\hat{G}_V$	-	✓	$(0, \mathbf{1}, \mathbf{8})$

Table 2.4: The matter content of model 1. All superfields of chiral fermions live on a brane and all Higgs-type superfields and gauge vector fields live in the bulk. The superscript $f = 1, 2, 3$ denotes the generations. Neutrino superfields may be included straightforwardly.

Superfields	Brane	Bulk	$U(1)_Y \times SU(2)_L \times SU(3)_c$
$\hat{q}^{1,2}$	-	✓	$(\frac{1}{6}, \mathbf{2}, \mathbf{3})$
$\hat{d}^{1,2}$	-	✓	$(\frac{1}{3}, \mathbf{1}, \overline{\mathbf{3}})$
$\hat{u}^{1,2}$	-	✓	$(-\frac{2}{3}, \mathbf{1}, \overline{\mathbf{3}})$
$\hat{l}^{1,2}$	-	✓	$(-\frac{1}{2}, \mathbf{2}, \mathbf{1})$
$\hat{e}^{1,2}$	-	✓	$(1, \mathbf{1}, \mathbf{1})$
$\hat{q}^3$	✓	-	$(\frac{1}{6}, \mathbf{2}, \mathbf{3})$
$\hat{d}^3$	✓	-	$(\frac{1}{3}, \mathbf{1}, \overline{\mathbf{3}})$
$\hat{u}^3$	✓	-	$(-\frac{2}{3}, \mathbf{1}, \overline{\mathbf{3}})$
$\hat{l}^3$	✓	-	$(-\frac{1}{2}, \mathbf{2}, \mathbf{1})$
$\hat{e}^3$	✓	-	$(1, \mathbf{1}, \mathbf{1})$
$\hat{H}_d$	-	✓	$(-\frac{1}{2}, \mathbf{2}, \mathbf{1})$
$\hat{H}_u$	-	✓	$(\frac{1}{2}, \mathbf{2}, \mathbf{1})$
$\hat{F}_-$	-	✓	$(-1, \mathbf{1}, \mathbf{1})$
$\hat{F}_+$	-	✓	$(1, \mathbf{1}, \mathbf{1})$
$\hat{B}_V$	-	✓	$(0, \mathbf{1}, \mathbf{1})$
$\hat{W}_V$	-	✓	$(0, \mathbf{3}, \mathbf{1})$
$\hat{G}_V$	-	✓	$(0, \mathbf{1}, \mathbf{8})$

Table 2.5: The matter content of model 2.

2.7.2 Running parameters

It is particularly interesting to understand and compare the behaviour of the various running parameters of these theories compared to the more usual four dimensional MSSM. The behaviour of the various parameters as a function of renormalisation scale for model 1 is pictured in figure 2.15. Of particular note is that unification happens much earlier if the size of the extra dimension is large [118] , than the usual four dimensional case. One also finds that the top Yukawa reduces rather significantly and becomes of similar order to the other Yukawa couplings near the unification scale. In addition one finds that even for initially vanishing A-terms the A_t term may become multi-TeV in value at the electoweak scale, which is encouraging from the perspective of obtaining the observed 125 GeV Higgs mass. It is also the case (bottom left) that the gluino mass can become much hearvier than the other gauginos allowing for the theory to still have a light bino and wino whilst allowing for a gluino above current exclusions.

The first model may be compared with model 2 similarly presented in figure 2.16 and in table 2.5. In these figures it is notable that that gauge couplings quite nearly unify but the gauge couplings rise rather than fall, after the KK modes start to take effect in the RGEs. The Y_t still decreases in value, although now rather interestingly the A_t becomes so quickly negative that it can quickly overcompensate the effect of the gluino soft mass, and for very large radius, the A_t running may even return on itself. Again the wino and bino soft terms can be much smaller than that of the gluino, even starting from the same initial value.

2.7.3 Supersymmetry breaking in benchmark models

So far our exploration has been reasonably agnostic about how supersymmetry is broken, since the main feature of the models presented in the previous sections are their RGEs. In what follows we will simply refer to sets of RGEs we used, as models.

There are however a number of ways that have been proposed for the parametrisation of supersymmetry breaking in a five dimensional scenario. In this section we wish to identify these scenarios and look at their patterns of supersymmetry breaking which define their possible high scale spectra.

Our first benchmark scenario is the simple CMSSM spectrum, however since easier generation of A-terms during running is a key feature of five dimensional running, we will always take $A_i = 0$ case for which the difference between five and four dimensional theories is the most visible. This implies a very simple type of spectrum with just two free parameters $M_{\frac{1}{2}}$ and m_0:

$$M_i = M_{\frac{1}{2}} \quad , \quad m^2_{\tilde{f}} = m^2_0 \quad , \quad A_i = 0, \tag{2.127}$$

defined at the unification scale.

The second benchmark model is gauge mediation (GMSB). in this type of models there is an additional characteristic scale at which SUSY is broken, which for brevity we will labelled M. For the five dimensional RGEs to have an impact on the spectrum and

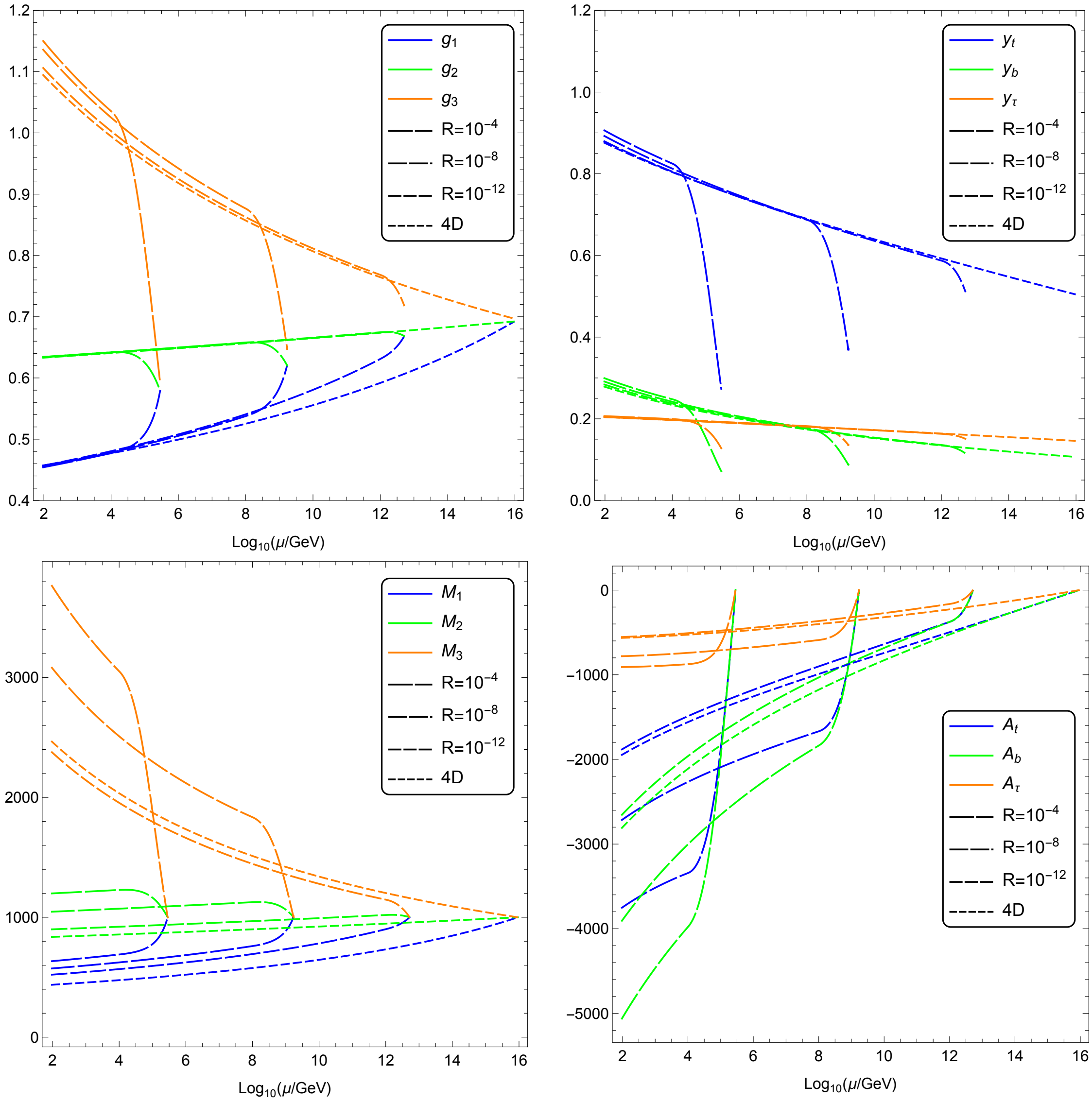

Figure 2.15: *Model 1 running of gauge coupling constants $g_i(\mu)$ (top left panel), 3rd generation Yukawa couplings (top right panel), trilinear soft terms (bottom right panel) and gaugino soft terms (bottom left panel) with compactification scales $1/R \sim 10^4\,\text{GeV}$, $10^8\,\text{GeV}$ & $10^{12}\,\text{GeV}$, as a function of Log$_{10}(\mu/\text{GeV})$. In this example all soft terms were set to $M_{SUSY} = 1\,\text{TeV}$* at the unification scale (defined by $g_1 = g_2$), except the trilinear soft terms (A_i) which were set to 0.

to not simply be an effective four dimensional theory with a low SUSY breaking scale we wish that M is at least $O(1/R)$ and possibly nearer $M_{\text{unification}}$. The soft terms in five

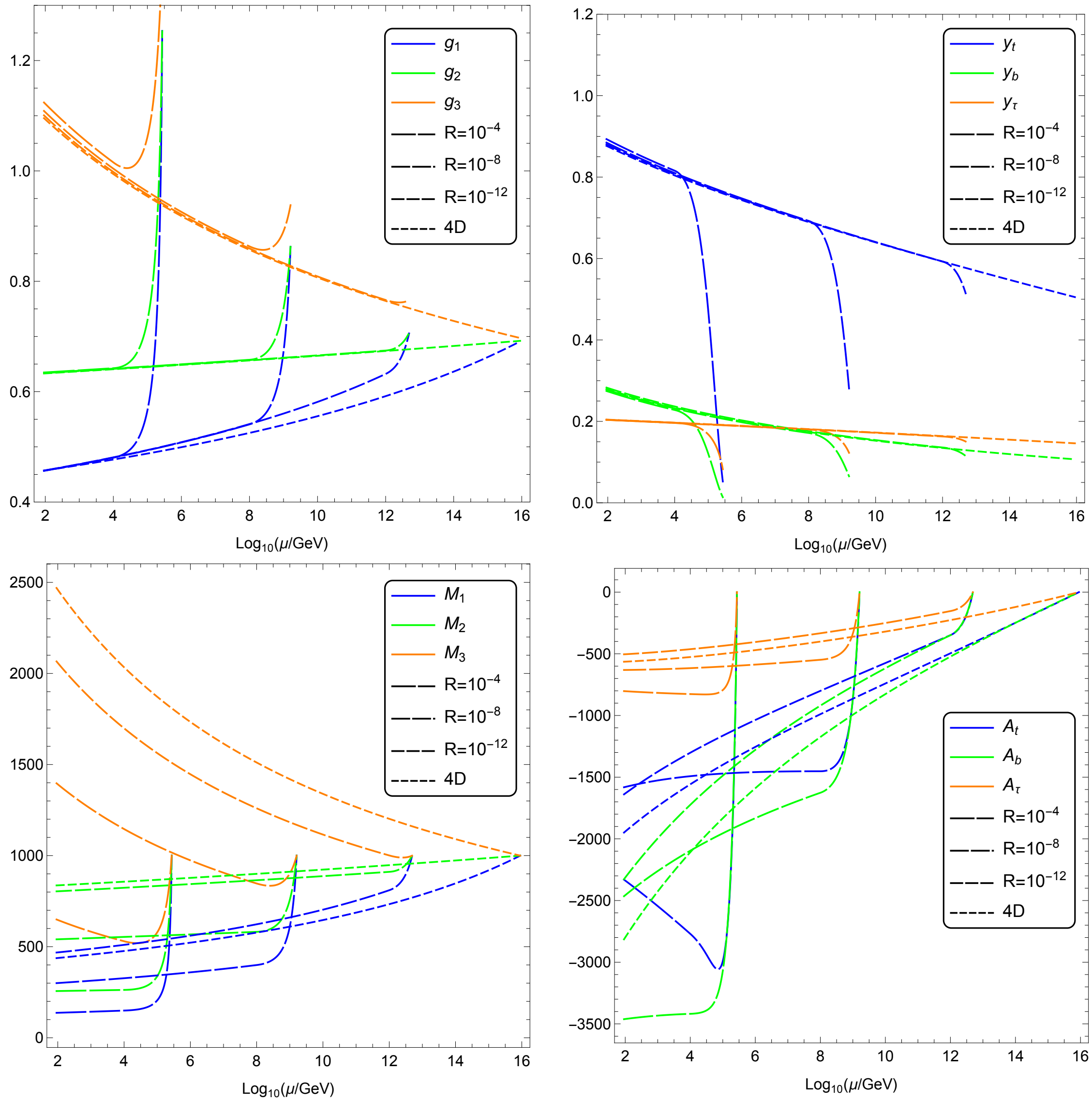

Figure 2.16: *Model 2 running of gauge coupling constants* $g_i(\mu)$ *(top left panel), 3rd generation Yukawa couplings (top right panel), trilinear soft terms (bottom right panel) and gaugino soft terms (bottom left panel) with compactification scales* $1/R \sim 10^4\,\mathrm{GeV}$, $10^8\,\mathrm{GeV}$ *&* $10^{12}\,\mathrm{GeV}$, *as a function of Log*$_{10}(\mu/\mathrm{GeV})$. *In this example all soft terms were set to* $M_{SUSY} = 1\,\mathrm{TeV}$ at the unification scale (defined by $g_1 = g_2$), except the trilinear soft terms (A_i) which were set to 0.

dimensional GMSB, at the breaking scale, are then given by

$$M_r = \left(\frac{\alpha_r}{4\pi}\right)\left(\frac{F}{M}\right) \quad , \quad m_{\tilde{f}}^2 \simeq 2\sum_r C_{\tilde{f}}^r \left(\frac{\alpha_r}{4\pi}\right)^2 \left(\frac{F}{M}\right)^2 \left(\frac{1}{MR}\right)^2 \quad , \quad A_i = 0, \tag{2.128}$$

where F and M are the free parameters we will scan over. This analysis is the first implementation of five dimensional GMSB soft masses [119, 120, 112, 113, 121], with five dimensional RGEs [108, 107]. In both model 1 and 2 we will take the supersymmetry breaking to be on the opposite brane to the matter, and both brane and bulk matter are essentially suppressed by the effect of the extra dimension, as in the above equation.

Our final benchmark scenario comes from an attempt to create a natural SUSY breaking scenario using new features possible in a five dimensional theory. The renormalisation group equations of model 1 may be used to explore a scenario as pictured in figure 2.17. In this model the 3rd generation is located on one brane and the 1st and 2nd generation on another, along with the supersymmetry breaking sector. The effects of supersymmetry breaking are mediated by gauge forces [122] (but one can also easily consider gravity mediation too in this context) and the result is that the 1st and 2nd generation and also the gauginos will receive normal (4D) GMSB soft mass contributions but the 3rd generation will be heavily suppressed [121, 113, 107, 108]. The soft mass matrix for squarks and sleptons takes the form

$$m_{\tilde{f}}^2(M_{\cancel{SUSY}}) \sim \Lambda^2 \begin{pmatrix} 1 & 0 & 0 \\ 0 & 1 & 0 \\ 0 & 0 & 0 \end{pmatrix} + ... \tag{2.129}$$

leading to an interesting natural SUSY spectrum of lighter 3rd generation squarks. This scenario suggests that natural SUSY softer terms are imprinted due to the 'geometry' of the theory. We will consider such a natural spectrum in context of minimal gauge mediation, the resulting soft terms are similar to those in(2.128), however now only third generation sfermions are suppressed by $1/(MR)^2$. In the text we will refer to this as an nMGM spectrum. Needless to say, a similar model may be constructed using brane to brane gravity mediation. It would also be interesting to discuss models with H_u and H_d localised alongside the 3rd families, however it would require a much more serious modification of the RGEs of our Model 1 and 2, consequently we postpone that discussion to future work.

2.7.4 Electroweak symmetry breaking and naturalness

One important feature of a model is whether its parameter space can accommodate electroweak symmetry breaking. Figure 2.18 shows regions in the parameter space of our models where the breaking does not occur or which violate direct detection bounds summarised in table 2.6 [63]. Exclusions corresponding to varying size of the extra dimension (including the $4D$ case) are plotted together. For standard CMSSM and MGM boundary conditions Model 1 predicts rather standard spectra of sparticles quite similar to the $4D$ case. However Model 2 due to much lower gaugino masses compared to the A-terms allows us to obtain very light stops and maximal mixing even despite A-terms vanishing at the unification scale. In fact for large $R = 10^{-4}$ the peculiar shape of the CMSSM excluded region in model 2 comes from obtaining too light stops that would have already been observed.

The MGM excluded region comes from the interplay between large scalar masses we obtain at the scale M when $M = 1/R$, and when they are generated during 5D modified

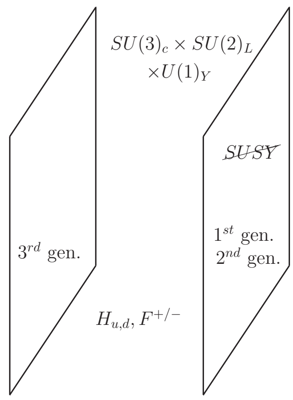

Figure 2.17: *Pictorial to represent the location of matter in the five dimensional model resulting in a natural SUSY breaking scenario with GMSB (nMGM spectrum) and model 1 RGEs.*

particle	mass bound in GeV
$\tilde{g}$	1200
$\tilde{q}_{1,2}$	800
$\tilde{t}$	700
$\tilde{b}$	650
$\tilde{\chi}_1^{\pm}$	92
$\tilde{\chi}_1^{0}$	46

Table 2.6: *Experimental exclusion limits used*

running between $1/R$ and $M >> 1/R$. The minimal stop mass is obtained between these two situations and results in excluded part on the left hand side of middle row in Figure 2.18 where the small stop soft mass fails to push m_{H_u} to negative values and break electroweak symmetry.

This is also visible in nMGM plot on the bottom row of Figure 2.18. However here the problem is more severe since m_{H_u} is not suppressed by $1/(MR)$ at the SUSY breaking scale, and a much bigger part of the parameter space is excluded. For nMGM spectrum this problem appears also for very small $1/(MR)$, because in this part of the parameter space the difference between Higgs and stop soft masses is the largest. These two effects lead to appearance of a window of allowed parameter space which is very interesting, since it is in that window, that we obtain the highest Higgs mass.

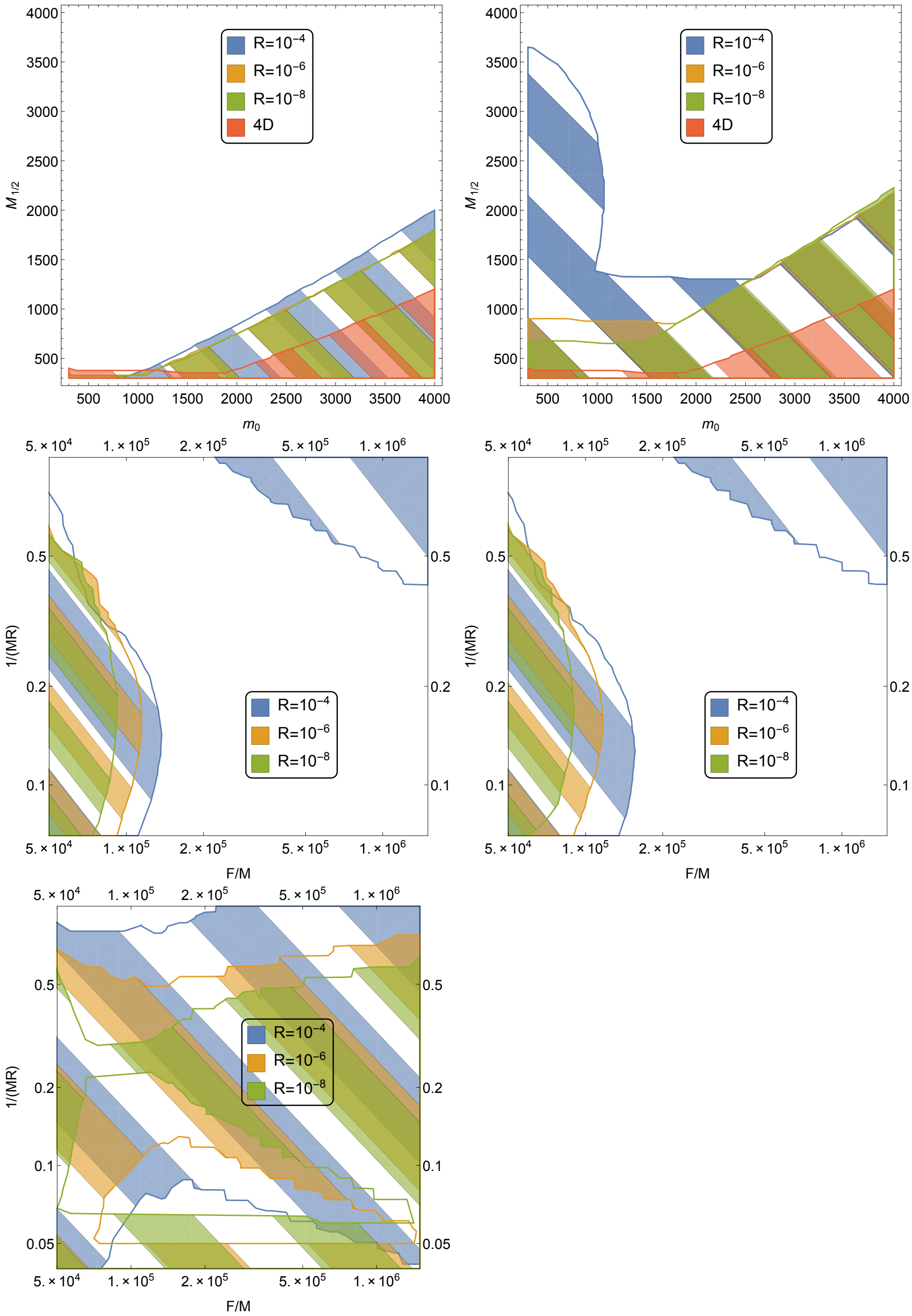

Figure 2.18: *Striped regions of the CMSSM (top row) MGM (middle row) and nMGM (bottom row) parameter space cannot accommodate electroweak symmetry breaking or are already excluded by direct searches. Left hand side plot shows results for model 1 and right hand side for model 2. Both show different sizes of the extra dimension and CMSSM shows the 4D case as well.*

2.7.5 Naturalness in benchmark scenarios

In MSSM-like theories, at a finite loop order, electroweak symmetry breaking is radiatively induced. The up-Higgs soft mass is driven to negative values, leading to

$$-\frac{1}{2}M_z^2 = m_{H_u}^2(\Lambda) + \delta m_{H_u}^2 + |\mu|^2 + \mathcal{O}\left(\tan\beta^{-2}\right) \tag{2.130}$$

At leading order, the running of this soft mass in four dimensions follows

$$\delta m_{H_u}^2 \sim -\frac{3}{8\pi^2} y_t^2 (m_{Q_3}^2 + m_{U_3}^2 + A_t^2) \mathrm{Log}\left(\frac{M_{SUSY}}{M_S}\right) \tag{2.131}$$

In five dimensional models the RGEs are rather different due to the power law contributions and one finds

$$\delta m_{H_u}^2 \sim -\frac{3}{8\pi^2} y_t^2 (m_{Q_3}^2 + m_{U_3}^2 + A_t^2) \left[\mathrm{Log}\left(\frac{1}{RM_S}\right) + M_{SUSY}R\right] \tag{2.132}$$

One might have expected a significant contribution to fine tuning from the power law contribution. However four and five dimensional theories actually have similar fine tuning as the much faster power law contribution can dominate the running for only a very small range of scales if the spectra we are comparing are similar. And so the final amount of fine-tuning for a given scenario depends mostly on the resulting spectrum rather than on the amount of power law running. This is quantified in figure 2.19, where in numerical calculations we use a standard fine-tuning measure with respect to parameter a defined in (2.69).Figure 2.19 shows resulting fine-tuning as a function of Higgs mass for different sizes of the extra dimension as well as the result one would obtain from $4D$ running. the top row shows results obtained assuming CMSSM-like soft terms (with $A_i = 0$), the middle row shows gauge mediated boundary conditions and the bottom plot shows the nMGM ones.

The results in left panel show model 1 which gives a rather standard prediction despite power law contribution to running. However model 2 shown on the right hand side allows us to reduce fine-tuning very significantly. The reason are the gaugino masses that decrease during 5D part of the running (as shown in Figure 2.16). This protects the soft terms from the usual increase due to the heavy gluino. Since the A-terms do not grow proportionally to scalar masses we can easily achieve maximal mixing scenario for the light stops as shown in Figure 2.20. We can see that its their direct detection bound is precisely what gives us the lower bound on fine-tuning we can see in model 2 with $R = 10^{-4}$.

The bottom plot shows nMGM result which turns out quite similar to MGM and CMSSM model 1 results. The reason for this is that in model 1 the least fine tuned results are those for which $M >> 1/R$. Thus the scalar masses are initially very small and have to be generated with modified running. Consequently the 3rd family part of the spectra are very similar. The correction introduced by nMGM relies only on larger subleading corrections to the Higgs mass from first two families and other Higgs sector scalars. Unfortunately fine-tuning price of these corrections is larger than their contribution to the Higgs mass and the results are slightly more fine tuned than those from standard MGM or CMSSM soft terms.

CMSSM							
Model:	1			2			$4D$
R:	10^{-4}	10^{-6}	10^{-8}	10^{-4}	10^{-6}	10^{-8}	$4D$
$\tilde{q}_{1,2}$	3.14	3.45	3.84	1.76	2.40	3.23	4.58
$\tilde{t}_1$	2.44	2.82	3.1	0.75	1.1	2.2	3.59
$\tilde{\chi}_1^0$	0.85	1.02	1.23	0.21	0.38	0.81	1.26
$\tilde{m}_A$	1.82	2.20	2.50	2.1	2.3	2.4	2.77
$\Delta/10^3$	3.5	4.0	4.6	0.9	1.5	3	5.3

MGM							
Model:	1			2			$4D$
R:	10^{-4}	10^{-6}	10^{-8}	10^{-4}	10^{-6}	10^{-8}	$4D$
$\tilde{q}_{1,2}$	3.12	3.45	3.84	1.76	2.40	3.23	4.59
$\tilde{t}_1$	2.57	2.77	3.18	0.81	1.47	2.2	3.92
$\tilde{\chi}_1^0$	0.80	0.91	1.08	0.17	0.37	0.81	1.32
$\tilde{m}_A$	1.82	2.20	2.44	1.43	1.8	1.90	2.31
$\Delta/10^3$	3.6	4.0	4.6	0.95	1.85	3.19	6.01

nMGM				
Model:	1			$4D$
R:	10^{-4}	10^{-6}	10^{-8}	$4D$
$\tilde{q}_{1,2}$	3.81	4.41	5.69	6.41
$\tilde{t}_1$	2.33	2.64	3.15	3.69
$\tilde{\chi}_1^0$	0.79	0.93	1.01	1.05
$\tilde{m}_A$	1.92	2.36	2.92	3.31
$\Delta/10^3$	3.7	4.2	5.2	6.0

Table 2.7: Masses of superpartners (in TeV) for spectra which minimize fine-tuning for $m_h = 125\,\mathrm{GeV}$

A large qualitative difference between MGM and nMGM becomes visible for Higgs masses slightly higher than the observed one. This comes from the part of parameter space which predicts successful electroweak symmetry breaking in nMGM. As explained in the beginning of this section, the problem is a result of the exclusion appearing in nMGM for very small $1/MR$. Where we cannot break electroweak symmetry because radiative correction to the unsuppressed soft Higgs mass coming from highly suppressed stop mass is to small, and the former never runs negative. This becomes visible for higher Higgs masses because very small $1/MR$ is the part of the parameter space where we obtain highest Higgs masses. Another very important feature of 5D models is the possibility to bring superpartner masses within the LHC reach for points predicting minimal fine-tuning. This is illustrated in Table 2.7 which shows spectra corresponding to lowest obtained fine tuning for $m_h = 125\,\mathrm{GeV}$.

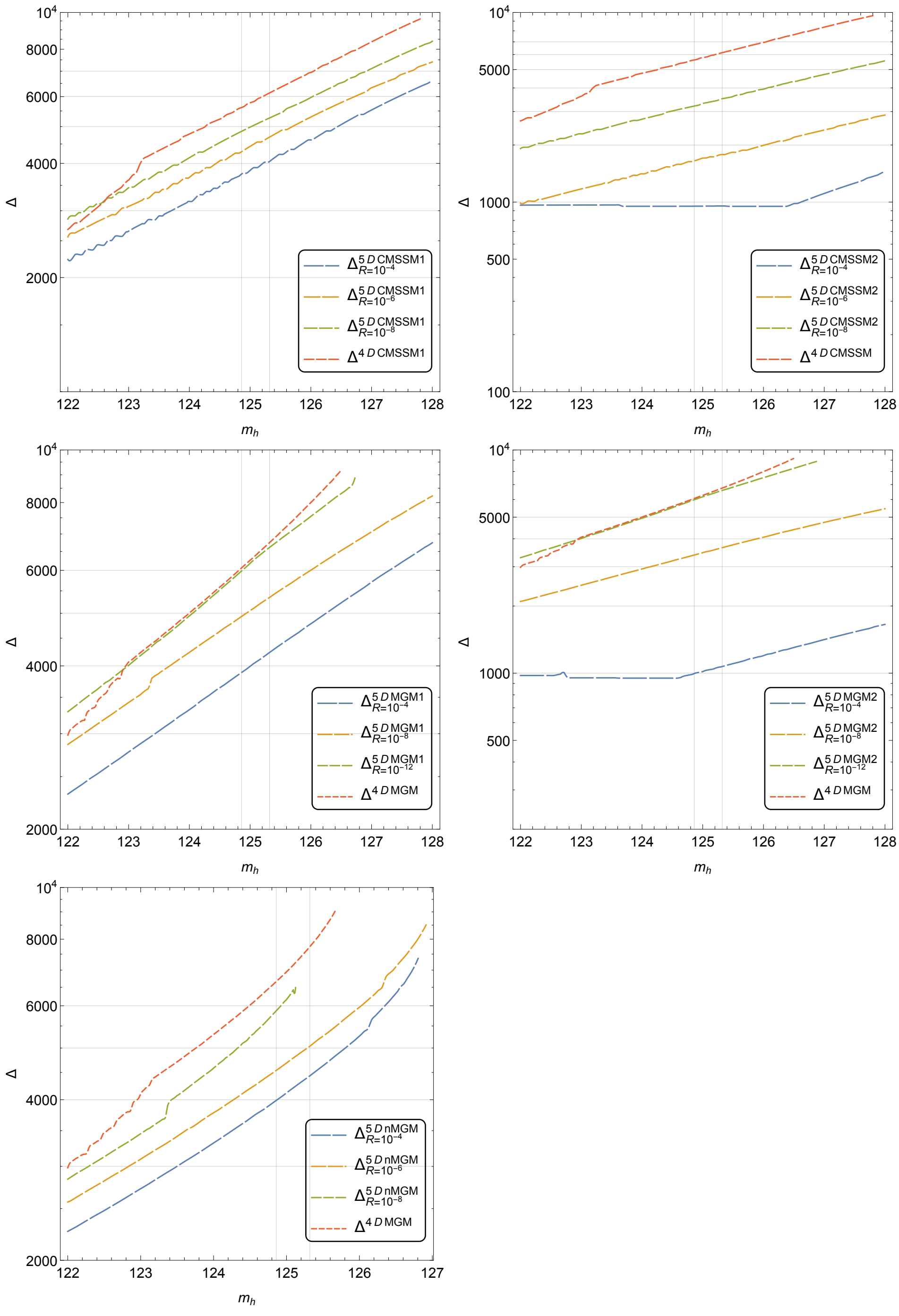

Figure 2.19: *Fine-tuning as a function of Higgs mass for different sizes of the extra dimension for models 1 (left hand side) and 2 (right hand side) with CMSSM (top row), MGM (middle row) and nMGM (bottom row) spectra as well as the 4D results.*

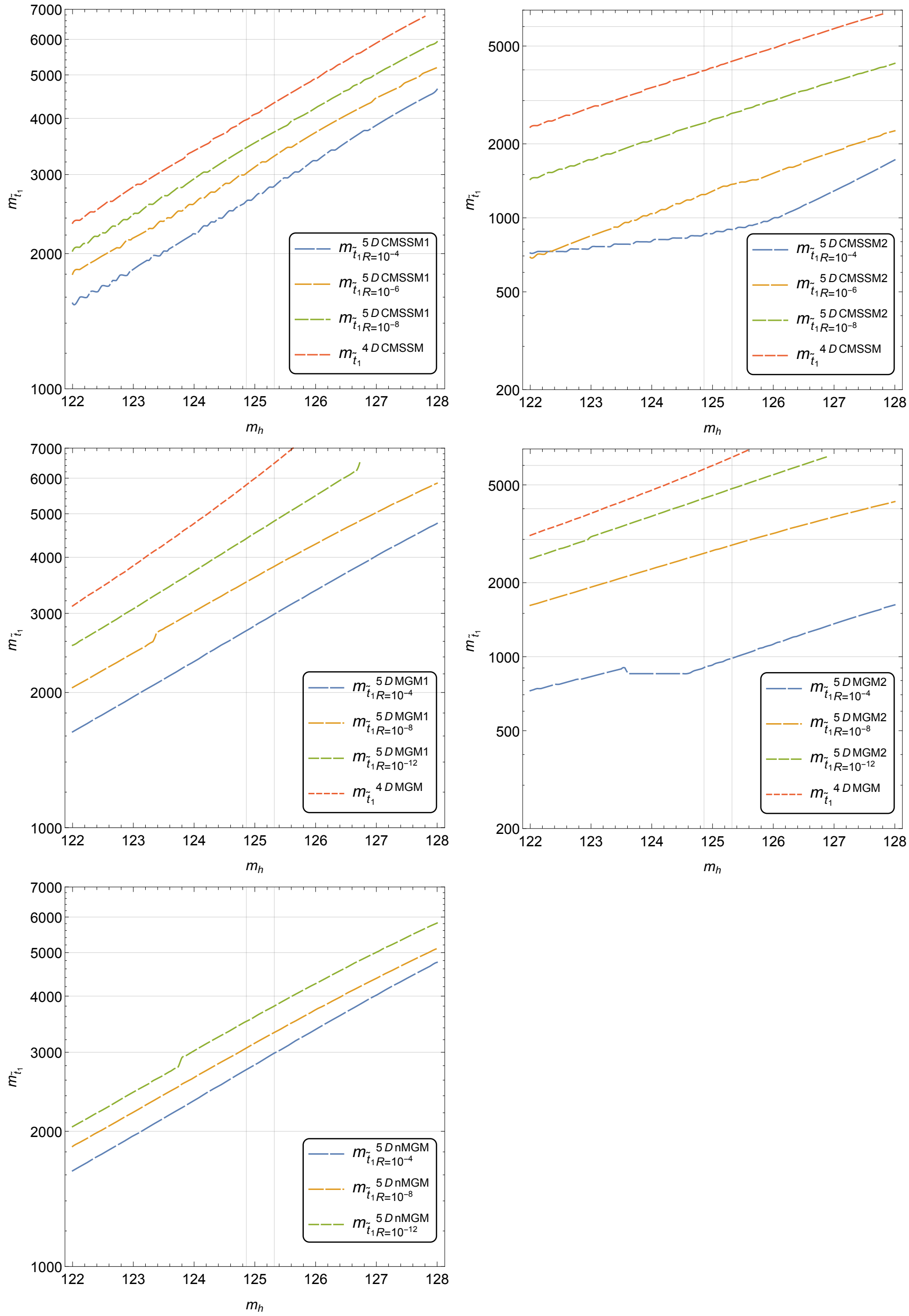

Figure 2.20: *minimal possible lighter stop mass as a function of Higgs mass for different sizes of the extra dimension for models 1 (left hand side) and 2 (right hand side) with CMSSM (top row), MGM (middle row) and nMGM (bottom row) spectra as well as the 4D result.*

2.7.6 Summary

In this section we explored the implementation of the five dimensional renormalisation group equations in a number of supersymmetric extensions of the MSSM, into a full C++ spectrum generator, along with self energy corrections for the Higgs mass.

Our key result is showing that modified five dimensional RGEs can result in spectra very different from the usual $4D$ case. This is because in 5D the heavy gluino does not necessarily dominate running of other soft terms during power law running, as in our model 2. Thus we can easily obtain maximal stop mixing and much less fine-tuned spectra, even with standard sets of soft terms at the SUSY breaking scale.

This is also very interesting because in 5D models the least fine tuned spectra with correct Higgs mass can easily predict soft superpartner masses within LHC reach, even for standard patterns of soft terms. Curiously, this means the most interesting parts of the parameter space can be probed during next run of the LHC, which is not usually the case in 4D models.

We explored models where the 1st and 2nd generation are in the bulk and a model in which the 1st and 2nd generation is on the same brane as the supersymmetry breaking sector and the 3rd generation is located on an opposite brane, resulting in a spectrum of stops lighter than other squarks. Obtaining lighter stop soft terms at the SUSY breaking scale did not result in a more natural spectrum. The reason is the non negligible fine-tuning price of heavier first two generations and heavier Higgs sector which give only a subleading correction to the light Higgs mass.

The final advantage is a low scale of unification of gauge couplings and a low supersymmetry breaking scale. And also much better unification of Yukawa couplings (especially in model 2) which gives hope for a very interesting five dimensional UV completion of such models.

Chapter 3

Vacuum stability

3.1 Introduction

The discovery of the 125 GeV Higgs boson, and absence of experimental signature of a new physical state in the LHC experiments makes it very important to search for possible windows towards new phenomena within the SM itself. One of such possible windows is the investigation of the structure of the effective potential in the SM which has already been the subject of considerable activity [123, 124, 125, 126, 127, 128, 129, 18, 130].

The study of the renormalisation group improved SM effective potential reveals an interesting structure at field strenghts higher than approximately 10^{11} GeV. These new features depend critically on the precise value of the Higgs mass and the top quark Yukawa coupling. In particular, one finds that for the central value of the top mass and for the central value of the measured Higgs mass the physical electroweak symmetry breaking minimum is not the global minimum of the potential. Thus the electroweak minimum is unstable with respect to the tunneling from the physical EW minimum to the deeper minimum located at very large Higgs field strength values. The computed lifetime of the metastable SM vacuum turns out larger than the presently estimated age of the Universe, however the instability border in the SM parameter space looks uncomfortably close. This suggests that the result is rather sensitive to various types of modifications that can from various BSM extensions.

We will begin by reviewing the well known standard model stability calculation, and subsequently move towards finer issues connected with this computation such as the issue of gauge invariance and gravitational corrections to the lifetime estimation. Finally we will discuss the impact of new physics on the vacuum stability.

3.2 Lifetime of the Standard Model vacuum

The starting point in this discussion is the effective potential of the SM which we discussed in Section 1.3.2. As noted there, the potential of SM has another very deep minimum separated from the electroweak one by a potential barrier shown in Figure 3.1. The electroweak vacuum is unstable due to possible tunnelling through the barrier. In

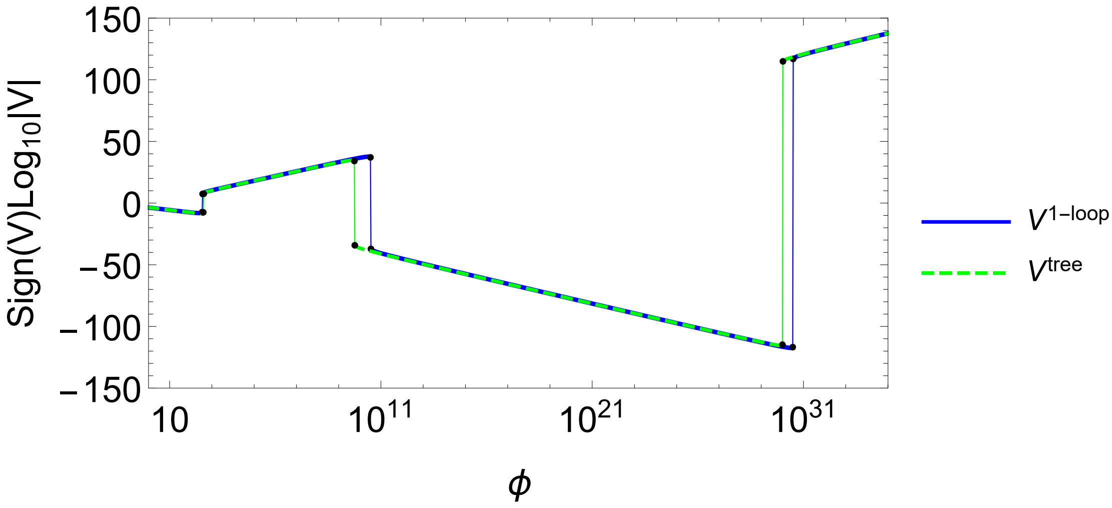

Figure 3.1: *RGE improved Standard Model potential at the tree level and including one loop correction*

this situation the superplanckian global minimum is called the *true vacuum* while the electroweak one is called *false vacuum.* In this section we will review the semi-classical method of computation of the vacuum's lifetime, describing the tunnelling as nucleation of true vacuum bubbles within the false vacuum [131, 132].

Based on analogy with usual quantum mechanics, the method is based on finding a so called bounce solution describing the nucleating bubble. The bounce is a solution to the euclidean version of the equation of motion which interpolates between the false and true vacua. As in case of quantum mechanics the nucleation probability is exponentially suppressed with the action of the bounce. Thus finding a bounce with minimal action is equivalent to obtaining the usual variational solution needed in all tunnelling problems.

It was shown in [133] that the solution of lowest action is spherically symmetric. In the euclidean metric an $O(4)$ symmetric solution depends only on $s = \sqrt{\vec{x}^2 + x_4^2}$. This means solving the scalars equation of motion of the form

$$\ddot{\phi} + \frac{3}{s}\dot{\phi} = \frac{\partial V(\phi)}{\partial \phi}, \tag{3.1}$$

with a dot denoting a derivative with respect to s.

$$\begin{aligned} \dot{\phi}(0) &= 0 \\ \phi(\infty) &= \phi_{fv} \end{aligned} \tag{3.2}$$

The first boundary condition is necessary for the solution to be non-singular at $s = 0$. The second one means our solution corresponds to a bubble forming within the homogeneous configuration of metastable vacuum, without this the solutions would not match at infinity the action would diverge. The euclidean action of the bounce is simply given by

$$S_E = \int d^4x \left\{ \frac{1}{2}\sum_{\alpha=1}^{4}\left(\frac{\partial\phi(\mathbf{x})}{\partial x^\alpha}\right)^2 + V(\phi(\mathbf{x}))\right\} = 2\pi^2 \int dss^3 \left(\frac{1}{2}\dot{\phi}^2(s) + V(\phi(s))\right), \quad (3.3)$$

which allows us to calculate decay probability

$$dp = dtd^3x \frac{S_E^2}{4\pi^2} \left| \frac{det'[-\partial^2 + V''(\phi)]}{det[-\partial^2 + V''(\phi_{\min})]} \right|^{-1/2} e^{-S_E}. \quad (3.4)$$

To obtain the expected lifetime we simply integrate that probability over the volume of the universe. It is a valid assumption to approximate this size as that of a cube of size $T_U = 10^{10}$yr. We define the expected lifetime τ as time at which the integrated decay probability is equal to 1. For now we can also approximate the determinant and normalization prefactor by another dimensionfull quantity encountered in our problem, namely the width of the barrier $\phi_0 = \phi(0)$. The error introduced that way is small compared to uncertainty in determination of action, because lifetime depends only on fourth power of ϕ_0 while its dependence on action is exponential. Our final approximation of the vacuum's lifetime reads

$$\frac{\tau}{T_U} = \frac{1}{\phi_0^4 T_U^4} e^{S_E}. \quad (3.5)$$

In the following subsections we will present the known analytical approximations of the bounce and compare them results with our precise numerical solution.

3.2.1 Analytical approximation

Possibly the most simplified estimate for the lifetime of electroweak vacuum reads

$$\frac{\tau}{T_U} \sim \frac{1}{\Lambda^4 T_U^4} e^{\frac{8\pi^2}{3|\lambda(\Lambda)|}}, \quad (3.6)$$

where $\lambda(\mu)$ is the running Higgs quartic coupling. The scale Λ is chosen to minimize the negative value of $\lambda(\Lambda)$ so that our result is actually a lower bound on the lifetime. The rationale behind the above formula is as follows. The classical Lagrangian

$$\mathcal{L} = \frac{1}{2}(\partial\phi)^2 - \frac{\lambda_c}{4}\phi^4, \quad (3.7)$$

where this time λ_c is just a negative constant, admits a bounce solution describing the decay of $\phi = 0$ configuration, whose action is $S = \frac{8\pi^2}{3}\frac{1}{\lambda_c}$ [134]. Hence, after reinterpretation of the Lagrangian (3.7) as a quantum Lagrangian, our formula (3.5) describes space-density of the tunneling rate. Due to classical scale invariance of the Lagrangian, one has no dimensionfull quantity to fill in above except the renormalization scale Λ at which we calculate the quartic coupling λ.

Thus using this approximation and neglecting the explicit mass term in the standard model Lagrangian the whole calculation requires only finding the minimum of the Higgs quartic coupling λ. The key here is very precise determination of the quartic since the value of the minimum is often very close to zero and even a small correction used in (3.6) can change the result dramatically. We use NNLO order initial conditions for the running couplings calculated at the top mass scale $\mu = m_t$ from top and Higgs physical masses [123]

$$
\begin{aligned}
g_1 &= \sqrt{\frac{5}{3}}\left(0.3583 + 0.00011 \times (m_t - 173.34)\right), \\
g_2 &= 0.64779 + 0.00004 \times (m_t - 173.34)\,, \\
g_3 &= 1.1666 - 0.00046 \times (m_t - 173.34), \\
y_t &= 0.93690 + 0.00556 \times (m_t - 173.34), \\
m &= 131.55 + 0.94 \times (m_h - 125.15) + 0.17 \times (m_t - 173.34), \\
\lambda &= 0.12604 + 0.00206 \times (m_h - 125.15) - 0.00004 \times (m_t - 173.34).
\end{aligned} \tag{3.8}
$$

We calculate the evolution using three loop renormalisation group equations from [123]. Figure 3.2 shows the SM phase diagram calculated using (3.6), using only running Higgs

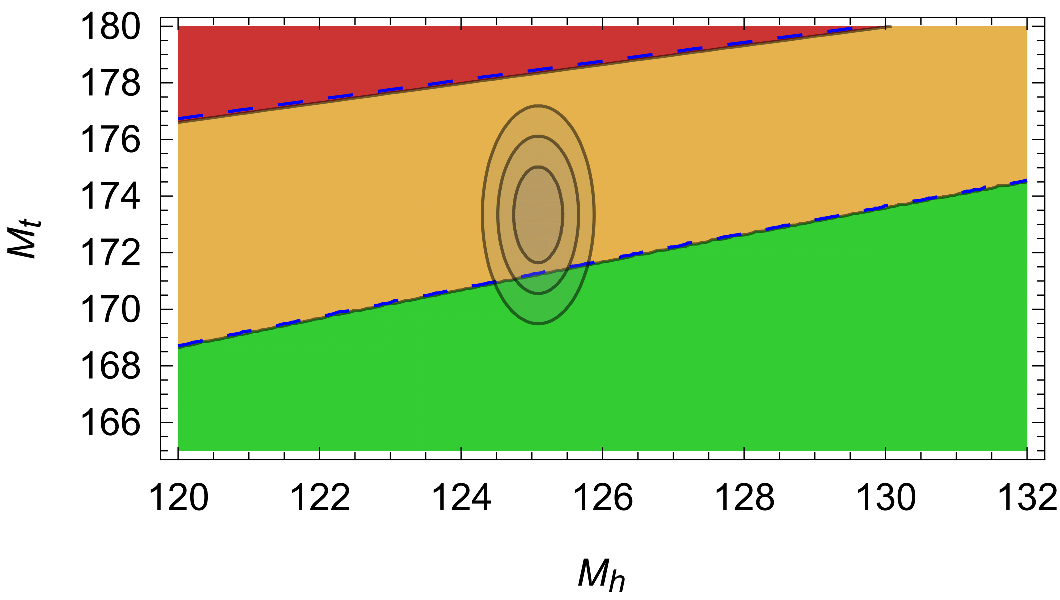

Figure 3.2: *Phase diagram of the electroweak vacuum calculated using only Higgs quartic coupling and the full one-loop potential (dashed lines). Green region corresponds to absolute stability, the yellow region to metastability while the red region is unstable.*

Quartic λ and the effective Higgs potential λ_{eff} described in Section 1.3.2. We also plot the experimental ellipsis showing the observed top and Higgs masses at one two and three sigma significance. We can see that the SM vacuum is most likely metastable (yellow region) which means the other minimum exists within the potential but the expected lifetime of the electroweak vacuum is longer than the observed lifetime of the Universe.

This result means the standard model does not need to be modified due to vacuum instability, the current situation is phenomenologically acceptable. However the uncomfortably small distance to the instability border makes it very important to check the impact of any extension of SM on the vacuum stability. We will discuss such examples in the following sections.

We can also see that the correction coming from using a full one loop potential instead of the tree level approximation, is small and makes the potential slightly more stable.

3.2.2 Gauge independence

Our next step is verifying the gauge independence of the above results. Even though we know an observable such as the lifetime has to be gauge independent, verifying this feature explicitly can lead to better understanding of the approximations we have to take during the calculation.

We will now use gauge invariance to further justify approximations from the previous subsection. After renormalisation the effective Lagrangian would be rather

$$\mathcal{L} = \frac{1}{2} Z(\mu) \left(\partial\phi\right)^2 - \frac{\lambda(\mu)}{4} Z(\mu)^2 \phi^4 \ . \tag{3.9}$$

This form is correct only at the lowest level of perturbative calculation, when logarithmic loop correnctions are not yet included. Simply using the coefficient before ϕ^4 as our effective coupling would result in a lifetime different than in the previous subsection, namely

$$\frac{\tau}{T_U} \sim \frac{1}{\Lambda^4 T_U^4} e^{\frac{8\pi^2}{3} \frac{1}{|Z^2(\Lambda)\lambda(\Lambda)|}} \ , \tag{3.10}$$

where

$$Z(\mu)^{\frac{1}{2}} = e^{-\int_{M_t}^{\mu} \gamma(\tilde{\mu})\, \mathrm{d}\log(\tilde{\mu})} \tag{3.11}$$

Going to higher loop orders introduces more complicated dependence on ϕ. Now we notice that, for one, the full coefficients in front of both the kinetic and quartic terms are dimensionless and thus, absent any dimensionfull parameters in the theory, they may depend on μ only via ϕ/μ. Also the running of Z and $Z^2\lambda$ captures these coefficients' dependence on μ, so it cancels between running couplings and explicit dependence of loop corrections. In conclusion, it is justified to replace μ from (3.9) with the field, $\mu \to \phi$, and claim that the resulting μ-independent function of ϕ well approximates the full effective quantum Lagrangian. This leaves us with

$$\mathcal{L} = \frac{1}{2} \left(\partial \left(Z^{\frac{1}{2}}(\phi)\phi\right)\right)^2 - \frac{\lambda(\phi)}{4} Z^2(\phi)\phi^4 \ . \tag{3.12}$$

This brings us to our point. $|Z^2\lambda|$ in (3.10) should be replaced by $|\lambda|$ alone bringing us back to (3.6). From the point of view of the Lagrangian (3.12), it makes sense to redefine the field variable by $\tilde{\phi} = Z^{\frac{1}{2}}(\phi)\phi$, thus eliminating $Z(\mu)$. There is a way to show that this is in fact the correct approach. Namely, the anomalous dimension is gauge-dependent,

$$\gamma = \frac{1}{16\pi^2} \left(\frac{3}{20}\zeta g_1^2 + \frac{3}{4}\zeta g_2^2 + \frac{9}{4} g_2^2 + \frac{9}{20} g_1^2 - 3y_t^2 - 3y_b^2 - y_\tau^2 \right) \tag{3.13}$$

,where ζ is the gauge fixing parameter in the Fermi gauge [135]. This makes (3.10) very sensitive to the values of gauge fixing parameters, however, absence of Z trivially makes it gauge-independent again. Simple as it sounds, throwing away Z's may seem controversial, because it means treating μ, substituted by ϕ, as a spacetime dependent configuration, and thus hitting $Z(\phi(x))$ with ∂_μ in (3.12).

In our present case of the Standard Model, difference between (3.6) and (3.10) is significant. $Z^2(\mu)$ changes from 1 at the scale of the top quark mass, m_{top}, to about 0.8 closer to the Planck scale. This translates to the exponent in (3.10) increasing from 1800 to roughly 2100. Correspondingly the lifetime of the vacuum computed via (3.10) is only around 10^{529} as compared to 10^{676} when using (3.6). Figure 3.3 illustrates gauge dependence of the action, for the Fermi gauges, with $\xi = \xi_W(m_{top}) = \xi_B(m_{top})$ [135]. The

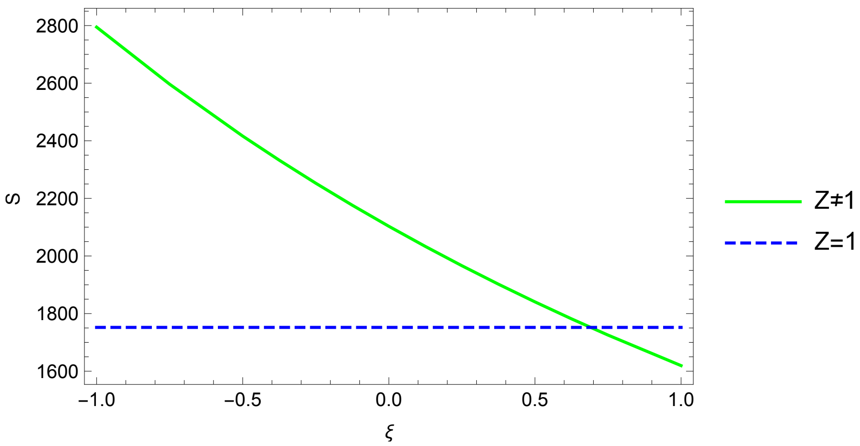

Figure 3.3: *Solid curve: gauge dependence of the bounce action obtained neglecting Z factor in front of the kinetic term. Dashed line: the bounce action after the redefinition $\tilde{\phi} = Z^{\frac{1}{2}}(\phi)\phi$. ξ is the gauge fixing parameter.*

most commonly used Landau gauge belongs to this this class, and corresponds to the choice of $\xi = 0$.

The crucial result here is that using (3.10) with field renormalisation even in Landau gauge results in an action which is significantly bigger than the correct result with $Z = 1$. Thus these results would predict a vacuum far more stable than the correct treatment of (3.6).

3.2.3 Numerical calculation

In this section we will discuss the validity of the simple approximation obtained in the previous subsections. The only way to make sure that our analytical approximation is accurate is through numerically finding the full bounce solution.

As noted already in [131], our EOM (3.1) can be thought of as an equation of motion of a praticle in potential $-V$ with an uncommon friction term $3/s$ and s playng the role of time. Very schematically our boundary conditions (3.2) correspond to our particle starting with zero speed on the slope of the higher maximum (true vacuum in terms of $+V$). To satisfy the second boundary condition we have to find a starting point such that at infinite s the particle comes to rest at the lower maximum (false vacuum). This is sketched on Figure 3.4.

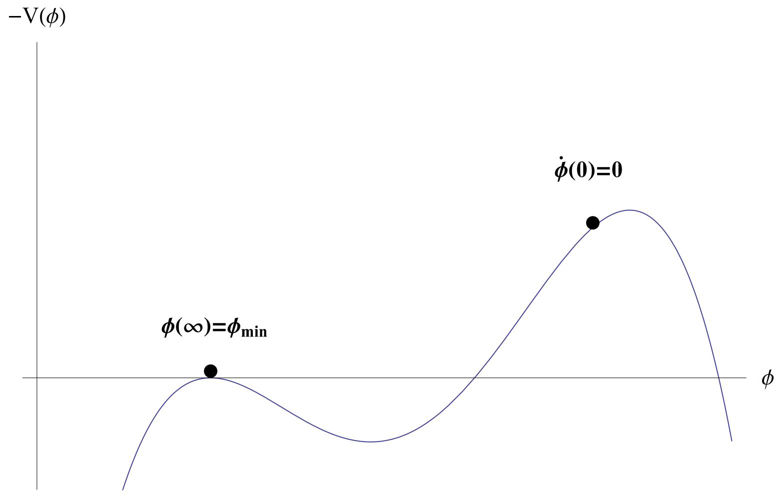

Figure 3.4: *Illustration of the boundary conditions* (3.2).

The numerical procedure we used is based on an overshot/undershot method. First we solve starting from the true vaccuum at very small $s = \epsilon$ and expanding the solution into a series to get

$$\begin{aligned} \phi &\approx \phi_0 + \frac{\epsilon^2}{8} \frac{\partial V(\phi)}{\partial \phi}\bigg|_{\phi=\phi_0}, \\ \dot{\phi} &\approx \frac{\epsilon}{4} \frac{\partial V(\phi)}{\partial \phi}\bigg|_{\phi=\phi_0}. \end{aligned} \tag{3.14}$$

Now we simply have to find the correct starting point ϕ_0. Stating infinitely close to the top of the higher maximum, the particle can spend infinitely long time there, so it is always possible to eliminate the friction and overshot the other maximum. Conversely starting to low we wont have enough energy to climb the lower minimum. From continuity of the solutions we know our desired result lies somewhere between the two and we can use a simple bisection in ϕ_0 to find the correct value for which $\phi(\infty)$ is the electroweak minimum.

To double check we solve the equation of motion again, this time starting from the electroweak minimum. To begin, we expand the field and potential around the minimum

$$\begin{aligned} \phi &\approx \phi_{\min} + \phi_\infty, \\ \frac{\partial V(\phi)}{\partial \phi} &\approx m^2 \phi_\infty. \end{aligned} \tag{3.15}$$

Thus we get a simplified EOM which is solved by modified Bessel functions, so we can express our initial conditions as

$$\phi_\infty = A\,\frac{K_1(s)}{s}, \tag{3.16}$$

$$\dot{\phi}_\infty = -A\,\frac{K_2(s)}{s}. \tag{3.17}$$

Next we solve these to obtain $\dot{\phi}_\infty$ as a function of ϕ_∞. We then again use simple bisection to find ϕ_∞ which minimizes the field derivative at a very small $s = \epsilon$ near the true vacuum.

The case of the Standard Model is still numerically challenging because the are very far away and we have to solve the equation of motion through sixteen orders of magnitude in the field ϕ. Nevertheless this only means we need enough precision in setting the initial conditions, before we are able to find the desired solution. Figure 3.5 shows the resulting bounce solutions.

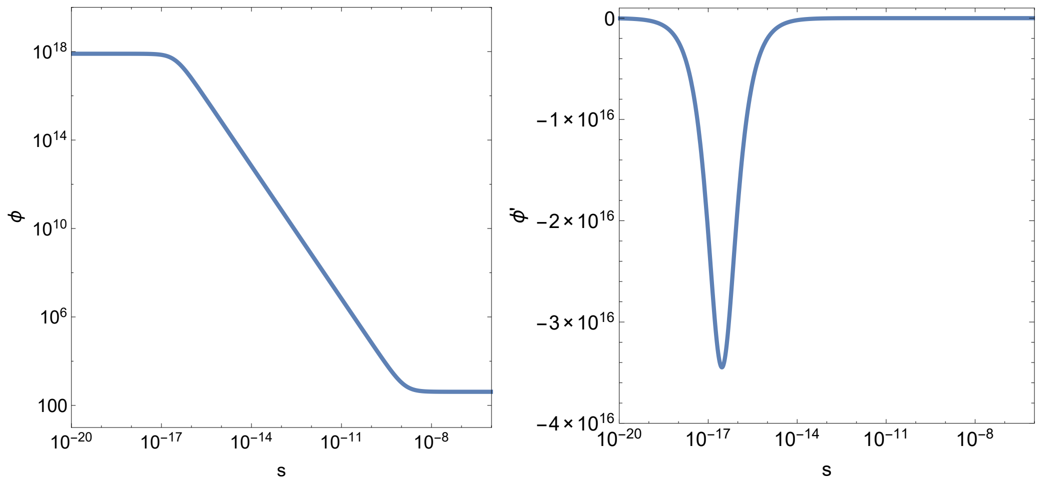

Figure 3.5: *Field configuration corresponding to the bounce solution in the Standard Model (left panel) and the derivative of the field (right panel)* (3.2).

The results from our numerical procedure turn out to be in perfect agreement with the Analytical approximation discussed in the previous sections, the difference in the resulting lifetime is of order of a few percent. The exact value we obtain is $\tau = 9.84 \times 10^{528}$. This confirms that the Standard Model is a consistent theory. No modification is required to explain why the electroweak vacuum live as long as it did already.

3.3 The impact of new physics on vacuum stability

Now we can proceed to include extensions of the standard model, with the goal of discussing their impact on the stability of the electroweak vacuum. We will describe such extension in its generic form of nonrenormalisable operators. Specifically we will supplement the SM potential with two higher dimensional interactions λ_6 and λ_8 suppressed by a large mass scale M:

$$V = -m^2\phi^2 + \frac{\lambda}{4}\phi^4 + \frac{\lambda_6}{6!}\frac{\phi^6}{M^2} + \frac{\lambda_8}{8!}\frac{\phi^8}{M^4}. \tag{3.18}$$

In previous section we discussed that effects of radiative corrections to SM couplings on the vacuum decay are large and so these couplings require precise determination. In order to include RGE effects of the new couplings we computed one-loop corrections associated with the new interactions. The correction to the running of the quatric Higgs coupling is of the form

$$\Delta\beta_\lambda = \frac{\lambda_6}{16\pi^2}\frac{m^2}{M^2}, \tag{3.19}$$

and its contribution is negligible for $m << M$. One-loop beta functions of new couplings take the form

$$\begin{aligned} 16\pi^2\beta_{\lambda_6} &= \lambda_8\frac{m^2}{M^2} + 15\lambda_6 6\lambda - 6\lambda_6\left(\frac{9}{4}g_2^2 + \frac{9}{20}g_1^2 - 3y_t^2\right), \\ 16\pi^2\beta_{\lambda_8} &= 35\lambda_6^2 + 28\lambda_8 6\lambda - 8\lambda_8\left(\frac{9}{4}g_2^2 + \frac{9}{20}g_1^2 - 3y_t^2\right). \end{aligned} \tag{3.20}$$

Figure 3.6 shows an example of running of the new couplings. We can see that while λ_6 varies only by roughly twenty percent, the running of λ_8 is very fast and can have significant consequences. Figure 3.7 shows the resulting potential with $\lambda_6(M_p) = -1$,

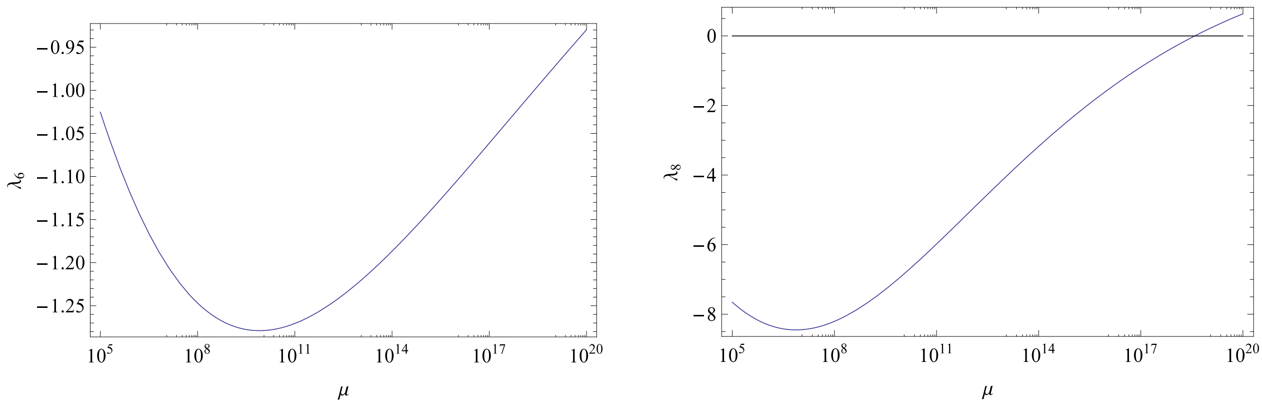

Figure 3.6: Example solution of RGEs for couplings $\lambda_6(M_p) = -1$ and $\lambda_8(M_p) = -0.1$.

$\lambda_8(M_p) = -0.1$ and suppression scale $M = M_p$. As we see the result of negative λ_6 is a new very deep minimum forming close to the cut-off scale M. We could use a more common electroweak basis used in SM [136] which means nonrenormalisable couplings of the form

$$V_{\mathrm{nonr}} = \frac{\lambda_6}{6!}\frac{|H^\dagger H|^3}{M^2} + \frac{\lambda_8}{8!}\frac{|H^\dagger H|^4}{M^4}. \tag{3.21}$$

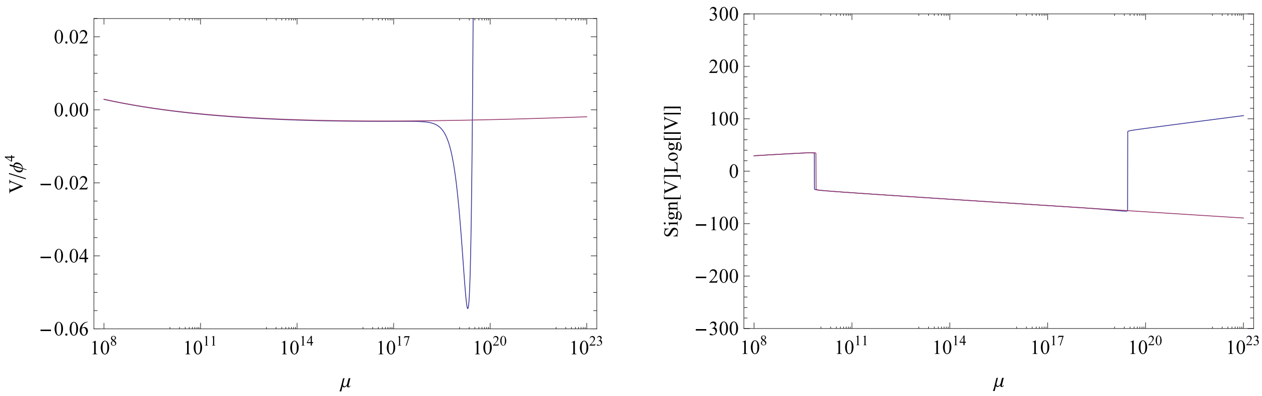

Figure 3.7: Potential corresponding to couplings from Figure 3.6 (blue line) together with the Standard Model potential (purple line).

This gives slightly different coefficients than those in (3.20) due to contributions from three additional scalars in the Higgs doublets

$$\begin{aligned} 16\pi^2\beta_{\lambda_6} &= \frac{10}{7}\lambda_8\frac{m^2}{M^2} + 18\lambda_6 6\lambda - 6\lambda_6\left(\frac{9}{4}g_2^2 + \frac{9}{20}g_1^2 - 3y_t^2\right), \\ 16\pi^2\beta_{\lambda_8} &= \frac{7}{5}28\lambda_6^2 + 30\lambda_8 6\lambda - 8\lambda_8\left(\frac{9}{4}g_2^2 + \frac{9}{20}g_1^2 - 3y_t^2\right), \end{aligned} \tag{3.22}$$

which agrees with [137]. However we have checked that difference between (3.20) and (3.22) has negligible impact on our results here and in the following sections.

3.3.1 Analytical solution

As discussed in the previous section the simplest scheme for estimating the vacuums lifetime, amounts to calculating the quantity in (3.5) as

$$\frac{\tau}{T_U} = \frac{1}{\Lambda_B^4 T_U^4} e^{\frac{8\pi^2}{3|\lambda_{eff}(\Lambda_B)|}}, \tag{3.23}$$

where $\frac{\lambda_{eff}(\phi)}{4} = \frac{V_{eff}(\phi)}{\phi^4}$, V_{eff} being the effective potential, and Λ_B denoting the renormalisation scale for which λ_{eff} is minimised. This approach is based on the fact that in the Standard Model the minimum of λ is very flat and so, for a wide range of energy scales, λ_{eff} is close to a negative constant $\lambda_c \approx -0.013$. Now we have to incorporate the new couplings which gives $\lambda_{eff} = \lambda_{eff}^{\rm SM}(\phi) + \frac{4}{6!}\frac{\lambda_6}{M_P^2}\phi^2 + \frac{4}{8!}\frac{\lambda_8}{M_P^4}\phi^4$. We will discuss two approaches. Firstly we also completely ignore the RGE-running of λ_6 and λ_8. Then we include them in the set of our RGE equations and calculate their scale dependence according to (3.20).

For constant λ_6 and λ_8, the effective λ_{eff} does not have a global minimum for $\lambda_8 < 0$, and we can calculate the value (3.23) only for the range of positive λ_8's. The left panel of Figure 3.8 shows a contour plot of the resulting lifetime, or more precisely $\log_{10}\frac{\tau}{T_U}$. In the region where λ_6 is negative enough, λ_{eff} develops new minimum (as compared to SM) at scales close to M_P and the exponent in (3.23) becomes small, rendering the vacuum short-lived. Our next step is to include the running of λ_6 and λ_8. As we can see in the right hand

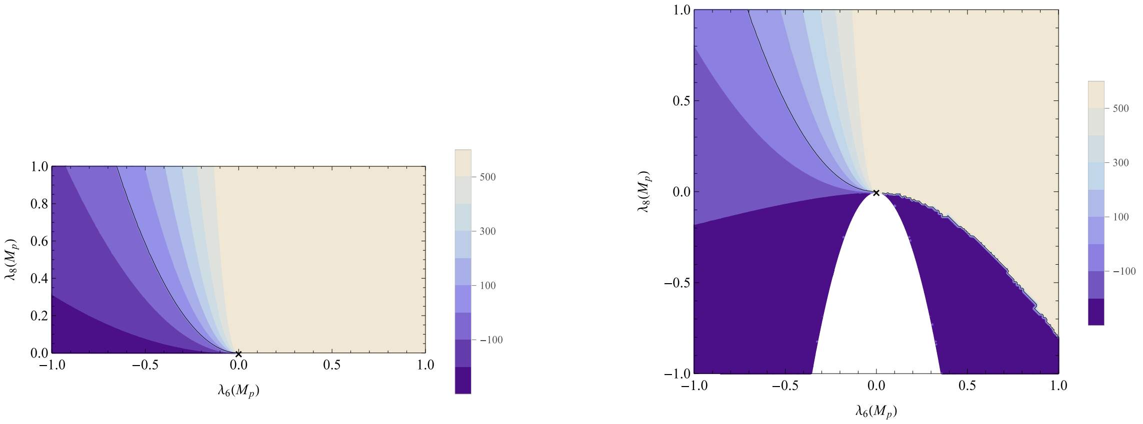

Figure 3.8: Decimal logatihm of lifetime of the universe in units of T_U as a function of the nonrenormalisable λ_6 and λ_8 couplings, calculated with formula (3.23). For λ_6 and λ_8 kept constant (left panel) and λ_6 and λ_8 scale dependent and satisfying their one-loop RGE's (right panel).

side panel of Figure 3.8 it has small influence on the position of the $\log_{10}\frac{\tau}{T_U}=0$ contour. The most significant change is that now, even when we set a negative value of λ_8 at the Planck scale, it eventually becomes positive and so λ_{eff} possesses a global minimum, thus enabling us to use the formula (3.23). The region where λ_{eff} does not develop a global minimum at the renormalisation scale lower than M_P^2 was excluded (white color). Another analytical approximation allowing us to find an approximate bounce solution (originally presented in [134] and recently used in [130]) would be to aproximate the potential with a constant sewn together with a linear function at a certain point, as in

$$V_\eta(\phi)=\begin{cases}-\frac{b_\eta}{4}\phi^4\,, & \phi\leqslant\eta\\ -\frac{b_\eta}{4}\eta^4-K\,(\phi-\eta)\,, & \phi\;>\eta\end{cases}\,, \tag{3.24}$$

where $\frac{b_\eta}{4}=\frac{-V_{eff}(\eta)}{\eta^4}=\frac{-\lambda_{eff}(\eta)}{4}$. The problem is that one always needs to choose the sewing point η and the slope parameter K, to approximate the effective potential so the results are more arbitrary than in the previous method.

The solution exists if the ratio of derivatives at η, $-\gamma=\frac{b_\eta\eta^3}{K}$, obeys $0<-\gamma<1$, [134]. Then the action of a bounce is given by $S_\eta=\dfrac{8\pi^2}{3}\dfrac{1}{b_\eta}(1-(\gamma+1)^4)$, and its starting point, $\phi_0=\eta(2+\gamma)$, lies in the linear part of V_η. In the case when $-\gamma\geqslant 1$, all the bounce solutions lie in the quartic part of V_η only and the effect of sewing it with the linear function amounts to arbitrarily choosing the value of quartic coupling $\lambda_{eff}(\eta)$.

Generally to for V_η to reproduce the shape of V_{eff} near the global minimum, one has to chose $-\gamma$ close to 1 and η of the order of M_P. Thus, the main effect of lowering the action in (3.5) by the nonrenormalisable operators comes from the increase of $|\lambda_{eff}|$, exactly as in the previously described simpler scheme. To check this, we have calculated the $\log_{10}\frac{\tau}{T_U}$, putting $-K = V'_{eff}(\eta)$ and η equal to the potentials inflection point $(V''_{eff}(\eta) = 0$. The results were very similar to the ones presented above, particularly the $\log_{10}\frac{\tau}{T_U} = 0$ contour remained unchanged.

3.3.2 Numerical result

The numerical procedure we used is exactly the same as the one we used in case of the Standard Model as described in Section 3.2.3. The only difference is a different form of the potential including the new interactions.

The resulting lifetimes are shown in Figure 3.9 for constant couplings λ_6 and λ_8. Its

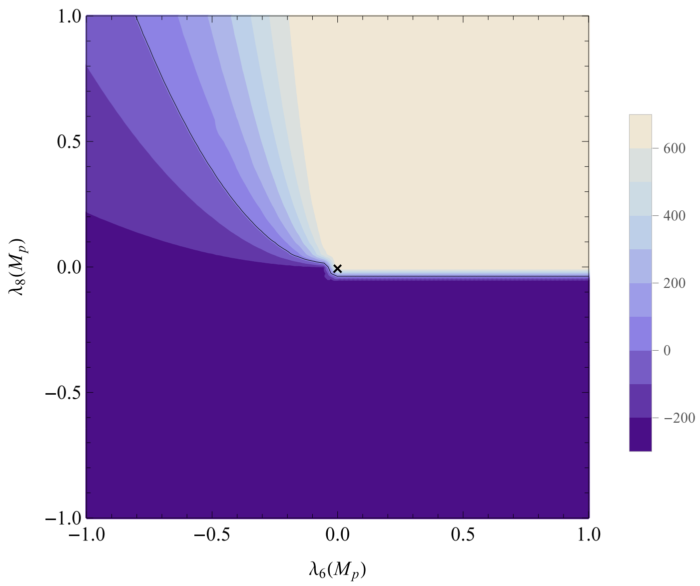

Figure 3.9: Decimal logarithm of lifetime of the universe in units of T_U as a function of constant couplings λ_6 and λ_8.

important to distinguish 3 areas in Figure 3.9. The first one with both new couplings positive corresponds to the SM potential stabilised by new interactions at the Planck scale. The resulting lifetimes are very close to SM one, because the bounce solution within SM probes field values much smaller than Planck mass $(\phi_0 < M_p)$. The second region with $\lambda_8 < 0$ corresponds to a potential unbounded from below, and this whole region predicts very unstable potentials. The last important region has positive λ_8 but negative λ_6, and corresponds to a potential with a new minimum around the Planck scale.

To increase the accuracy of above prediction we solved the equation of motion (3.1) numerically taking into account the 1-loop running of λ_6 and λ_8 from equation (3.20) together with 3-loop Standard Model RGEs. The resulting lifetimes are shown in Figure 3.10.

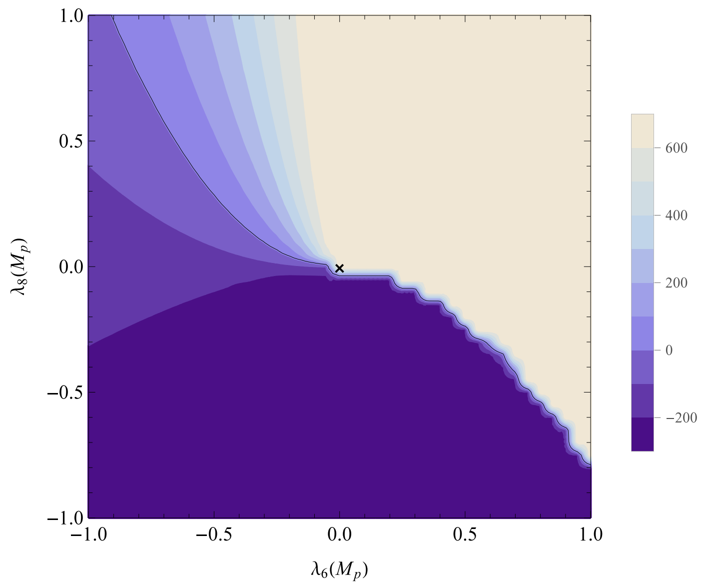

Figure 3.10: Decimal logarithm of lifetime of the universe in units of T_U as a function of running couplings λ_6 and λ_8 calculated at the scale M.

Examples of running of new couplings in Figure 3.6 show that their values, especially λ_8 can change significantly. The most important qualitative difference comes from the λ_6^2 contribution to the running of λ_8 (see equation (3.20)). In the Figure 3.6 we see that for large enough λ_6 it can stabilize the potential by pushing λ_8 to positive values not far above the Planck scale, when $\lambda_8(M_p)$ is negative but has small enough modulus. This effect bends the metastability curve in Figure 3.10 towards more negative λ_8 near edges of the plot where $|\lambda_6|$ is large.

3.3.3 Accuracy Comparison

Figure 3.11 shows comparison of metastability/instability boundaries obtained using the methods described in previous subsections. The analytical approximation is accurate enough for qualitative discussion, however more careful numerical analysis results in a larger metastability region. The same can be said about the impact of the running of nonrenormalisable couplings.

3.3.4 Standard Model phase diagram

To illustrate effects of new nonrenormalisable operators on Standard model vacuum stability in Figure 3.12 we show the well known standard model phase diagram (see for example [123]) and the same diagram after including new operators, respectively $\lambda_6(M_p) = -1/2, -1$ and $\lambda_8(M_p) = 1, 1/2$. Above results clearly show that nonrenormalisable interactions suppressed by the Planck mass can drastically change the SM phase diagram, by pushing electroweak vacuum towards the instability region.

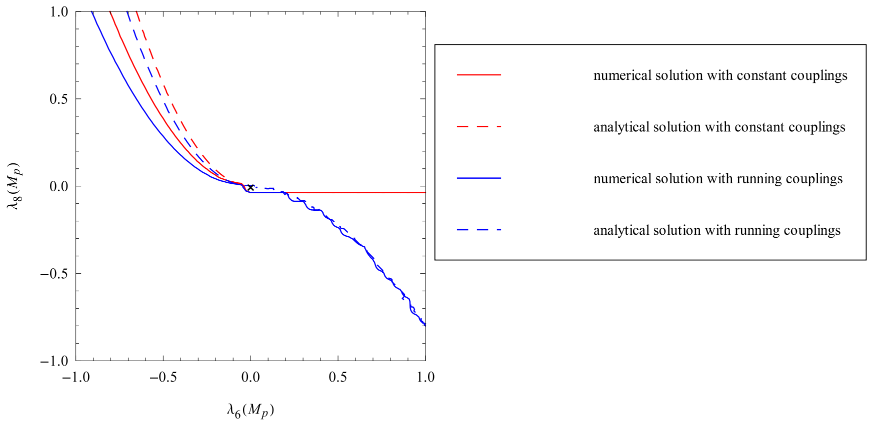

Figure 3.11: Contours corresponding to metastability boundary ($\tau = T_u$) obtained using four different methods.

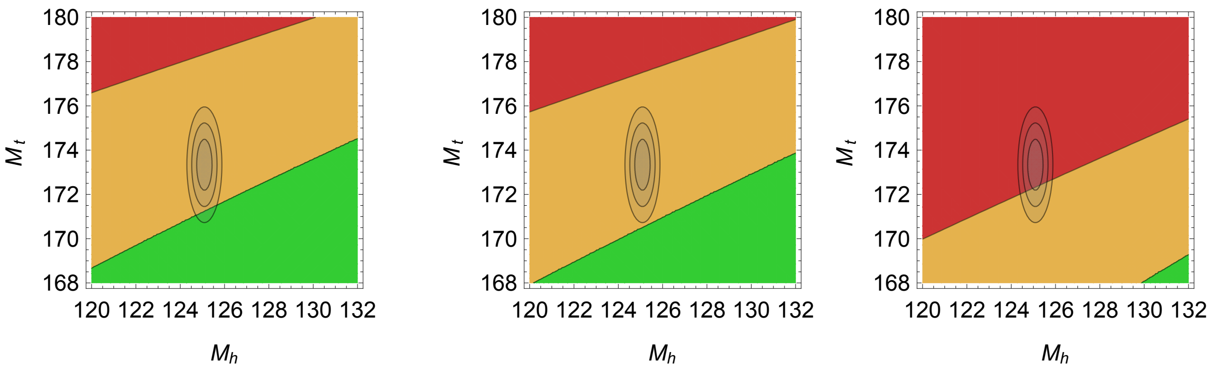

Figure 3.12: Standard Model phase diagram (left panel), the same diagram after including new operators $\lambda_6(M_p) = -1/2$ and $\lambda_8(M_p) = 1$ (middle panel) and $\lambda_6(M_p) = -1$ and $\lambda_8(M_p) = 1/2$ (right panel). The green region corresponds to absolute stability, the yellow region is metastable and the red one corresponds to rapid instability.

3.3.5 Magnitude of the suppression scale

In this section we will discuss how lowering the suppression scale of our nonrenormalisable interactions M in (3.18) changes the results from previous subsections. To analyse this problem qualitatively it is enough to use the analytical approximation we presented in section 3.3.1 . When the nonrenormalisable couplings are positive, lowering the suppression scale M corresponds simply to making the potential positive not far above the scale M. The action (exponent in (3.23)) increases because the position of the minimum of λ_{eff} shifts towards smaller energy scales and the value of $|\lambda_{eff}|$ decreases, which is shown in Figur 3.13. In the case with positive λ_8 and negative λ_6 this dependence is smaller as shown in Figure 3.14. The new minimum is much deeper and changing the scale, changes λ_{eff} by a small fraction of its value. Thus the resulting lifetimes are much less scale dependent. In fact, in this case scale dependence of lifetime comes mostly from the prefactor

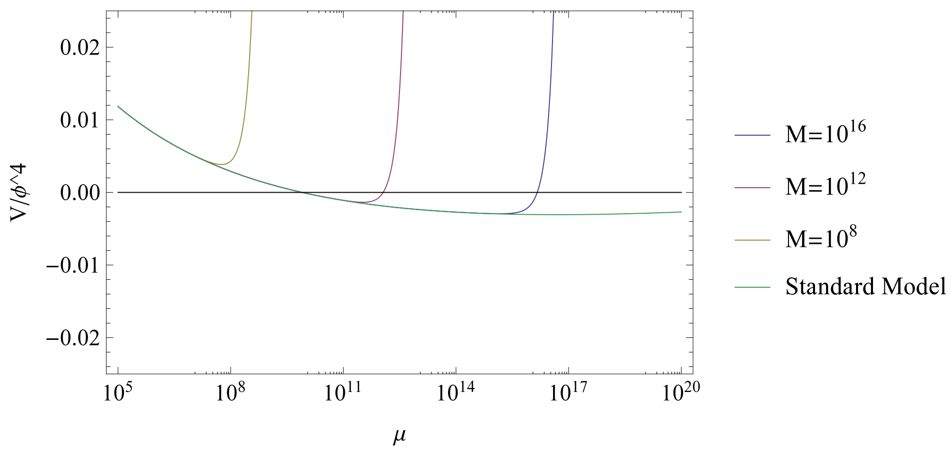

Figure 3.13: Scale dependence of $\frac{\lambda_{eff}}{4} = \frac{V}{\phi^4}$ with $\lambda_6 = \lambda_8 = 1$ for different values of suppression scale M. The lifetimes corresponding to suppression scales $M = 10^8, 10^{12}, 10^{16}$ are, respectively, $\log_{10}(\frac{\tau}{T_U}) = \infty, 1302, 581$ while for the Standard Model $\log_{10}(\frac{\tau}{T_U}) = 540$.

in (3.23), because the size of the bounce is $\phi_0 \approx \mu_{min} \propto M$.

The last possibility is a potential unbounded from below which again corresponds to unstable potentials, that depend on M very weakly as in the previous case. The conclusion is that changing the suppression scale cannot save an unstable solution.

3.4 Summary

We prepared a map of the vacua in the SM extended by nonrenormalisable scalar couplings, taking into account the running of the new couplings and going beyond the standard assumptions taken when calculating the lifetime of the metastable vacuum. We verified the correctness of quasi-analytic approximations of the effective potential widely used in the literature for calculatinon the tunneling rate, [134]. It is important to check the validity of such approximation and to search through a relatively wide scope of new couplings to find the actual behaviour of the scalar potential. The tool we used in this case is direct numerical analysis, which however is not so straightforward due to large separation of scales. Our result is that the simplified analytical approach represents reasonably well the actual numerical results.

In general, we also confirm that it is relatively easy to destabilise the SM with the help of the Planck scale suppressed scalar operators. In fact its possible to destabilise the electroweak vacuum by new interactions at any scale while making it absolutely stable requires cut-off scales lover than roughly 10^{11} GeV.

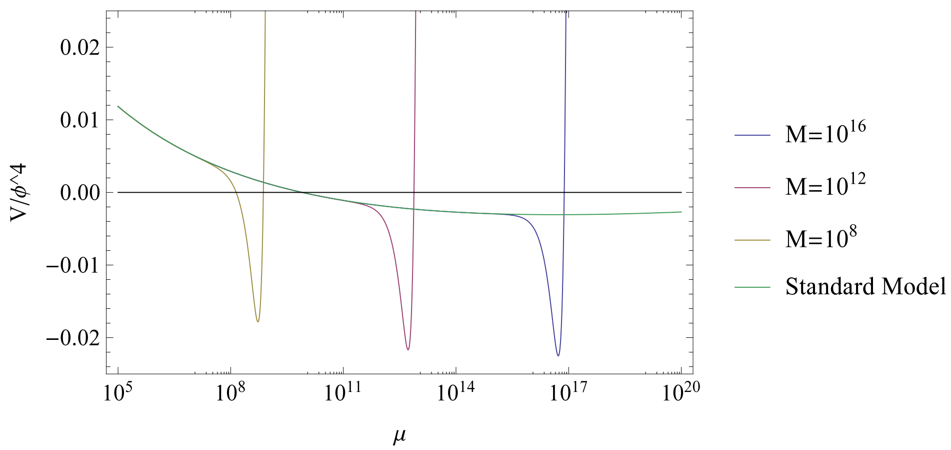

Figure 3.14: Scale dependence of $\frac{\lambda_{eff}}{4} = \frac{V}{\phi^4}$ with $\lambda_6 = -1$ and $\lambda_8 = 1$ for different values of suppression scale M. The lifetimes corresponding to suppression scales $M = 10^8, 10^{12}, 10^{16}$, are, respectively, $\log_{10}(\frac{\tau}{T_U}) = -45, -90, -110$ while for the Standard Model $\log_{10}(\frac{\tau}{T_U}) = 540$.

3.5 Gravitational corrections

In this section we will discuss gravitational corrections to the vacuum decay process. We begin by discussing the gravitational backreaction on a simple toy model.

3.5.1 Toy Model

We will consider a very simple model describing a single neutral scalar field. Our Lagrangian takes the form

$$\mathcal{L} = \frac{R}{2\kappa} + \frac{1}{2}(\partial\phi)^2 - \frac{1}{2}\xi R\phi^2 - V, \qquad V = -a^2(3b-1)\phi^2 + a(b-1)\phi^3 + \frac{1}{4}\phi^4 + C. \tag{3.25}$$

The potential is intentionally very simple with two minima at $\phi = 0$ and $\phi = 2a$. We will always consider a scenario when the field is initially in a homogeneous configuration in the false vacuum at $\phi = \phi_{\mathrm{f}} = 0$ which we will denote by V_{f}. And consider tunnelling to the true vacuum at $\phi = \phi_{\mathrm{t}} = 2a$ denoted by V_{t}.

In the previous sections we could always shift the whole potential by a constant. Now including gravity gives the value of the potential an interpretation of the vacuum energy and thus a very significant role. We will see that the character of our background solution, so the false vacuum energy is crucial in these considerations. To discuss this effect we will use the constant C to change the character of our initial false vacuum.

We will focus on two examples of potentials, first with a de Sitter false vacuum (for $C > 0$) and the second one with a Minkowski false vacuum (for $C = 0$). These example potentials are plotted in Figure 3.15 with $a = 1/2$ and $C = 1/100$ such that the true vacuum is positioned at the Planck scale, for different values of b. We also use natural units where $M_p = 1$.

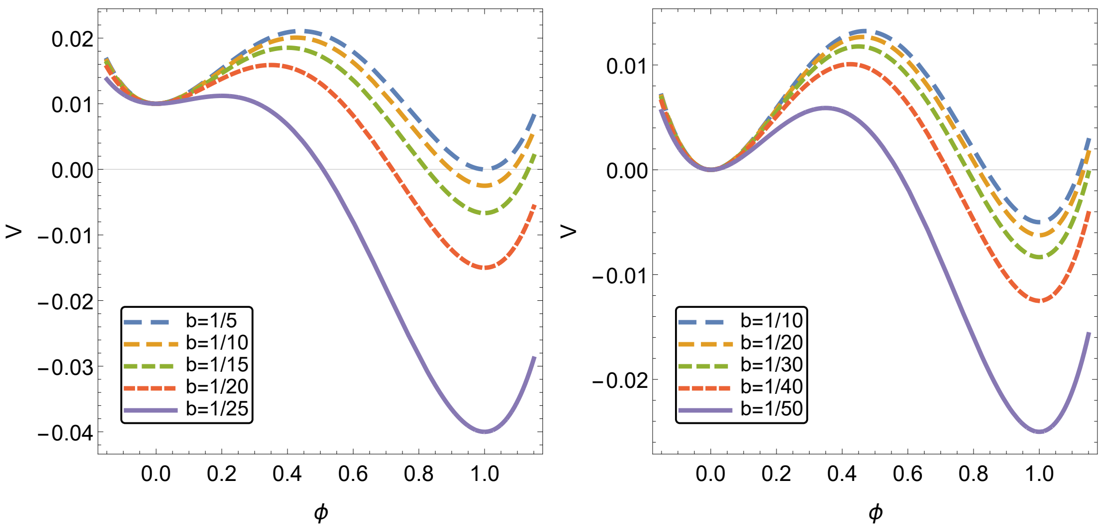

Figure 3.15: Our toy model potential. Left panel: dS false vacuum and AdS true vacuum. Right Panel: Minkowski false and vacuum AdS true vacuum.

3.5.2 Gravitational impact on bubble formation

We will consider and compare thwo different methods of obtaining the vacuums lifetime

- Numerical determination of instanton action neglecting gravity with a thin wall approximation of gravitational correction [138].
- Full numerical calculation including gravitational effects.

We will be most interested in the third case, where we will use the standard formalism of Coleman and De Luccia (CDL) [138], assuming that vacuum decay proceeds through nucleation of true vacuum bubbles within our false vacuum. We will also compare a precise numerical result with results of the thin wall approximation [131, 138].

Action of an CDL instanton is the difference between the instanton solution and the background. That is a homogeneous solution of the field residing in the false vacuum,

$$S = S[\phi_{\text{CDL}}] - S[\phi_{\text{f}}]. \tag{3.26}$$

We are interested in an $O(4)$ symmetric scalar field configuration $\phi = \phi(\tau)$, with the metric given by $ds^2 = d\tau^2 + r(\tau)^2(d\Omega)^2$. Here $d\Omega$ is an infinitesimal element of the $3D$ sphere, and $r(\tau)$ is the radius of that sphere. The resulting metric tensor is of the form of the FRW metric with the curvature parameter $k = +1$. Euclidean action in Einstein frame takes the form

$$S_E = 2\pi^2 \int d\tau \rho^3 \left(\frac{1}{2}\dot{\phi}^2 + V + \frac{1}{2}\frac{R}{\kappa}\right) , \tag{3.27}$$

since as in the usual FRW case $R = 6\left(\frac{\ddot{\rho}}{\rho} + \left(\frac{\dot{\rho}}{\rho}\right)^2 - \frac{1}{\rho^2}\right)$ and $\dot{\phi} = \frac{d\phi}{d\tau}$. The equation of motion of the scalar field reads

$$\ddot{\phi} + 3\frac{\dot{\rho}}{\rho}\dot{\phi} = \frac{\partial V}{\partial \phi}\,, \tag{3.28}$$

the second EOM is the Friedmann equation

$$\dot{\rho}^2 = 1 + \frac{\kappa\rho^2}{3}\left(\frac{1}{2}\dot{\phi}^2 - V\right)\,. \tag{3.29}$$

One can show that scale factor ρ crosses zero at least once [139]. Without loss of generality we chose value of τ of the first one to be $\tau = 0$, the other boundary is set at τ_{end}. The appropriate boundary conditions then are

$$\begin{aligned} \dot{\phi}(0) = \dot{\phi}(\tau_{\text{end}}) &= 0 \\ \rho(0) &= 0 \\ \rho(\tau_{\text{end}}) &= 0, \quad (\text{for dS}) \\ \rho(\tau_{\text{end}}) &= \rho_{\text{end}} \neq 0, \quad (\text{for Minkowski})\,. \end{aligned} \tag{3.30}$$

We can also simplify the action using EOMs and integrating by parts

$$\begin{aligned} S_E &= 2\pi^2 \int_0^{\tau_{\max}} d\tau \rho^3 \left(\frac{1}{2}\dot{\phi}^2 + V + \frac{1}{2}\frac{R}{\kappa}\right) \\ &= 2\pi^2 \int_0^{\tau_{\max}} d\tau \left(\rho^3\left(\frac{1}{2}\dot{\phi}^2 + V\right) + \frac{3}{\kappa}\left(\ddot{\rho}\rho^2 + \dot{\rho}^2\rho - \rho\right)\right) \\ &= 4\pi^2 \int_0^{\tau_{\max}} d\tau \left(\rho^3 V - \frac{3\rho}{\kappa}\right) + \frac{6\pi^2}{\kappa}\rho^2\dot{\rho}\Big|_{\tau=\tau_{\max}}\,. \end{aligned}$$

Now we can proceed and find the solutions we need to compute the action. To find the simpler background solution we will use the first Friedmann equation (3.29) assuming a constant field configuration $\dot{\phi} = 0$, which gives a solution for ρ,

$$\begin{aligned} \rho &= \frac{1}{\sqrt{\frac{\kappa V_{\text{f}}}{3}}} \sin\left(t\sqrt{\frac{\kappa V_{\text{f}}}{3}}\right)\,, \quad (\text{for dS}) \\ \rho &= t, \quad (\text{for Minkowski}) \end{aligned} \tag{3.31}$$

For dS and Minkowski false vacua false vacua of interest to us we have

$$\begin{aligned} S[\phi_{\text{f}}] &= -\frac{24\pi^2}{V_{\text{f}}}, \quad (\text{for dS}) \\ S[\phi_{\text{f}}] &= 0, \quad (\text{for Minkowski}) \end{aligned} \tag{3.32}$$

The next step is the calculation of $S[\phi_{\text{CDL}}]$ which we will discuss in the following subsections.

3.5.3 Thin-wall approximation

We now proceed to the thin-wall inclusion of gravity. This method, described in detail in [138] assumes the true vacuum bubble stretches to some $\bar{\rho}$ taking a constant value V_t and beyond that our solution is identical to the false vacuum V_f. To integrate up to an arbitrary ρ which will play the role of the size of the bubble, we change the variables using (3.29)

$$d\tau = d\rho \left(1 - \frac{\kappa V}{3}\rho^2\right)^{-\frac{1}{2}} \tag{3.33}$$

And perform the integral in (3.31) to obtain action of the bubble

$$S = 2\pi^2 \left(S_\mathrm{w}\rho^3 + \frac{2}{\kappa^2}\left[\frac{1}{\Lambda_\mathrm{t}}\left(\left(1 - \Lambda_\mathrm{t}\rho^2\right)^{\frac{3}{2}} - 1\right) - \frac{1}{\Lambda_\mathrm{f}}\left(\left(1 - \Lambda_\mathrm{f}\rho^2\right)^{\frac{3}{2}} - 1\right)\right]\right), \tag{3.34}$$

where S_w is the action of the bubble wall, and $\Lambda_i = \kappa V_i/3$. Next we find $\hat{\rho}$ such that the above action is stationary,

$$\hat{\rho}^2 = \frac{1}{\Lambda_\mathrm{t} + \left(\frac{\gamma_\mathrm{t}}{\kappa S_\mathrm{w}}\right)^2} = \frac{1}{\Lambda_\mathrm{f} + \left(\frac{\gamma_\mathrm{f}}{\kappa S_\mathrm{w}}\right)^2}, \tag{3.35}$$

where $\gamma_\mathrm{t} = \left(\frac{\kappa S_\mathrm{w}}{2}\right)^2 - \Lambda_\mathrm{t} + \Lambda_\mathrm{f}$ and $\gamma_\mathrm{f} = \left(\frac{\kappa S_\mathrm{w}}{2}\right)^2 - \Lambda_\mathrm{f} + \Lambda_\mathrm{t}$. For this solution to exist we require $\gamma_\mathrm{t} > 0$ and $\gamma_\mathrm{f} < 0$. Using these results in 3.34 we finally obtain

$$S = 2\pi^2 \left(\frac{S_\mathrm{w}}{\left(\Lambda_\mathrm{t} + \frac{\gamma_\mathrm{t}^2}{\kappa^2 S_\mathrm{w}^2}\right)^{\frac{3}{2}}} + \frac{2}{\kappa^2}\left[\frac{1}{\Lambda_\mathrm{t}}\left(\left(\frac{1}{1 + \frac{\Lambda_\mathrm{t}\kappa^2 S_\mathrm{w}^2}{\gamma_\mathrm{t}^2}}\right)^{\frac{3}{2}} - 1\right) - \frac{1}{\Lambda_\mathrm{f}}\left(\left(\frac{1}{1 + \frac{\Lambda_\mathrm{f}\kappa^2 S_\mathrm{w}^2}{\gamma_\mathrm{f}^2}}\right)^{\frac{3}{2}} - 1\right)\right]\right). \tag{3.36}$$

Within the thinn-wall approximation, the bubble tension can be expressed through size of the bubble in flat spacetime ρ_0 as $S_\mathrm{w} = (V_\mathrm{f} - V_\mathrm{t})\rho_0/3$. Thin-wall result neglecting gravity for parameter ρ_0 reads [131]

$$\rho_0 = \frac{3}{V_\mathrm{t} - V_\mathrm{f}} \int_{\phi_\mathrm{f}}^{\phi_\mathrm{t}} d\phi \sqrt{2\left(V - V_\mathrm{f}\right)}. \tag{3.37}$$

To improve the thin-wall gravity correction we numerically solve the EOM neglecting gravity to find the correct ρ_0 and the correct bubble wall tension. This procedure is identical to the one discussed in Subsection 3.2.3, the difference is using the toy potential (3.25) instead of the SM one. Figure 3.16 shows the resulting difference between the simple thin-wall approximation of ρ_0 in flat spacetime and our numerical result taking $\rho_0 = \rho(\phi = (V_\mathrm{f} - V_\mathrm{t})/2)$.

Results for the bounce action neglecting gravity and the thin-wall correction are both presented and discussed together with the full numerical results including gravity, discussed in the next subsection.

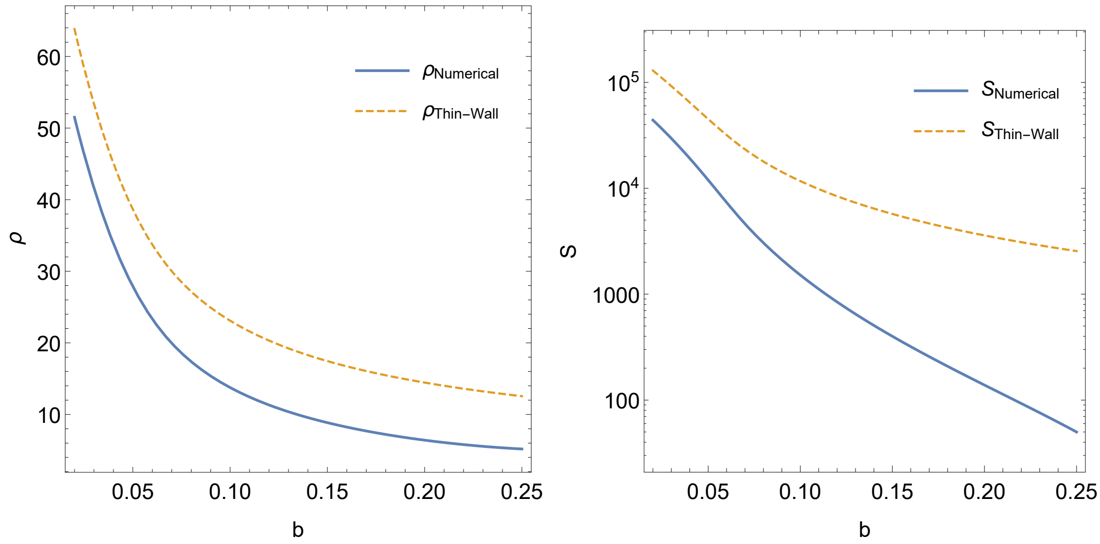

Figure 3.16: Left panel: Size of the bounce ρ obtained using thin-wall and by numerically solving the full EOM. Right Panel: Action of the bounce obtained using thin-wall and using numerical solution of the full EOM. Both results neglect any gravity corrections.

3.5.4 Numerical CDL instanton calculation

For practical purposes, numerically it is more its more convenient to solve the second Friedmann equation,

$$\ddot{\rho} = \frac{\kappa\rho}{3}\left(-\dot{\phi}^2 - V\right), \tag{3.38}$$

rather than the first one. Its also very useful to express the curvature using the scalar field,

$$R = 6\left(\frac{\ddot{\rho}}{\rho} + \left(\frac{\dot{\rho}}{\rho}\right)^2 - \frac{1}{\rho^2}\right) = \kappa\left(\dot{\phi}^2 + 4V\right) \tag{3.39}$$

which allows us to avoid numerical problems when ρ approaches zero.

We find initial values for our numerical EOM solutions by expanding the functions ϕ and ρ for very small $t = \epsilon$ around $\dot{\phi}(0) = \rho(0) = 0$ as in (3.30) obtaining

$$\begin{aligned}
\phi(\epsilon) &\approx \phi_0 + \frac{\epsilon^2}{2}\frac{\partial V}{\partial \phi}\bigg|_{\phi=\phi_0}, \\
\rho(\epsilon) &\approx \epsilon + \frac{\epsilon^2}{2}\frac{\kappa V}{3}\bigg|_{\phi=\phi_0}.
\end{aligned}$$

The final initial condition needed for our equations is the initial field value ϕ_0. We find the correct value of this parameter corresponding to a CDL instanton by a simple undershoot/overshoot method just as in the flat spacetime. Figure 3.17 shows the resulting bubble profiles.

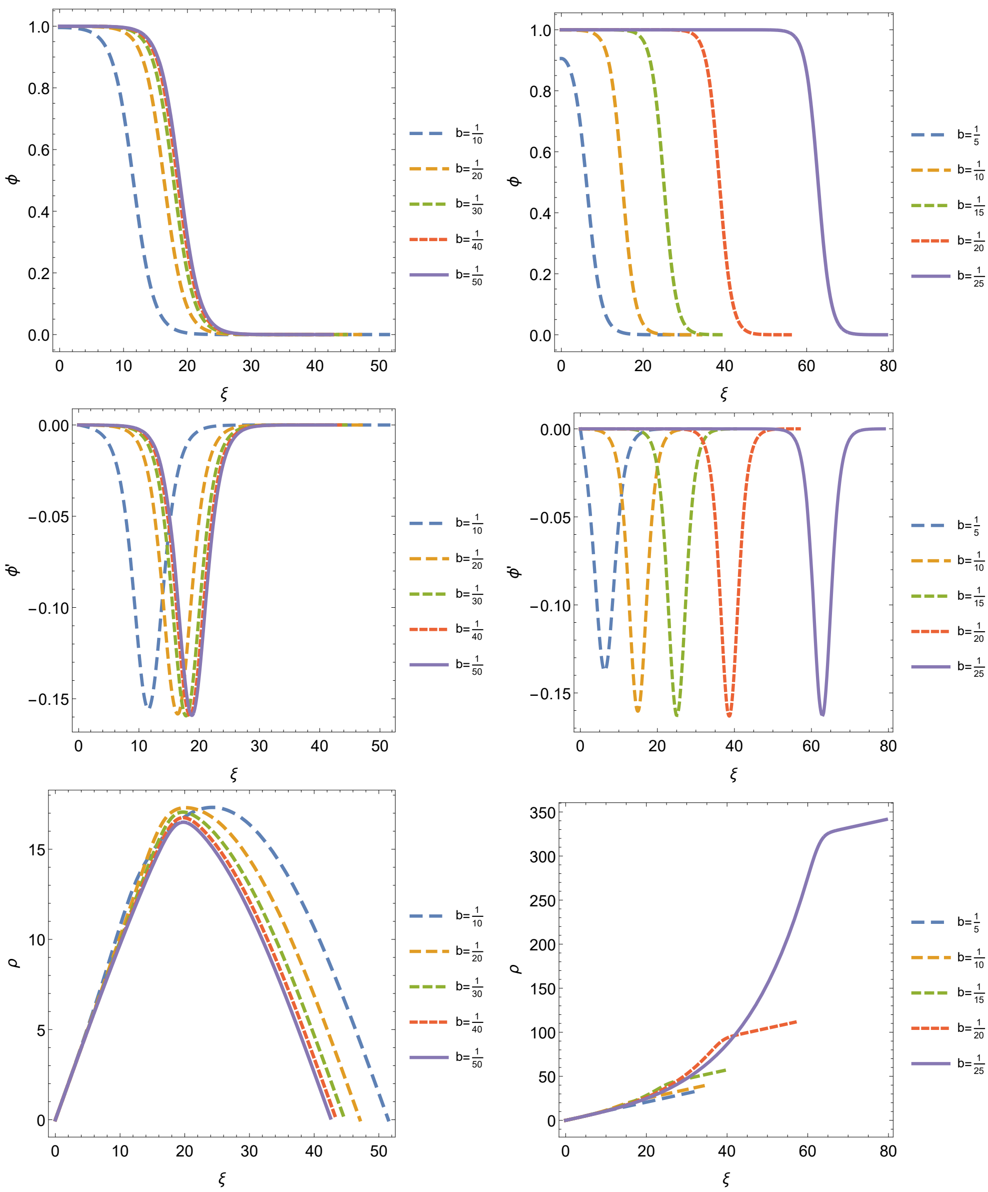

Figure 3.17: CDL bubble profiles. Left panel: tunnelling from dS false vacuum to AdS true vacuum. Right Panel: tunnelling from Minkowski false vacuum to AdS true vacuum.

After finding the CDL solution for $\phi(\tau)$ and $\rho(\tau)$ we numerically perform the action integral in a form (3.31). Now we have all the elements needed to obtain our final result for the action (3.26). Figure 3.18 shows the action of our CDL instantons with various false vacuum energy densities parametrised by c parameter ($c = 0$ corresponds to a Minkowski background). Flat background bounce action and thin-wall approximation of gravity discussed in Subsection 3.5.3 are also shown.

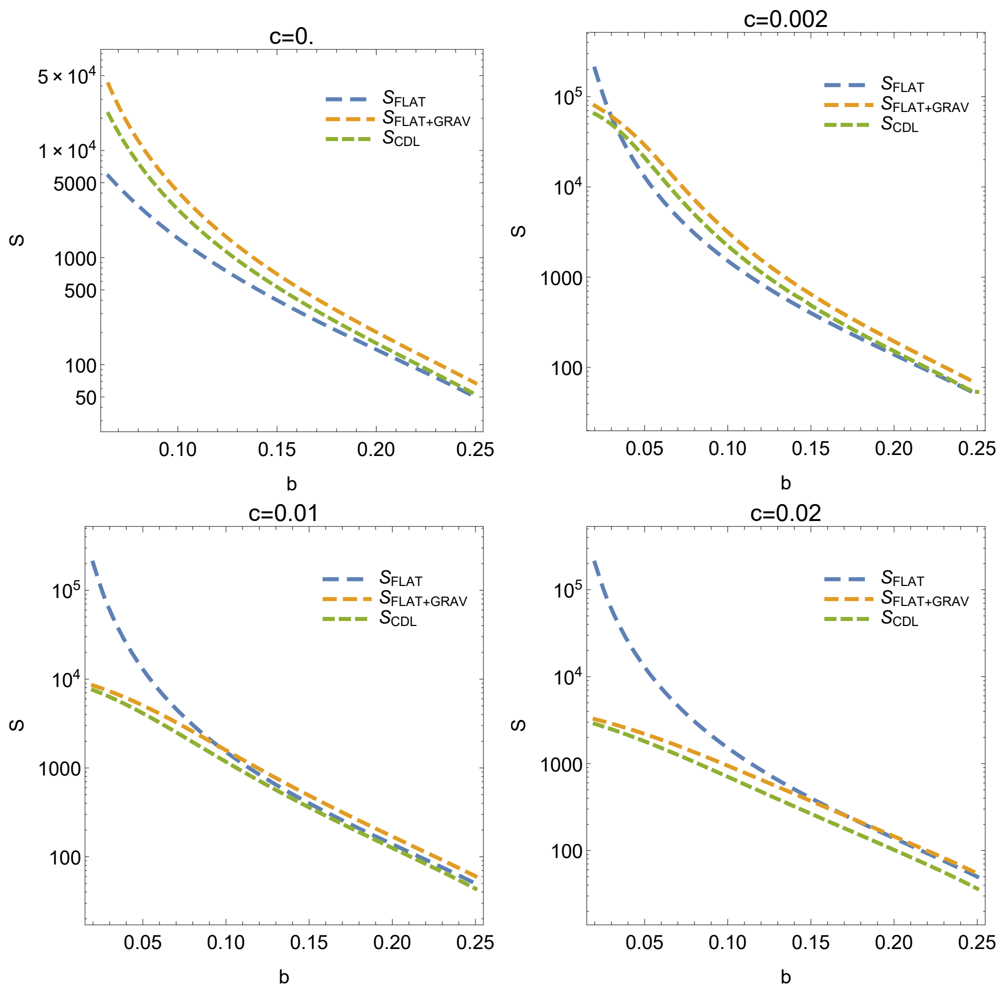

Figure 3.18: Left panel: action of CDL instanton tunnelling from a dS false vacuum to an AdS true vacuum. Right Panel: action of CDL instanton from Minkowski false vacuum to an AdS true vacuum.

As we can see tunneling from a Minkowski false vacuum is heavily suppressed. There is a minimal splitting between vacua below which gravitational effects disable the tunnelling completely.

Tunneling from an AdS false vacuum is completely different. Gravitational effects facilitate the bubble nucleation. This happens because a CdL instanton does not necessarily need to connect the two vacua it only connects different sides of the barrier. The horizon shrinks with increasing c (look at lower left panel of Figure 3.17) so our instanton which needs to fit inside does the same, which results in smaller action. This effect is illustrated in Figure 3.19 showing instantons for several values of constant added to the potential c.

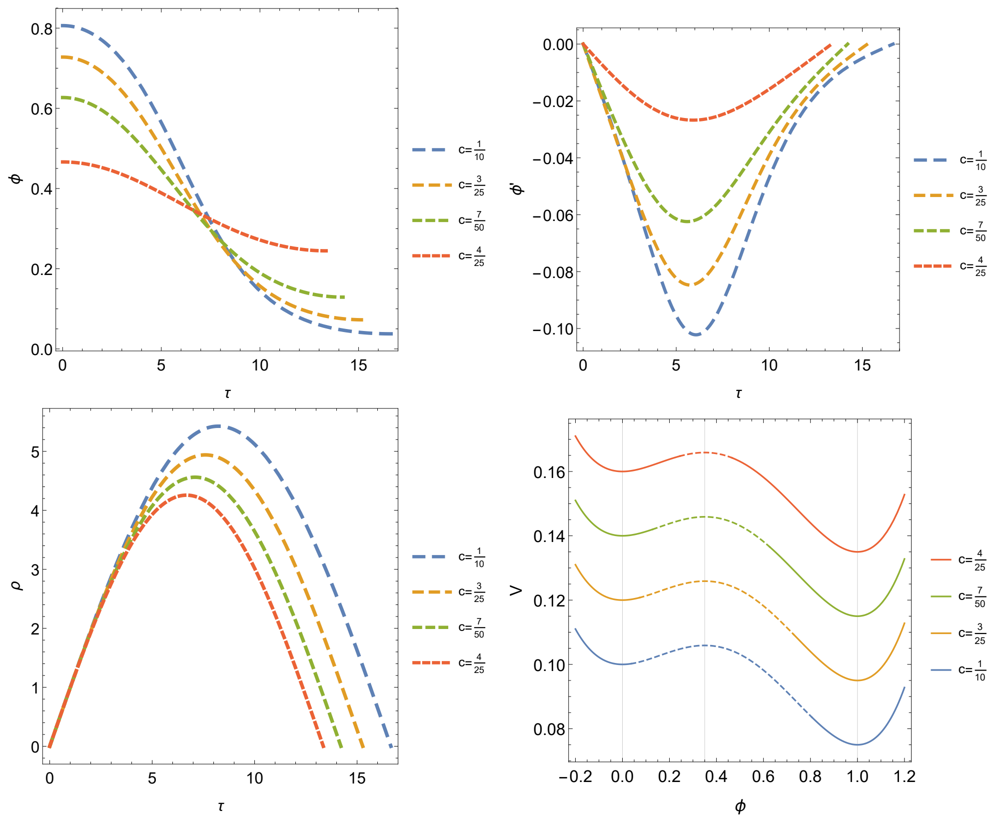

Figure 3.19: Top row: CDL bubble profiles and their derivatives. Bottom row: scale factors (left panel) and potentials with dashed out parts probed by CDL instantons tunneling through the barrier.

3.5.5 Summary and situation in the SM

The first problem in discussion of the SM case is the uncertainty of the depth of the vacuum. Looking at (3.32) we see that this is an important issue since the vacuum positioned at $V \approx 10^{-120}$ introduces yet another very different scale in the problem. However, based on our discussion from the previous section its not difficult to discuss the effect quantitatively. The SM case is similar to our toy potential with very small cosmological constant c and very large separation of energies of the vacua (large b). Looking at the top row of 3.18 we can safely say that the correction will be a very small increase of the action. The same conclusion comes from applying the simple thin-wall correction in SM. This happens because in the SM the bubble which forms is of subatomic size (see Figure 3.5) vastly smaller than the scale at which the spacetime curvature becomes important or even observable. Thus our bounce is very similar to the flat spacetime case, because at the scale of its size the background is to a great approximation flat.

Chapter 4

Electroweak baryogenesis in modified cosmologies

4.1 Introduction

Now we turn to another problem of the Standard Model, namely explaining the observed matter-antimatter asymmetry. Creating such asymmetry requires the so called Sakharov's conditions to be fulfilled [24]. These are:

- baryon number violation,
- C and CP violation,
- departure from thermal equilibrium.

We now know that electroweak symmetry is broken due to the vacuum expectation value (vev) of a scalar field. However, the symmetry was restored in the early Universe due to high temperature modifications of the Higgs boson properties. We will study a baryogenesis scenario [20, 21, 22, 23] in which the observed baryon asymmetry of the Universe is created during the phase transition between the symmetric phase and the phase with broken electroweak symmetry.

The last of Sakharov's conditions can be fulfilled if the electroweak phase transition is first order. However, in the Standard Model (SM) it is second order for a Higgs mass of 125 GeV, and the field transitions smoothly into its new non-symmetric minimum which develops as the temperature drops. Thus, models of electroweak baryogenesis require new physics near the electroweak scale in order to generate a barrier between the symmetric phase and the broken phase [25, 26]. Figure 4.1 illustrates this point, showing the thermally corrected potentials in the SM an its extension which we will discuss in this chapter. The dynamics of a phase transition from a symmetric phase in the hot early Universe to the present-day broken phase at low temperature is described by finite-temperature field theory. While the high-temperature Higgs dynamics is not directly measurable at a collider, it is tightly related to the currently probed zero-temperature potential.

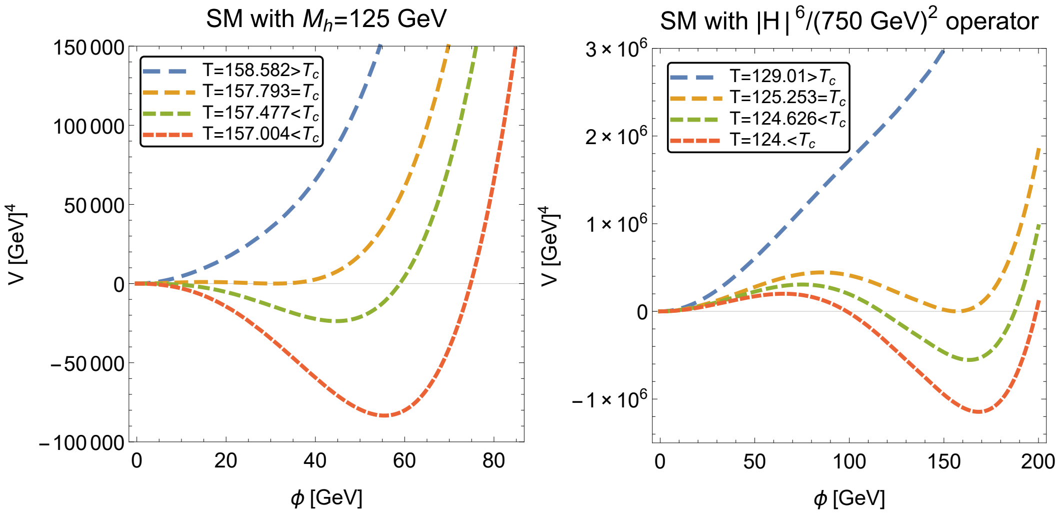

Figure 4.1: *Thermally corrected potential of the SM (left panel) and its modification through 2* $|H|^6$ *operator that we will discuss in this chapter.*

Models realising EWBG gained renewed attention recently, as the experimental accuracy with which we know the Higgs properties increases and models predicting modification to its potential can be probed [27, 28].

We will discuss modification of SM in its generic form of nonrenormalisable interactions. Specifically we will supplement the SM Higgs potential with non-renormalisable dimension six operator, suppressed by a cutoff scale Λ. It has already been shown that this model can facilitate a first-order phase transition, depending on the value of Λ [140, 141]. Such modifications arise naturally from any UV complete model once the heavy states are integrated out and can describe the theory at energies below the mass of the heavy state Λ. However, here we will not discuss a particular high energy model, but try to discuss all of their possible modifications of the Higgs potential by including a nonrenormalisable modification of the Higgs potential through $|H|^6$ operator.

We will be most interested in how the bounds one can put on EWBG models depend on the cosmological history of the universe. In the standard cosmological model, the Universe is radiation-dominated from the end of reheating following inflation, to the time of matter-radiation equality, around $400,000$ years after the Big Bang. During this time, a plethora of phase transitions occurred, among them the EWPT at a scale around $T \sim 100\,\text{GeV}$. While the good agreement between Big Bang nucleosynthesis (BBN) models and measurements of the primordial elemental abundances imply that the Universe was radiation-dominated during and after BBN ($T \lesssim 1\,\text{MeV}$), the expansion history before BBN is still very poorly constrained. This means that the energy density in the early Universe could have been dominated by components which have sufficiently decayed or transformed into radiation, hence their presence may not show up through measurements of the energy density at later epochs. Virtually all extensions of the SM predict new particles or energy constituents, and so the question of how those will impact the early Universe arises naturally.

The difficulty for electroweak baryogenesis (EWBG) that we will discuss arises when the Universe returns to thermal equilibrium after the phase transition. Then, the same sphaleron processes that could have created the baryon asymmetry during the transition can wash it away, if their damping in the broken phase is not sufficient. One way to avoid this problem is to generate a large potential barrier, such that these processes are sufficiently damped after the transition. However, cosmological freeze-out due to a fast expansion of the Universe works in the same direction, see [142, 143]. In order to obtain a higher expansion rate of the Universe than in the standard case, we require that the dominant energy density during EWBG decreases faster than radiation which has to dominate the Universe later during BBN. We will remain agnostic to what cosmological model modifies the evolution of the Universe during this early epoch. Indeed, our results are applicable to a large class of cosmological models and do not depend on the detailed implementation of such models.

4.2 Description of the model

In order to facilitate a first-order phase transition of electroweak symmetry breaking (EWSB), we need to extend the Standard Model. There are numerous models in the literature that accomplish this. We will discuss the simplest and most generic idea which does not introduce new propagating degrees of freedom, but only a single higher-dimensional operator $|H|^6$. This can create a potential barrier between two local minima at the critical temperature, thereby achieving the first-order phase transition as the temperature drops. In this section we review the details of this model and also the finite temperature field theory formalism needed to investigate the phase transition.

4.2.1 SM with a ϕ^6 coupling

We will now describe the particle physics dynamics of an extension of SM with additional $|H|^6$ coupling suppressed by a certain energy scale Λ. Above that scale, new degrees of freedom become fully dynamical, and the underlying particle model cannot be described in the language of our effective theory. Restricting ourselves to processes around the electroweak scale, we will consider the following potential

$$V(H) = -m^2|H|^2 + \lambda|H|^4 + \frac{1}{\Lambda^2}|H|^6, \tag{4.1}$$

with $H^T = (\chi_1 + i\chi_2, \varphi + i\chi_3)/\sqrt{2}$. We assume only the real part of the neutral component has a vev: $\varphi = \phi + v$. The physical Higgs boson is ϕ, which leads to the following tree level potential

$$V(\phi)^{tree} = -\frac{m^2}{2}\phi^2 + \frac{\lambda}{4}\phi^4 + \frac{1}{8}\frac{\phi^6}{\Lambda^2}. \tag{4.2}$$

The field-dependent masses take the form

$$\begin{aligned}
m_h^2(\phi) &= -m^2 + 3\lambda\phi^2 + \frac{15}{4}\frac{\phi^4}{\Lambda^2}, \\
m_{\chi_i}^2(\phi) &= -m^2 + \lambda\phi^2 + \frac{3}{4}\frac{\phi^4}{\Lambda^2}, \\
m_W^2(\phi) &= \frac{g^2}{4}\phi^2, \quad m_Z^2(\phi) = \frac{g^2+g'^2}{4}\phi^2, \qquad m_t^2(\phi) = \frac{y_t^2}{2}\phi^2,
\end{aligned} \tag{4.3}$$

where g, g' and y_t are the gauge boson and Yukawa couplings, respectively.

Following the prescription from [141], where a very similar potential was considered, we include thermal and loop corrections as follows,

$$\begin{aligned}
V_{eff}(\phi, T) = -\frac{m^2}{2}\phi^2 + \frac{\lambda}{4}\phi^4 + \frac{1}{8}\frac{\phi^6}{\Lambda^2} &+ \sum_{i=h,\chi,W,Z,t} n_i \frac{m_i^4(\phi)}{64\pi^2}\left[\log\frac{m_i^2(\phi)}{\mu^2} - C_i\right] \\
&+ \sum_{i=h,\chi,W,Z} \frac{n_i T^4}{2\pi^2} J_b\left(\frac{m_i^2(\phi)}{T^2}\right) + \sum_{i=t} \frac{n_i T^4}{2\pi^2} J_f\left(\frac{m_i^2(\phi)}{T^2}\right) \\
&+ \sum_{i=h,\chi,W,Z,\gamma} \frac{\bar{n}_i T}{12\pi}\left[m_i^3(\phi) - \left(m_i^2(\phi) + \Pi_i(T)\right)^{3/2}\right].
\end{aligned} \tag{4.4}$$

The coefficients read $n_{\{h,\chi,W,Z,t\}} = \{1, 3, 6, 3, -12\}$, $\bar{n}_{\{h,\chi,W,Z,t\}} = \{1, 3, 2, 1, 1\}$, and the functions J are given by

$$J_{b/f}\left(\frac{m_i^2(\phi)}{T^2}\right) = \int_0^\infty dk\, k^2 \log\left[1 \mp \exp\left(-\sqrt{\frac{k^2 + m_i^2(\phi)}{T^2}}\right)\right]. \tag{4.5}$$

The thermal mass corrections Π_i in (4.4) result from the *ring-improvement* of the finite temperature potential, which is a resummation of the so-called *daisy* diagrams that become enhanced at high temperature in the limit of zero boson mass. In our model, these mass shifts read [144, 141]

$$\begin{aligned}
\Pi_{h,\chi_i}(T) &= \frac{T^2}{4v_0^2}\left(m_h^2 + 2m_W^2 + m_Z^2 + 2m_t^2\right) - \frac{3}{4}T^2\frac{v_0^2}{\Lambda^2} \\
\Pi_W(T) &= \frac{22}{3}\frac{m_W^2}{v_0^2}T^2
\end{aligned} \tag{4.6}$$

and the resulting masses of Z and γ ($m_{Z/\gamma}^2 + \Pi_{Z/\gamma}(T)$) are eigenvalues of the following mass matrix, including thermal corrections

$$\begin{pmatrix} \frac{1}{4}g^2\phi^2 + \frac{11}{6}g^2T^2 & -\frac{1}{4}g'^2g^2\phi^2 \\ -\frac{1}{4}g'^2g^2\phi^2 & \frac{1}{4}g'^2\phi^2 + \frac{11}{6}g'^2T^2 \end{pmatrix}. \tag{4.7}$$

There are certain conditions our model must fulfil to correctly predict known observations. Namely we require correct masses of the Higgs boson m_h =125.09 GeV , as well as those of the gauge bosons via the Higgs ground state of $v_0 := \langle\phi(T=0)\rangle = 246.2\,\text{GeV}$. These conditions predict the values of our model parameters λ and m, such that

$$V'_{eff}(\phi, T=0)|_{\phi=v_0} = 0, \quad V''_{eff}(\phi, T=0)|_{\phi=v_0} = m_h\,. \tag{4.8}$$

The resulting values of the parameters m and λ, as well as examples of potentials, are shown in Figure 4.2.

We will limit our considerations to cutoff scales smaller than $\Lambda \approx 1100$ GeV. Above that scale, the phase transition is as weak as in the Standard Model (SM) with $m_h \approx 80\,\text{GeV}$. For this value the barrier between vacua is negligible and lattice simulations show results characteristic for a second-order phase transition [145]. In that case, even if the sphalerons can be decoupled after the phase transition, no asymmetry will be created to begin with, so the model is ruled out anyway.

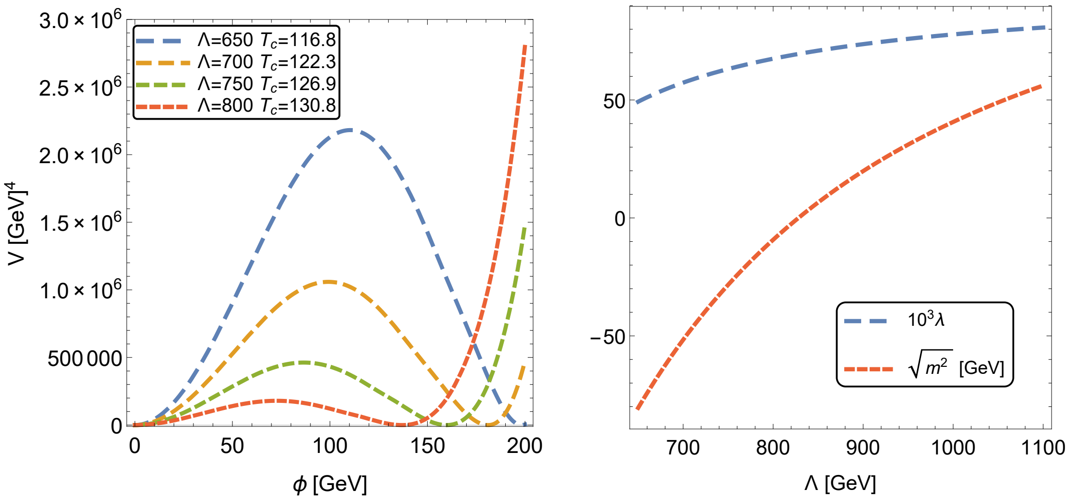

Figure 4.2: *The left panel shows examples of potentials at their critical temperatures for several values of* Λ. *The right panel depicts the values of* m *and* λ *as functions of* Λ *(all values except for the dimensionless* λ *are expressed in* GeV*).*

4.2.2 Experimental observables

While all UV complete models realizing EWBG predict various modifications of the Higgs properties, our effective theory differs from the SM only in terms of the Higgs potential. This approach is the simplest way to discuss the dynamics of the phase transition without specifying a UV completion. In the language of an effective theory, all other modifications of Higgs properties are simply unrelated. Thus, in this approach, the only modified measurable Higgs property is the triple-Higgs coupling. This observable is defined by the third derivative of the zero-temperature potential (4.4),

$$\lambda_3 = \frac{1}{6}\left.\frac{d^3V_{eff}(\phi, T=0)}{d\phi^3}\right|_{\phi=v_0}. \tag{4.9}$$

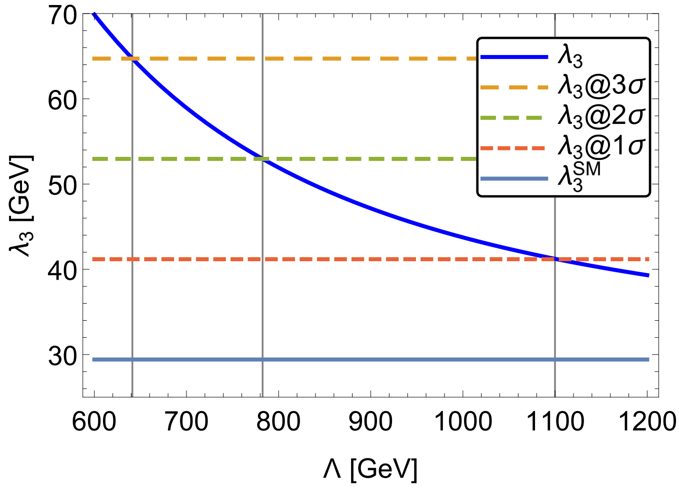

Figure 4.3: *Values of the triple Higgs coupling* λ_3 *as a function of the cutoff scale (dark blue line), along with the SM value (light blue) and HL-LHC experimental sensitivity at* 1, 2 *and* 3σ *(dashed lines). The thin vertical lines point to cutoff values corresponding to these bounds which are* $\Lambda \approx 1102, 783$ *and* 641 *GeV, respectively.*

Unfortunately this coupling can be measured only in double Higgs production events. Thus their measurement requires high-luminosity experiments, because the cross-section for producing a single Higgs boson is roughly three orders of magnitudes larger.

Even the future high-luminosity phase of the LHC (HL-LHC) will be able to determine the value of λ_3 with only about 40% accuracy [146, 147, 148, 149].

Figure 4.3 shows the value of λ_3 in our model as a function of the cutoff scale Λ, together with the SM value and the HL-LHC experimental sensitivities at 1, 2 and 3σ, respectively. As we can see, the smaller the cutoff scale (i.e., the larger the deviation from the SM), the larger the resulting λ_3 coupling. This observation allows us to explicitly calculate the reach of HL-LHC through λ_3 measurements, in terms of the cutoff scale of new physics. The resulting scales are $\Lambda \approx 1102, 783$ and 641 GeV, corresponding to 1, 2 and 3σ deviations in the measurement, respectively.

4.2.3 Dynamics of the phase transition

Below the critical temperature T_c, the minimum that breaks electroweak symmetry becomes the global minimum of the potential. This new minimum is still separated from the symmetric one by a potential barrier so the field resides in the symmetric local minimum. The phase transition proceeds via thermal tunnelling, described in terms of nucleation of bubbles of the broken phase (with non-zero vev) in the symmetric phase background. After nucleation the bubbles grow, converting false vacuum into true one, until the whole Universe transitions into the broken phase.

In the early Universe the dominant mechanism responsible for the phase transition is a high temperature sphaleron effect. We basically ask the question, what is the probability that the field will be pushed over the barrier by thermal fluctuations. First we must find the field configuration connecting the different sides of the barrier, which has the smallest action and so, requires the least energy to create. Such configuration is static, since any kinetic term contribution would be positive and could only increase the action. It is also the most symmetric one. With these assumptions the action reads

$$S_3(T) = 4\pi \int dr r^2 \left[\frac{1}{2} \left(\frac{d\phi}{dr} \right)^2 + V(\phi, T) \right] . \tag{4.10}$$

The resulting equation of motion for the field takes the form

$$\frac{d^2\phi}{dr^2} + \frac{2}{r}\frac{d\phi}{dr} + \frac{\partial V(\phi,T)}{\partial \phi} = 0. \tag{4.11}$$

The boundary conditions necessary to obtain a finite action read

$$\phi(r \to \infty) = 0 \quad \text{and} \quad \left.\frac{d\phi}{dr}\right|_{r=0} = 0, \tag{4.12}$$

then the solution describes an $O(3)$ symmetric bubble of the non-symmetric vacuum appearing in the symmetric vacuum background.

The crucial value for finding the temperature of the phase transition is the probability of nucleation of such a bubble. Assuming a Boltzmann distribution this probability per volume $\mathcal{V}$ is simply given by [150, 151]

$$\Gamma/\mathcal{V} \approx T^4 \exp\left(-\frac{S_3(T)}{T} \right), \tag{4.13}$$

Still the question at what temperature the phase transition will proceed and the bubbles will percolate also depends on the expansion rate of the Universe. We will assume that the phase transition occurs at a temperature T_n, at which at least one bubble appears in every horizon.

The usual assumption used in the literature is that for $T \approx \mathcal{O}(100\,\text{GeV})$ the Universe is dominated by radiation [152], whose energy density redshifts with scale factor a as

$$\tilde{\rho}_R = \frac{\rho_R}{a^4}. \tag{4.14}$$

Neglecting all the sub-dominant energy density components, we can solve the Friedmann equation (see Appendix A)

$$H^2 = \left(\frac{\dot{a}}{a} \right)^2 = \frac{8\pi}{3M_p^2} \frac{\rho_R}{a^4}, \tag{4.15}$$

and calculate the volume of the Universe as

$$\mathcal{V}_H(T) = \left(a \int \frac{dt}{a} \right)^3 = 8\zeta^3 \frac{M_p^3}{T^6}, \tag{4.16}$$

where $\zeta = \frac{1}{4\pi}\sqrt{\frac{45}{\pi g_*}} \approx 2\times10^{-3}$, assuming the SM number of degrees of freedom $g_* = 106.75$, which is approximately constant in the range of temperatures we are considering. Using (4.13), our condition for one bubble to be nucleated within each horizon then translates to

$$\int_{T_n}^{\infty} \Gamma dT = \int_{T_n}^{\infty} \frac{dT}{T}\left(\frac{2\zeta M_p}{T}\right)^4 \exp\left(-\frac{S_3(T)}{T}\right) = 1. \tag{4.17}$$

We are now ready to calculate the nucleation temperature. We first numerically find the bubble profiles (4.11) using an overshoot/undershoot algorithm. The procedure is identical to the one discussed in the SM vacuum instability case discussed in the previous Chapter in Section 3.2.3. In fact the EOMs we now solve differ only by a constant coefficient, and the boundary conditions are identical. This allows us to determine the action $S_3(T)$ via (4.10) as a function of temperature. Finally, we can integrate (4.17) to find the nucleation temperature T_n for all values of the cutoff scale Λ. Figure 4.4 shows an example of this procedure for $\Lambda = 750\,\mathrm{GeV}$. Left panel shows numerically obtained $S(T)/T$ function while right panel shows the corresponding potential in appropriate temperature range. Above

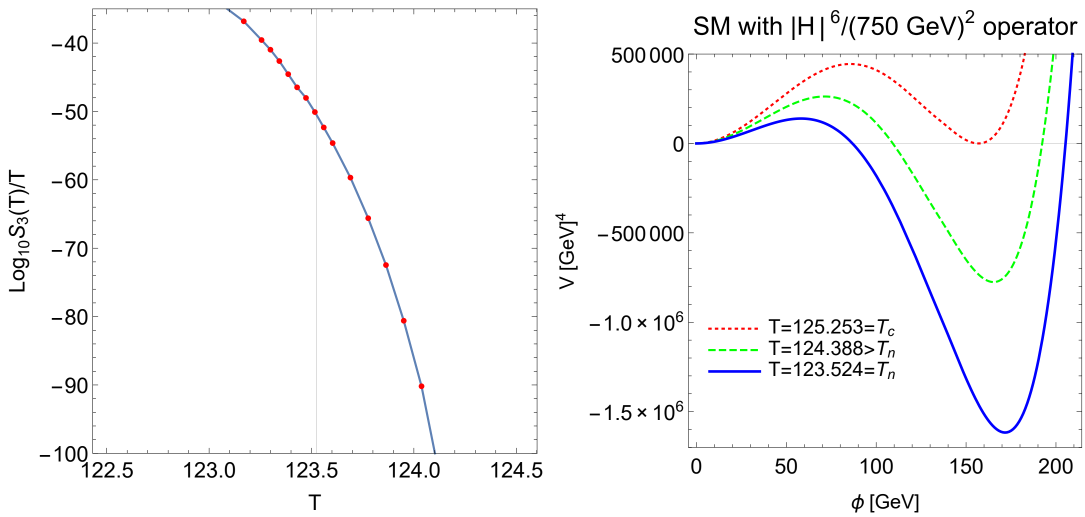

Figure 4.4: *Left panel: Numerically obtained $S(T)/T$ function, red points are results of the overshot/undershoot algorithm and the blue line results from interpolation between them. the vertical line shows the resulting nucleation temperature. Right panel: The corresponding potential in appropriate temperature range*

results clearly rely on our assumptions concerning radiation domination. Our next step will be introduction of a modification of the cosmological history.

4.2.4 Modification of the cosmological history

Now we will generalize the calculation from the previous section by including a modified expansion epoch before the usual radiation-dominated epoch. Our generalised cosmological model simply assumes a new energy density constituent ρ_S which redshifts faster than radiation, namely

$$\tilde{\rho}_S = \frac{\rho_S}{a^n}, \tag{4.18}$$

with $n > 4$. As we move towards earlier times, the new component quickly dominates the total energy density. Thus, at EWBG we can use a simplified Friedmann equation (see Appendix A), including only the new dominating component

$$H^2 = \left(\frac{\dot{a}}{a}\right)^2 = \frac{8\pi}{3M_p^2}\frac{\rho_S}{a^n}. \tag{4.19}$$

We performed the full calculation in which we include both radiation and the new component. However, the results can only be expressed using special functions, and we have found that the correction coming from not including the radiation component is completely negligible. Thus, for the sake of clarity we will present only the simplified calculation. Assuming that the new energy component does not interact with SM degrees of freedom, we can use the standard relationship between temperature and scale factor, namely

$$\tilde{\rho}_R = \frac{\rho_R}{a^4} = \frac{\pi^2}{30} g_* T^4, \tag{4.20}$$

which allows us to obtain the scale factor as a function of temperature. Analogously to the previous subsection, we now calculate the horizon volume

$$\mathcal{V}_H(T) = \left(a\int\frac{dt}{a}\right)^3 = \frac{M_p^3 2^{\frac{3}{8}(5n-4)}\left(\frac{\pi}{3}\right)^{\frac{3(n-4)}{8}}\xi^{\frac{3n}{4}}{\rho_R}^{3n/8}}{(n-2)^3 T^{\frac{3n}{2}}{\rho_S}^{3/2}}. \tag{4.21}$$

Using (4.13), the condition for one bubble to be nucleated within each horizon now reads

$$\int_{T_n}^{\infty}\Gamma dT = \int_{T_n}^{\infty}\frac{dT}{T}\frac{M_p^4 2^{\frac{5n-6}{2}}\left(\frac{3}{\pi}\right)^{\frac{4-n}{2}}\xi^n {\rho_R}^{\frac{n}{2}}}{(n-2)^3 T^{2n-4}{\rho_S}^2}\exp\left(-\frac{S_3(T)}{T}\right) = 1. \tag{4.22}$$

Our goal is to parametrize the cosmological modification. We are able to do this using the Friedmann equation, that allows us to express the new energy density as a function of the ratio of the modified Hubble parameter to the standard radiation-dominated case H/H_R, as follows

$$\rho_S = \left(\left(\frac{H}{H_R}\right)^2 - 1\right)\rho_R\left(\frac{\pi^2 T^4}{30}\right)^{\frac{n-4}{4}}\left(\frac{\rho_R}{g_*}\right)^{\frac{4-n}{4}} \quad , \quad \rho_R = \frac{\pi^2}{30}g_* T^4. \tag{4.23}$$

From now on we will use H/H_R as a measure of modification of cosmology. Of course there are also experimental bounds we can put on such modification and consequently on H/H_R. We will discuss these bounds in the next section.

Our next step is determination of the nucleation temperature. The steps are identical as those described in the previous subsection except for using (4.22) instead of (4.17). Figure 4.5 shows the resulting critical temperature T_c and the nucleation temperature T_n, as well as the ratio of the Higgs vev $v(T) := \langle \phi(T) \rangle$ to those temperatures, $v(T_c)/T_c$ and $v(T_n)/T_n$, as functions of the cutoff scale Λ, for the radiation-dominated case ($H = H_R$) and $n = 6$ (as for SFDM-domination) with $H = 10^3 H_R$ and $H = 10^6 H_R$, respectively. Also, values of the ratio of the vev to temperature $(v/T)_{\rm Sph}$ required in each of these cases by the sphaleron freeze-out which we will discuss in Subsection 4.2.6 are marked in the right panel.

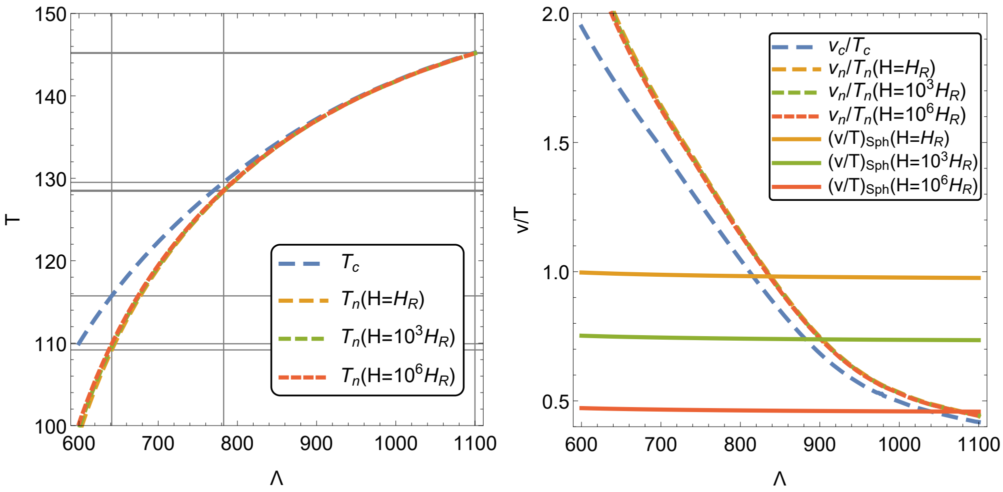

Figure 4.5: *left panel: The critical and nucleation temperatures (T_c and T_n) of our model with $n = 6$. The thin vertical lines highlight cutoff scales corresponding to experimental sensitivities, as shown in Figure 4.3, while the horizontal lines point to the temperatures corresponding to these values of Λ. Right panel: The ratios of vevs to the temperatures ($v(T_c)/T_c$ and $v(T_n)/T_n$), as a function of Λ (dashed lines). Also indicated are the sphaleron bounds on v/T for different expansion rates, as described in Sec.4.2.6 (solid lines).*

In the literature T_n is often approximated by T_c which does not require the computationally complicated nucleation calculation. The modification due to the proper calculation of the nucleation temperature can change the resulting bounds significantly, since the difference between these cases increases with the importance of the modification, which is largest in the most interesting range of small cutoff scales. However, the correction in (4.22) due to the modified expansion rate only appears in the factor in front of the exponential. Therefore, the results are nearly identical for very different ratios of H/H_R and different values of n.

4.2.5 Experimental bounds on cosmological modification

In this section, we will derive very generic bounds which have to be respected by cosmological models. These bounds come from our knowledge of the nucleosynthesis. Obtaining observed abundances of light elements precisely defines when the neutrons have to move out of thermal equilibrium to then recombine with protons and recreate observed abundances of light elements. We know this result quite precisely since neutrons decay very fast as long as they remain in equilibrium and interact with other particles. This practically gives us the expansion rate at the time of nucleosynthesis (see e.g. [153, 63]). However current measurements allow for some additional energy density components [154], traditionally given in terns of effective number of neutrinos. We start by translating this number the modification of the Hubble rate [155],

$$\left.\frac{H}{H_R}\right|_{\rm BBN} = \sqrt{1 + \frac{7}{43}\Delta N_{\nu_{\rm eff}}}. \tag{4.24}$$

We will assume $\Delta N_{\nu_{\rm eff}}$ is the difference between the SM radiation contribution $N = 3.046$ and the observed central value $N_{\nu_{\rm eff}} = 3.28$ from [153, 63] which corresponds to $H/H_R|_{\rm BBN} = 1.0187$. It is straightforward to calculate $H_{R,\rm BBN}$ using (4.20),

$$\rho_{R,\rm BBN} = \frac{\pi^2}{30} g_{*,\rm BBN} T_{\rm BBN}^4 \tag{4.25}$$

and the SM values, $T_{\rm BBN} = 1\,\text{MeV}$ and $g_{*,\rm BBN} = 43/4$.

The next step is to simply compute the energy density of the new component at the EWBG scale. We assume that $\rho_{R,\rm BBN}$ is composed of the SM radiation, while the remaining contribution corresponds to the new component $\rho_{S,\rm BBN}$. Again since the new componen quickly dominates in earlier times using the simplified Friedmann equation (4.19), we calculate H/H_R at the electroweak phase transition

$$\frac{H}{H_R} = \frac{1}{H_R}\sqrt{\frac{8\pi}{3M_p^2}\rho_{S,\rm BBN}\left(\frac{a_{\rm BBN}}{a}\right)^n} = \sqrt{\left(\left.\frac{H}{H_R}\right|_{\rm BBN}\right)^2 - 1}\left(\frac{T_{\rm BBN}}{T_n}\right)^{\frac{4-n}{2}}\left(\frac{g_{*,\rm BBN}}{g_*}\right)^{\frac{1-2n}{4}}. \tag{4.26}$$

As before, all values without subscript BBN should be calculated at T_n. The resulting maximal modification of the expansion rate for different cosmological models in the interesting temperature range $T \in [100, 150]$ GeV is shown in Figure 4.6. For the $n = 6$ example, this corresponds to a maximal H/H_R ratio between 6×10^5 and 9×10^5. This particular value of n is interesting because most of the usual models assuming the new energy density comes from a scalar field predict this value[156, 157, 143]. Above this value the speed of sound in the new medium would exceed the speed of sound if we assumed it is perfect fluid, so a more contrived explanation would be needed.

4.2.6 Modification of the sphaleron bound

We will not discuss the production of baryons during the phase transition, but rather the necessary condition for the baryon asymmetry not to be washed out after the phase transition. While the $SU(2)$ sphalerons can generate baryon asymmetry during the phase transition [21], they also dilute it after the phase transition is completed, and the system is returning to thermal equilibrium.

The $SU(2)$ sphalerons are suppressed in the broken phase due to the W bosons obtaining mass, and the weak interactions being able to act only on very short distances.

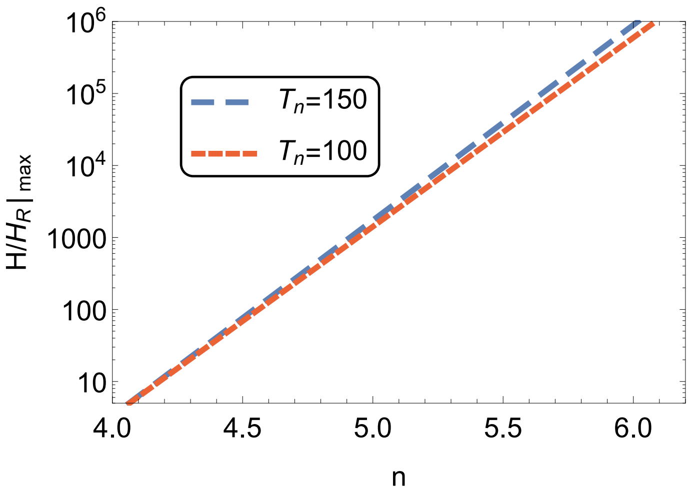

Figure 4.6: Maximal modification of the Hubble parameter calculated at the nucleation temperatures $T_n = 100$ GeV and $T_n = 150$ GeV, as a function of the parameter n which determines our cosmological model.

Hence, this suppression is proportional to the gauge boson masses and consequently to the Higgs vev right after the phase transition. If the barrier separating the vacua is too thin and the broken phase vev is too small, all the generated asymmetry can be washed out. This gives rise to the famous sphaleron bound usually expressed as [152]

$$\frac{v}{T} \gtrsim 1\,, \tag{4.27}$$

where the precise value varies in the literature depending on the approximations used in a particular paper.

Here we will use simple criterion for sphaleron freeze-out obtained by assuming that the sphaleron processes decouple when their rate becomes smaller than the expansion rate of the Universe, i.e., when $\Gamma \lessapprox H$. The sphaleron rate is given by [152]

$$\Gamma = 2.8 \times 10^5 T^4 \kappa \frac{g}{4\pi} \left(\frac{v}{T}\right)^7 \exp\left(-\frac{E_{\text{sph}}}{T}\right), \tag{4.28}$$

where the parameter κ is the functional determinant associated with fluctuations about the sphaleron. This parameter has been estimated to be in the range $10^{-4} \lesssim \kappa \lesssim 10^{-1}$.

The sphaleron energy E_{sph} is modified due to the cutoff Λ [140]. Due to the exponential dependence of the sphaleron rate on the energy, this can have a significant impact on the bounds we can place on Λ. In order to accurately calculate the sphaleron energy we find the sphaleron solution. We start with the ansatz [158] for the $SU(2)$ gauge field W and the scalar field ϕ,

$$W_i^a \sigma^a dx^i = -\frac{2i}{g} f(\xi) dU\, U^{-1}, \quad \phi = \frac{v_0}{\sqrt{2}} h(\xi) U \begin{pmatrix} 0 \\ 1 \end{pmatrix},$$

$\xi \to 0$	$\xi \to \infty$
$f \approx \xi^2/a_0^2$	$f \approx 1 - a_\infty \exp(-\xi/2)$
$h \approx \xi/b_0$	$h \approx 1 - (b_\infty/\xi)\exp(-\sqrt{\frac{2\lambda}{g^2}}\xi)$

Table 4.1: Analytic solutions of the asymptotic equations of motion (4.30) describing the sphaleron solution near the boundaries.

where $\xi = gv_0 r$, σ^a are the Pauli matrices and $U = \frac{1}{r}\begin{pmatrix} z & x+iy \\ -x+iy & z \end{pmatrix}$, while f and h are unknown functions of the single variable ξ. We will compute only the $SU(2)$ sphaleron, neglecting small corrections from $U(1)_Y$, as in [158]. With the above assumptions, the action of the sphaleron reads $E_{sph} = (4\pi v_0/g)E_0$ with

$$E_0 = \int_0^\infty d\xi \left(4f'^2 + \frac{8}{\xi^2}f^2(1-f)^2 + \frac{1}{2}\xi^2 h'^2 + h^2(1-f)^2 + \frac{\lambda}{4g^2}\xi^2(h^2-1)^2 + \frac{v_0^2}{8g^2\Lambda^2}\xi^2(h^2-1)^3\right). \tag{4.29}$$

Varying this action, we find the field equations for the functions f and h,

$$\begin{aligned} \xi^2\frac{d^2 f}{d\xi^2} &= 2f(1-f)(1-2f) - \frac{\xi^2}{4}h^2(1-f) \\ \frac{d}{d\xi}\left[\xi^2\frac{dh}{d\xi}\right] &= 2h(1-f)^2 + \frac{\lambda}{g^2}\xi^2(h^2-1)h + \frac{3}{4}\frac{v_0^2}{g^2\Lambda^2}\xi^2 h(h^2-1)^2. \end{aligned} \tag{4.30}$$

These are subject to the boundary conditions $f(0) = h(0) = 0$ and $f(\infty) = h(\infty) = 1$. In order to find the exact solutions, we start with the analytical solutions of the asymptotic equations, valid near the boundaries as shown in Table 4.1. Using these solutions to find our initial conditions at a certain very small and very large value of ξ, we numerically solve the full equations to a certain ξ_{match} where we compare the two solutions. Our procedure consists of randomly varying the initial parameters a_0, b_0, a_∞ and b_∞ and updating them if solutions with the new values match more closely. When both functions and their derivatives at ξ_{match} match with an accuracy of 10^{-6}, we consider the equations solved, and use that solution to calculate the resulting sphaleron energy, $E_{\rm sph} = (4\pi v/g)E_0$ from (4.29). Figure 4.7 shows the resulting sphaleron solutions for $\Lambda = 500\,\mathrm{GeV}$ and $\Lambda = 2000\,\mathrm{GeV}$ as well as the plot of resulting E_0 as a function of Λ. The solutions are nearly identical for very different cutoff scales shown. This is also reflected in the energy as E_0 changes only by a few percent over the whole range of Λ of interest to us.

We now have all the elements to rewrite the freeze-out condition $\Gamma \leq H$ as

$$\frac{v}{T} \geq \frac{g}{4\pi E_0}\ln\left(\frac{2.8\times 10^5 \kappa \frac{g}{4\pi}\left(\frac{v}{T}\right)^7}{H}\right), \tag{4.31}$$

where H is the Hubble rate calculated at the nucleation temperature T_n when the phase transition ends. We will choose $\kappa = 10^{-1}$, which gives the most stringent constraints. Figure 4.8 shows the resulting bound on v/T. For $H = H_R$ we obtain the standard sphaleron

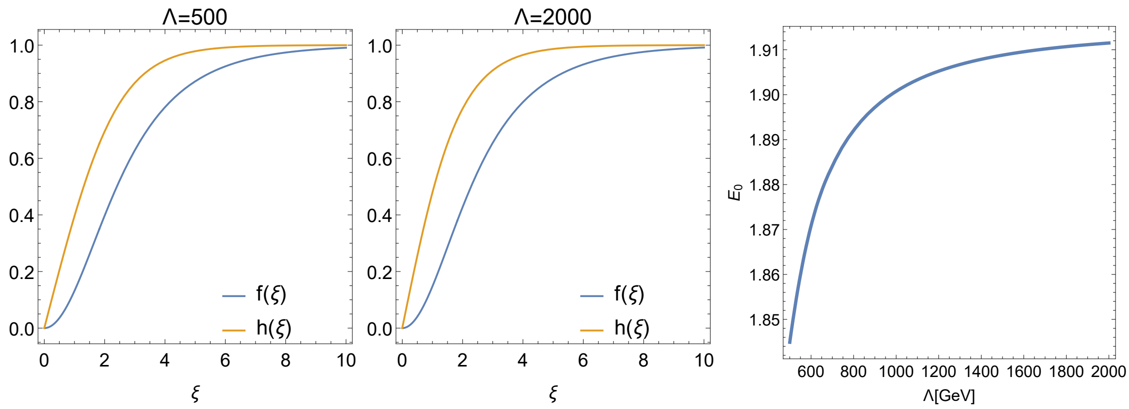

Figure 4.7: *$SU(2)$ phaleron solutions for* $\Lambda = 500\,\mathrm{GeV}$ *(left panel) and* $\Lambda = 2000\,\mathrm{GeV}$ *(middle panel) and E_0 as a function of Λ (right panel)*

bound (4.27) yet this bound lowers quickly and for $H = 10^6 H_R$ the required value is less than half of that value. Thus for perfectly reasonable and acceptable experimentally value of the expansion rate the bounds can be changed very significantly. We also show two different bounds due to the weak dependence of E_0 on Λ, however the difference between them is not significant.

We are finally in position to combine the v/T value required to decouple the sphalerons and preserve the asymmetry (4.31) with the v/T value we obtain as a function of the cutoff from Figure 4.5, along with the experimental constraints on the cutoff from Figure 4.3. Thus, we can determine the scale of new physics required to preserve the asymmetry as a function of the modified expansion rate H/H_R. We can also translate the maximal possible modification of the Hubble rate, discussed in Section 4.2.5, to an explicit bound on Λ for a wide class of cosmological models. Figure 4.9 shows the required value of Λ as a function of n, along with the experimental constraints, and the specific cosmological example for $n = 6$.

Our key result is that for $n = 6$, the minimal Λ required by the sphaleron bound is already very close to the value required for the first order phase transition (as discussed in Section 4.2.1). Thus, the modified cosmological history allows us to circumvent the sphaleron bound altogether, and the only bound given by current experiments is equivalent to the requirement of departure from thermal equilibrium.

4.3 Summary

In this chapter we studied the implications of a modified cosmological history for the electroweak baryogenesis scenario. We adopted a generic model in which the Higgs potential is modified by a non-renormalizable dimension six operator, suppressed by an appropriate new mass scale Λ.

We discussed a very generic model of cosmological modification with a single new energy density component which does not interact with SM degrees of freedom.

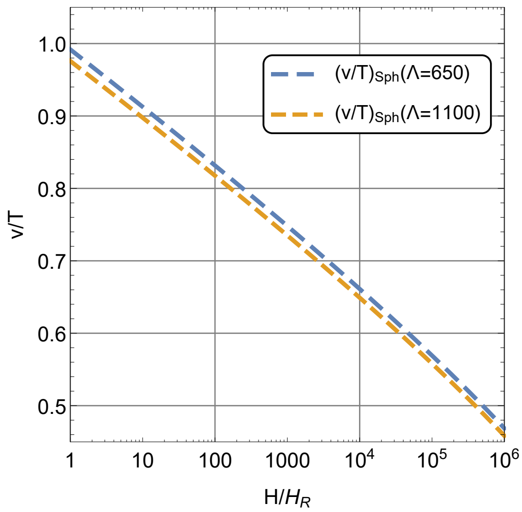

Figure 4.8: *Minimal value of v/T required to avoid wash-out of baryon asymmetry, as a function of the modified expansion rate H/H_R for several values of the cutoff Λ.*

We carefully computed the temperature at which the phase transition takes place, instead of using the approximation coming from the critical temperature, often used in the literature. This allowed us to include small corrections to the nucleation temperature due to a modification of the cosmological history. In all, using the nucleation temperature in the full calculation, rather than the critical temperature approximation, can change the final results significantly for the allowed parameter space.

Next, we described the modification of Standard Model $SU(2)$ sphalerons. This is the main source of modification resulting from the increased expansion rate. A higher expansion rate leads to a more readily achieved freeze-out of the sphalerons, thus preserving any baryons remaining after the phase transition. This in turn increases the scale of new physics Λ which is required for successful baryogenesis.

We find that this modification of the required Λ's, while numerically seemingly small (about 20% for $\rho_S \propto a^{-6}$), actually means circumventing the sphaleron bound altogether, because it brings us to the cutoff values required for a first order phase transition to begin with. The value $n = 6$, proves to be very interesting, since this is the smallest value allowing us to avoid the sphaleron bound. This particular value of n is important because most of the usual models assuming the new energy density comes from a scalar field predict this value[156, 157, 143]. Above this value the speed of sound in the new medium would exceed the speed of sound if we assumed it is perfect fluid, so a more contrived explanation would be needed. However more exotic models with even higher expansion rates (i.e., whose energy density would decay even faster than $\propto a^{-6}$) would not increase the allowed parameter space much further. On the particle experimental side cosmological modification with $n = 6$ means that our model can remain consistent within 1σ of the SM result, even with the bounds provided by the high luminosity stage of the LHC.

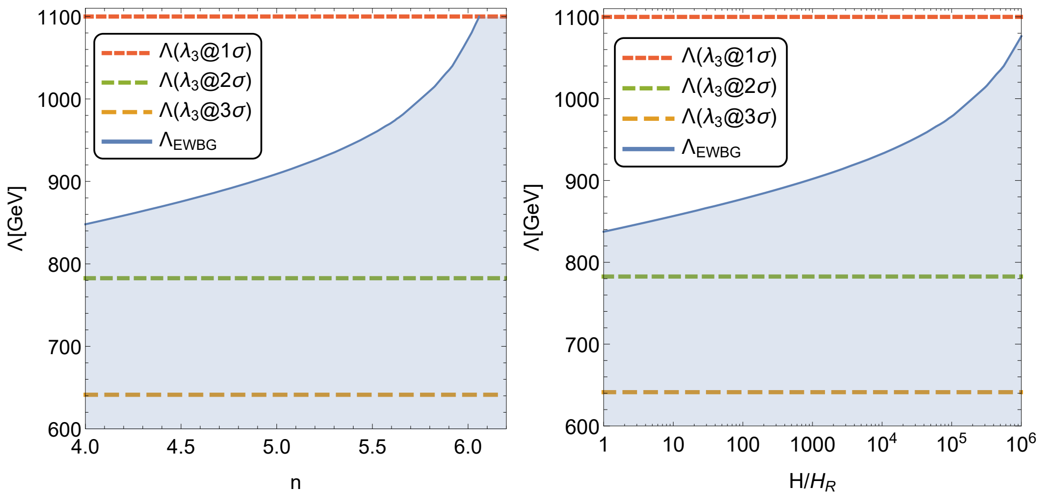

Figure 4.9: *Left panel: cutoff scale* Λ *required to preserve the baryon asymmetry (solid blue line) as a function of* n *which determines our cosmological model. Here we assumed maximal experimentally allowed assistance from cosmology. Right panel: cutoff scale* Λ *required for successful EWBG as a function of the expansion rate (solid blue curve) for* $n = 6$*. Both panels also show HL-LHC experimental constraints on* Λ *from its modification to* λ_3 *(horizontal dashed lines,* 1σ *(top) to* 3σ *(bottom)).*

Chapter 5

Summary of the thesis

Discovery of the Higgs boson has finally confirmed the Standard Model as the correct description of physics at the electroweak scale. We discussed its implications for the possible SM extensions needed at energy scales higher than the Fermi scale. Firstly, motivated by the hierarchy problem we discussed supersymmetric extensions of the SM. In our second step, taking a more pragmatic approach we discussed issues connected with vacuum stability of SM and its extension described by nonrenormalisable operators. Finally, we turned to baryon asymmetry using one of the simplest explanations utilising the electroweak phase transition itself.

5.1 Suprsymmetry

Supersymmetry remains the technically most attractive extension of the Standard Model motivated by its naturalness problem, which offers perturbativity and calculability up to the Planck scale. However, due to high Higgs boson mass, minimal realisations of such an extension suffer from a different, so called little, hierarchy problem. The issue arises because in minimal realisation of SUSY the Higgs mass is bounded from above by the Z boson mass. Raising it requires large quantum corrections which, in turn, require heavy supersymmetric particles, thus creating a new hierarchy between the electroweak scale ant the scale of superpartner masses.

We begun by discussing severity of the problem on the example of gauge mediated SUSY breaking models. These models are well motivated theoretically for example due to automatic limitation of flavour violation. However they are often believed to exhibit more severe hierarchy problem than other SUSY breaking models, due to their particular pattern of SUSY breaking parameters. Our key result was that fine-tuning in gauge mediated supersymmetry models is not larger than in a more standard gravity mediated case. The only drawback is the necessity to abandon the minimal realisation of gauge mediation in favour of more elaborate models with richer hidden sectors. Next we discussed bounds which can be put on supersymmetric theories due to one experimental result which does not fit SM prediction, namely the measurement of the anomalous magnetic moment of the muon. Assuming that SUSY is responsible for the $(g-2)_\mu$ anomaly leads to severe constraints on chargino and smuon masses. These in turn can be used to obtain a lower bound on $\tan\beta$, which we have finally translated into upper bound on the stop masses. This comes from the requirement that the predicted Higgs mass does not overshoot the experimental value. The LEP limits on the smuon and chargino masses result in an upper bound on the stop masses exceeding 10^3 TeV. However, even mild improvement of the LEP limits results in a significant improvement of this upper bound. Current LHC limits on smuon and chargino masses obtained for not too compressed gaugino and higgsino spectra reduce the upper bound on the stop masses to about 10 TeV. Future electron-positron collider operating at $\sqrt{s} = 500$ (1000) GeV would allow to set a solid upper bound on the stop masses of about 10 (5) TeV. Such stops should be discovered at the 100 TeV hadron collider. Thus our main conclusion is that, with the help of the discussed future colliders, SUSY should be discovered, if superpartners are responsible for the explanation of the $(g-2)_\mu$ anomaly. Next we turned to non-minimal supersymmetric models to verify to what extent the hierarchy problem of MSSM can be ameliorated. First we analyzed a single vectorlike top partner model, which is the simplest vectorlike extension of the MSSM. We showed that it can significantly help with the little hierarchy problem. After including all the constraints achievable at the HL-LHC, the resulting SUSY scale can be as low as 1.2 to 2.4 TeV for the simplest possible supersymmetry spectrum. These results are 3 to 5 times smaller compared to what otherwise would be allowed in the MSSM. We calculated and compared different experimental constraints the model will face after $300\,\text{fb}^{-1}$ of data are gathered at the HL-LHC. Our key result is that in majority of the parameter space the most constraining of the discussed bounds is the modification of the Higgs boson properties. Thus even a very simple vectorlike quark extension of MSSM can greatly reduce the little hierarchy problem of the MSSM, and careful measurements of Higgs boson observables would likely give first evidence of this scenario.

Our next step was modifying the minimal setup of the MSSM by introducing a large extra dimension. The biggest effect comes from the modification of the RGEs which exhibit power-like behaviour near the scale where the extra dimension becomes important. We implemented the modified RGEs for several models of the five dimensional extensions of the MSSM, into a full C++ spectrum generator, along with self energy corrections for the Higgs mass.

Our key result is showing that modified five dimensional RGEs can result in spectra very different from the usual $4D$ case. The reason is that in 5D the heavy gluino does not necessarily dominate running of other soft terms during power law running. Thus we can easily obtain maximal stop mixing and much less fine tuned spectra, even with standard sets of soft terms at the SUSY breaking scale.

This is also very interesting because in 5D models the least fine tuned spectra with correct Higgs mass can easily predict soft superpartner masses within LHC reach, even for standard patterns of soft terms. Thus in such models, the most interesting parts of the parameter space can be probed during next run of the LHC, which is not usually the case in the standard 4D case.

We also attempted creating a model of SUSY breaking predicting a more natural spectrum at the high scale utilising the extra dimension. We explored models where the

1st and 2nd generation are in the bulk and a model in which the 1st and 2nd generation is on the same brane as the supersymmetry breaking sector and the 3rd generation is located on an opposite brane, resulting in a spectrum of stops lighter than that of the other squarks. Obtaining lighter stop soft terms at the SUSY breaking scale did not result in a more natural spectrum. The reason is non negligible fine-tuning price of heavier first two generations and heavier Higgs sector which give only a subleading correction to the light Higgs mass.

The final advantage is a low scale of unification of gauge couplings and a low supersymmetry breaking scale. And also much better unification of Yukawa couplings is possible, giving hope for a very interesting five dimensional UV completion of such models.

5.2 Vacuum stability

In the next chapter we discussed and reviewed the vacuum stability issues in the Standard Model. We extended the discussion existing in the literature by explicitly finding the tunneling solution numerically, without using any analytical approximations. While the electroweak vacuum turns out to be unstable due to a new deeper minimum appearing in the potential for very large Higgs field values, the time it would take for the vacuum decay due to quantum fluctuations is much longer than the observed lifetime of the universe. Thus, while not very comforting, this situation is completely acceptable experimentally and no new physics is immediately necessary to save the consistency of the theory.

The next very interesting topic we addressed is how this situation changes once we include new physics. Our hope was to discuss as large class of models as possible and show the constraints resulting from requiring that they do not shorten the lifetime of the SM vacuum to much. To this end we focused on generic models parametrising the modification of SM using nonrenormalisable operators. We prepared a map of the vacua in the SM extended by nonrenormalisable scalar couplings also taking into account the running of the new couplings and going beyond the standard assumptions taken when calculating the lifetime of the metastable vacuum. Again we verified the correctness of quasi-analytic approximations of the effective potential widely used in the literature for calculation the tunnelling rate in modifications of SM.

In general, we also confirm that it is relatively easy to destabilise the SM, even with the help of the Planck scale suppressed scalar operators. In fact its possible to destabilise the electroweak vacuum by new interactions at any scale while making it absolutely stable requires sufficiently low cut-off scales not much larger than roughly 10^{11} GeV.

Our last step in this chapter was discussion of the impact of gravitational interactions on the vacuum decay. This issue has been discussed in the literature since the seventies. However, the curved background case is still quite poorly understood and explored as it is much more complicated than the usual flat space-time case.

We started by exploring the possible extent of such modification in a very simple and generic particle model describing a single scalar field with a simple potential. In the case when the unstable minimum has zero energy the gravitational correction usually quenches the vacuum decay due to gravitational back reaction. However the opposite effect is also possible, this happens when we have a large vacuum energy in our unstable minimum. Then the size of our de Sitter universe is finite and the size of the horizon limits the forming bubble. This affects bubbles for very small energy differences between the two vacua, which are usually very large, to overcome the wall tension with their interior negative energy contribution. Limiting the size of the bubble to the horizon volume also lowers its action accordingly.

We next turned to discussion of this impact in the SM case. The first problem in this discussion is the uncertainty of the position of the vacuum. This is an important issue since the vacuum positioned at $V \approx 10^{-120}$ introduces yet another very different scale in the problem. However we can still discuss the effect qualitatively. The SM case is similar to our toy potential with very small cosmological constant and very large separation of energies of the vacua. Thus we can safely say that the correction will be a very small increase of the action. The same conclusion comes from applying the simple thin-wall correction, also discussed in that chapter, to the SM. The simple explanation of this effect is as follows. In the SM the forming bubble is of subatomic size, vastly smaller than the scale at which the spacetime curvature becomes important or even observable. Thus our bounce is very similar to the flat spacetime case because at its scale the background is to a very good approximation flat.

5.3 Electroweak baryogenesis

In the next chapter we turned to yet another problem which is not accommodated in the SM. Namely the generation of matter anti-matter asymmetry required to correctly explain the experimental results. More specifically, we studied the implications of a modified cosmological history for the electroweak baryogenesis scenario.

On the particle physics side we adopted a generic model in which the Higgs potential is modified by a non-renormalizable dimension six operator, suppressed by an appropriate new mass scale Λ. On the cosmology side we used a generic model of cosmological modification with a single new energy density component which does not interact with SM degrees of freedom.

We carefully computed the temperature at which the phase transition takes place, instead of using the approximation coming from the critical temperature, often used in the literature. This allowed us to include corrections to the nucleation temperature due to a modification of the cosmological history. In general, using the nucleation temperature in the full calculation, rather than the critical temperature approximation, can change the final results significantly for the allowed parameter space, while the modification of said temperature from cosmological effects can safely be neglected.

Next, we described the modification of Standard Model $SU(2)$ sphalerons responsible for creation of the asymmetry during the phase transition. The same sphalerons on the other hand wash out the created asymmetry as the universe goes back to thermal equilibrium after the phase transition. This is the source of the most stringent constraint on such scenarios and also the main source of modification resulting from the increased expansion rate. A higher expansion rate leads to a more readily achieved freeze-out of the sphalerons, thus preserving any baryons remaining after the phase transition. This in turn increases the scale of new physics Λ which is required for successful baryogenesis.

We find that this modification of the required Λ's, while numerically seemingly small (about 20% for the new enegy component red-shifting as $\rho_S \propto a^{-6}$), actually means circumventing the sphaleron bound altogether, because it brings us to the cutoff values required for a first order phase transition.

The value $n = 6$ is particularly interesting, since not only it is the smallest value allowing us to avoid the sphaleron bound. It is also important because most of the typical models, assuming the new energy density comes from a scalar field, predict this value. Above this value the speed of sound in the new medium would exceed the speed of sound if we assumed it is perfect fluid, so a more contrived explanation would be needed. However more exotic models with even higher expansion rates (i.e., whose energy density would decay even faster than $\propto a^{-6}$) would not increase the allowed parameter space much further. On the particle experimental side cosmological modification with $n = 6$ means that our model can remain consistent within 1σ with the SM result, even with the bounds provided by the high luminosity stage of the LHC.

Appendix A

Introduction to FRW cosmology

We will begin our discussion with the cosmological principle, which states that, when viewed on a large enough scale, the universe is homogeneous and isotropic. Under this assumption also including the possible time dependence of the spatial component of the metric leads to the Friedman-Robertson-Walker (FRW) metric

$$ds^2 = -dt^2 + a(t)^2 \left[\frac{dr^2}{1-kr^2} dr^2 \left(d\theta^2 + \sin^2\theta d\phi^2 \right) \right] \tag{A.1}$$

where $a(t)$ is the dimensionless scale factor and k is the curvature of space. Thus the metric tensor is given by

$$g_{\mu\nu} = \left(-1, a(t)^2 \frac{dr^2}{1-kr^2}, a(t)^2 r^2, a(t)^2 r^2 \sin^2\theta d\phi^2 \right) \tag{A.2}$$

The spatial part of the metric is the most symmetric isotropic and homogeneous solution and can describe three different geometries of a spherical ($k > 0$), flat ($k = 0$), or hyperbolic ($k < 0$) space. All the physical distances change with the scale factor while the coordinate distances remain constant in time $d_{\mathrm{ph}} = a(t) d_{\mathrm{co}}$.

The matter can be described as a perfect fluid for which the energy-momentum tensor takes the form

$$T^{\mu}_{\nu} = (-\rho(t), p(t), p(t), p(t)) \tag{A.3}$$

where ρ is the density and p pressure. These also have to satisfy the continuity equation

$$\dot{\rho} + 3\frac{\dot{a}}{a}(\rho + p) \tag{A.4}$$

where a dot denotes a derivative with respect to time and we do not explicitly write out the time dependence. The last thing we need is the equation of state for our particular fluid. This is usually expressed as

$$\rho = \omega p, \tag{A.5}$$

where ω is the so called barotropic parameter. Together with the continuity equation (A.4) this gives

$$\rho \propto a^{-3(1+\omega)}, \tag{A.6}$$

and assuming that different components of the energy momentum tensor do not interact we obtain the same equation for each of them separately.

Using all above results in the Einstein equation we obtain the two Friedman equations. First of them governs the evolution of the scale factor

$$\left(\frac{\dot{a}}{a}\right)^2 = \frac{8\pi G}{3}\rho - \frac{k}{a^2} + \frac{\Lambda}{3} \tag{A.7}$$

where Λ is the cosmological constant. In the early universe case both the curvature and cosmological constant terms are much smaller than SM radiation contribution (and any additional perfect fluid) and can safely be neglected.

Bibliography

[1] Zygmunt Lalak and Marek Lewicki. Fine-tuning in GGM and the 126 GeV Higgs particle. *JHEP*, 05:125, 2013. arXiv:1302.6546, doi:10.1007/JHEP05(2013)125.

[2] Zygmunt Lalak, Marek Lewicki, and Paweł Olszewski. Higher-order scalar interactions and SM vacuum stability. *JHEP*, 05:119, 2014. arXiv:1402.3826, doi:10.1007/JHEP05(2014)119.

[3] Marcin Badziak, Zygmunt Lalak, Marek Lewicki, Marek Olechowski, and Stefan Pokorski. Upper bounds on sparticle masses from muon g-2 and the Higgs mass and the complementarity of future colliders. *JHEP*, 03:003, 2015. arXiv:1411.1450, doi:10.1007/JHEP03(2015)003.

[4] Zygmunt Lalak, Marek Lewicki, and James D. Wells. Higgs boson mass and high-luminosity LHC probes of supersymmetry with vectorlike top quark. *Phys. Rev.*, D91(9):095022, 2015. arXiv:1502.05702, doi:10.1103/PhysRevD.91.095022.

[5] Zygmunt Lalak, Marek Lewicki, and Paweł Olszewski. Hints of BSM physics in the SM effective potential. *PoS*, CORFU2014:106, 2015. arXiv:1505.05505.

[6] Zygmunt Lalak, Marek Lewicki, Moritz McGarrie, and Paweł Olszewski. Features of electroweak symmetry breaking in five dimensional SUSY models. *JHEP*, 11:137, 2015. arXiv:1508.05105, doi:10.1007/JHEP11(2015)137.

[7] Zygmunt Lalak, Marek Lewicki, and Paweł Olszewski. Standard Model vacuum stability in the presence of gauge invariant nonrenormalizable operators. In *18th International Conference From the Planck Scale to the Electroweak Scale (Planck 2015) Ioannina, Greece, May 25-29, 2015*, 2015. URL: http://inspirehep.net/record/1397189/files/arXiv:1510.02797.pdf, arXiv:1510.02797.

[8] Marek Lewicki, Tanja Rindler-Daller, and James D. Wells. Enabling Electroweak Baryogenesis through Dark Matter. *JHEP*, 06:055, 2016. arXiv:1601.01681, doi:10.1007/JHEP06(2016)055.

[9] S. L. Glashow. Partial Symmetries of Weak Interactions. *Nucl. Phys.*, 22:579–588, 1961. doi:10.1016/0029-5582(61)90469-2.

[10] Steven Weinberg. A Model of Leptons. *Phys. Rev. Lett.*, 19:1264–1266, 1967. doi:10.1103/PhysRevLett.19.1264.

[11] Abdus Salam. Weak and Electromagnetic Interactions. *Conf. Proc.*, C680519:367–377, 1968.

[12] Peter W. Higgs. Broken symmetries, massless particles and gauge fields. *Phys. Lett.*, 12:132–133, 1964. doi:10.1016/0031-9163(64)91136-9.

[13] F. Englert and R. Brout. Broken Symmetry and the Mass of Gauge Vector Mesons. *Phys. Rev. Lett.*, 13:321–323, 1964. doi:10.1103/PhysRevLett.13.321.

[14] G. S. Guralnik, C. R. Hagen, and T. W. B. Kibble. Global Conservation Laws and Massless Particles. *Phys. Rev. Lett.*, 13:585–587, 1964. doi:10.1103/PhysRevLett.13.585.

[15] Georges Aad et al. Observation of a new particle in the search for the Standard Model Higgs boson with the ATLAS detector at the LHC. *Phys. Lett.*, B716:1–29, 2012. arXiv:1207.7214, doi:10.1016/j.physletb.2012.08.020.

[16] Serguei Chatrchyan et al. Observation of a new boson at a mass of 125 GeV with the CMS experiment at the LHC. *Phys. Lett.*, B716:30–61, 2012. arXiv:1207.7235, doi:10.1016/j.physletb.2012.08.021.

[17] Sidney R. Coleman and Erick J. Weinberg. Radiative Corrections as the Origin of Spontaneous Symmetry Breaking. *Phys. Rev.*, D7:1888–1910, 1973. doi:10.1103/PhysRevD.7.1888.

[18] J. A. Casas, J. R. Espinosa, and M. Quiros. Improved Higgs mass stability bound in the standard model and implications for supersymmetry. *Phys. Lett.*, B342:171–179, 1995. arXiv:hep-ph/9409458, doi:10.1016/0370-2693(94)01404-Z.

[19] T. P. Cheng, E. Eichten, and Ling-Fong Li. Higgs Phenomena in Asymptotically Free Gauge Theories. *Phys. Rev.*, D9:2259, 1974. doi:10.1103/PhysRevD.9.2259.

[20] V. A. Kuzmin, V. A. Rubakov, and M. E. Shaposhnikov. On the Anomalous Electroweak Baryon Number Nonconservation in the Early Universe. *Phys. Lett.*, B155:36, 1985. doi:10.1016/0370-2693(85)91028-7.

[21] Andrew G. Cohen, D. B. Kaplan, and A. E. Nelson. Progress in electroweak baryogenesis. *Ann. Rev. Nucl. Part. Sci.*, 43:27–70, 1993. arXiv:hep-ph/9302210, doi:10.1146/annurev.ns.43.120193.000331.

[22] Antonio Riotto and Mark Trodden. Recent progress in baryogenesis. *Ann. Rev. Nucl. Part. Sci.*, 49:35–75, 1999. arXiv:hep-ph/9901362, doi:10.1146/annurev.nucl.49.1.35.

[23] David E. Morrissey and Michael J. Ramsey-Musolf. Electroweak baryogenesis. *New J. Phys.*, 14:125003, 2012. arXiv:1206.2942, doi:10.1088/1367-2630/14/12/125003.

[24] A. D. Sakharov. Violation of CP Invariance, c Asymmetry, and Baryon Asymmetry of the Universe. *Pisma Zh. Eksp. Teor. Fiz.*, 5:32–35, 1967. [Usp. Fiz. Nauk161,61(1991)]. doi:10.1070/PU1991v034n05ABEH002497.

[25] Peter Brockway Arnold and Olivier Espinosa. The Effective potential and first order phase transitions: Beyond leading-order. *Phys. Rev.*, D47:3546, 1993. [Erratum: Phys. Rev.D50,6662(1994)]. arXiv:hep-ph/9212235, doi:10.1103/PhysRevD.50.6662,10.1103/PhysRevD.47.3546.

[26] K. Kajantie, M. Laine, K. Rummukainen, and Mikhail E. Shaposhnikov. A Nonperturbative analysis of the finite T phase transition in SU(2) x U(1) electroweak theory. *Nucl. Phys.*, B493:413–438, 1997. arXiv:hep-lat/9612006, doi:10.1016/S0550-3213(97)00164-8.

[27] Timothy Cohen, David E. Morrissey, and Aaron Pierce. Electroweak Baryogenesis and Higgs Signatures. *Phys. Rev.*, D86:013009, 2012. arXiv:1203.2924, doi:10.1103/PhysRevD.86.013009.

[28] Andrey Katz and Maxim Perelstein. Higgs Couplings and Electroweak Phase Transition. *JHEP*, 07:108, 2014. arXiv:1401.1827, doi:10.1007/JHEP07(2014)108.

[29] Sidney R. Coleman and J. Mandula. All Possible Symmetries of the S Matrix. *Phys. Rev.*, 159:1251–1256, 1967. doi:10.1103/PhysRev.159.1251.

[30] Rudolf Haag, Jan T. Lopuszanski, and Martin Sohnius. All Possible Generators of Supersymmetries of the s Matrix. *Nucl. Phys.*, B88:257, 1975. doi:10.1016/0550-3213(75)90279-5.

[31] J. Wess and B. Zumino. A Lagrangian Model Invariant Under Supergauge Transformations. *Phys. Lett.*, B49:52, 1974. doi:10.1016/0370-2693(74)90578-4.

[32] J. Wess and J. Bagger. *Supersymmetry and supergravity.* 1992.

[33] Stephen P. Martin. A Supersymmetry primer. 1997. [Adv. Ser. Direct. High Energy Phys.18,1(1998)]. arXiv:hep-ph/9709356, doi:10.1142/9789812839657_0001,10.1142/9789814307505_0001.

[34] Giorgio Gamberini, Giovanni Ridolfi, and Fabio Zwirner. On Radiative Gauge Symmetry Breaking in the Minimal Supersymmetric Model. *Nucl. Phys.*, B331:331–349, 1990. doi:10.1016/0550-3213(90)90211-U.

[35] John R. Ellis, Giovanni Ridolfi, and Fabio Zwirner. Radiative corrections to the masses of supersymmetric Higgs bosons. *Phys. Lett.*, B257:83–91, 1991. doi:10.1016/0370-2693(91)90863-L.

[36] Piotr H. Chankowski, John R. Ellis, Marek Olechowski, and Stefan Pokorski. Haggling over the fine tuning price of LEP. *Nucl. Phys.*, B544:39–63, 1999. arXiv:hep-ph/9808275, doi:10.1016/S0550-3213(99)00025-5.

[37] B.C. Allanach. SOFTSUSY: a program for calculating supersymmetric spectra. *Comput.Phys.Commun.*, 143:305–331, 2002. arXiv:hep-ph/0104145, doi:10.1016/S0010-4655(01)00460-X.

[38] Werner Porod. SPheno, a program for calculating supersymmetric spectra, SUSY particle decays and SUSY particle production at e+ e- colliders. *Comput.Phys.Commun.*, 153:275–315, 2003. arXiv:hep-ph/0301101, doi:10.1016/S0010-4655(03)00222-4.

[39] Abdelhak Djouadi, Jean-Loic Kneur, and Gilbert Moultaka. SuSpect: A Fortran code for the supersymmetric and Higgs particle spectrum in the MSSM. *Comput.Phys.Commun.*, 176:426–455, 2007. arXiv:hep-ph/0211331, doi:10.1016/j.cpc.2006.11.009.

[40] L.V. Avdeev and M. Yu. Kalmykov. Pole masses of quarks in dimensional reduction. *Nucl.Phys.*, B502:419–435, 1997. arXiv:hep-ph/9701308, doi:10.1016/S0550-3213(97)00404-5.

[41] Damien M. Pierce, Jonathan A. Bagger, Konstantin T. Matchev, and Renjie Zhang. Precision corrections in the minimal supersymmetric standard model. *Nucl.Phys.*, B491:3–67, 1997. arXiv:hep-ph/9606211, doi:10.1016/S0550-3213(96)00683-9.

[42] Peter Z. Skands, B.C. Allanach, H. Baer, C. Balazs, G. Belanger, et al. SUSY Les Houches accord: Interfacing SUSY spectrum calculators, decay packages, and event generators. *JHEP*, 0407:036, 2004. arXiv:hep-ph/0311123, doi:10.1088/1126-6708/2004/07/036.

[43] Howard Baer, Javier Ferrandis, Kirill Melnikov, and Xerxes Tata. Relating bottom quark mass in DR-BAR and MS-BAR regularization schemes. *Phys.Rev.*, D66:074007, 2002. arXiv:hep-ph/0207126, doi:10.1103/PhysRevD.66.074007.

[44] Youichi Yamada. Two loop renormalization of tan beta and its gauge dependence. *Phys.Lett.*, B530:174–178, 2002. arXiv:hep-ph/0112251, doi:10.1016/S0370-2693(02)01324-2.

[45] Athanasios Dedes and Pietro Slavich. Two loop corrections to radiative electroweak symmetry breaking in the MSSM. *Nucl.Phys.*, B657:333–354, 2003. arXiv:hep-ph/0212132, doi:10.1016/S0550-3213(03)00173-1.

[46] Athanasios Dedes, Giuseppe Degrassi, and Pietro Slavich. On the two loop Yukawa corrections to the MSSM Higgs boson masses at large tan beta. *Nucl.Phys.*, B672:144–162, 2003. arXiv:hep-ph/0305127, doi:10.1016/j.nuclphysb.2003.08.033.

[47] A. Brignole, G. Degrassi, P. Slavich, and F. Zwirner. On the two loop sbottom corrections to the neutral Higgs boson masses in the MSSM. *Nucl.Phys.*, B643:79–92, 2002. arXiv:hep-ph/0206101, doi:10.1016/S0550-3213(02)00748-4.

[48] Andrea Brignole, Giuseppe Degrassi, Pietro Slavich, and Fabio Zwirner. On the O(alpha(t)**2) two loop corrections to the neutral Higgs boson masses in the MSSM. *Nucl.Phys.*, B631:195–218, 2002. arXiv:hep-ph/0112177, doi:10.1016/S0550-3213(02)00184-0.

[49] Giuseppe Degrassi, Pietro Slavich, and Fabio Zwirner. On the neutral Higgs boson masses in the MSSM for arbitrary stop mixing. *Nucl.Phys.*, B611:403–422, 2001. arXiv:hep-ph/0105096, doi:10.1016/S0550-3213(01)00343-1.

[50] J.M. Frere, D.R.T. Jones, and S. Raby. Fermion Masses and Induction of the Weak Scale by Supergravity. *Nucl.Phys.*, B222:11, 1983. doi:10.1016/0550-3213(83)90606-5.

[51] Luis Alvarez-Gaume, J. Polchinski, and Mark B. Wise. Minimal Low-Energy Supergravity. *Nucl.Phys.*, B221:495, 1983. doi:10.1016/0550-3213(83)90591-6.

[52] J.P. Derendinger and Carlos A. Savoy. Quantum Effects and SU(2) x U(1) Breaking in Supergravity Gauge Theories. *Nucl.Phys.*, B237:307, 1984. doi:10.1016/0550-3213(84)90162-7.

[53] C. Kounnas, A.B. Lahanas, Dimitri V. Nanopoulos, and M. Quiros. Low-Energy Behavior of Realistic Locally Supersymmetric Grand Unified Theories. *Nucl.Phys.*, B236:438, 1984. doi:10.1016/0550-3213(84)90545-5.

[54] Mark Claudson, Lawrence J. Hall, and Ian Hinchliffe. Low-Energy Supergravity: False Vacua and Vacuous Predictions. *Nucl.Phys.*, B228:501, 1983. doi:10.1016/0550-3213(83)90556-4.

[55] Patrick Meade, Nathan Seiberg, and David Shih. General Gauge Mediation. *Prog. Theor. Phys. Suppl.*, 177:143–158, 2009. arXiv:0801.3278, doi:10.1143/PTPS.177.143.

[56] Linda M. Carpenter, Michael Dine, Guido Festuccia, and John D. Mason. Implementing General Gauge Mediation. *Phys. Rev.*, D79:035002, 2009. arXiv:0805.2944, doi:10.1103/PhysRevD.79.035002.

[57] G. W. Bennett et al. Final Report of the Muon E821 Anomalous Magnetic Moment Measurement at BNL. *Phys. Rev.*, D73:072003, 2006. arXiv:hep-ex/0602035, doi:10.1103/PhysRevD.73.072003.

[58] Michel Davier, Andreas Hoecker, Bogdan Malaescu, and Zhiqing Zhang. Reevaluation of the Hadronic Contributions to the Muon g-2 and to alpha(MZ). *Eur. Phys. J.*, C71:1515, 2011. [Erratum: Eur. Phys. J.C72,1874(2012)]. arXiv:1010.4180, doi:10.1140/epjc/s10052-012-1874-8,10.1140/epjc/s10052-010-1515-z.

[59] Kaoru Hagiwara, Ruofan Liao, Alan D. Martin, Daisuke Nomura, and Thomas Teubner. (g-2) and alpha(MZ2) re-evaluated using new precise data. *J. Phys.*, G38:085003, 2011. arXiv:1105.3149, doi:10.1088/0954-3899/38/8/085003.

[60] M. Benayoun, P. David, L. DelBuono, and F. Jegerlehner. An Update of the HLS Estimate of the Muon g-2. *Eur. Phys. J.*, C73:2453, 2013. arXiv:1210.7184, doi:10.1140/epjc/s10052-013-2453-3.

[61] Takeo Moroi. The Muon anomalous magnetic dipole moment in the minimal supersymmetric standard model. *Phys. Rev.*, D53:6565–6575, 1996. [Erratum: Phys. Rev.D56,4424(1997)]. arXiv:hep-ph/9512396, doi:10.1103/PhysRevD.53.6565, 10.1103/PhysRevD.56.4424.

[62] Stephen P. Martin and James D. Wells. Muon anomalous magnetic dipole moment in supersymmetric theories. *Phys. Rev.*, D64:035003, 2001. arXiv:hep-ph/0103067, doi:10.1103/PhysRevD.64.035003.

[63] K. A. Olive et al. Review of Particle Physics. *Chin. Phys.*, C38:090001, 2014. doi:10.1088/1674-1137/38/9/090001.

[64] M. E. Cabrera, J. A. Casas, and A. Delgado. Upper Bounds on Superpartner Masses from Upper Bounds on the Higgs Boson Mass. *Phys. Rev. Lett.*, 108:021802, 2012. arXiv:1108.3867, doi:10.1103/PhysRevLett.108.021802.

[65] Gian F. Giudice and Alessandro Strumia. Probing High-Scale and Split Supersymmetry with Higgs Mass Measurements. *Nucl. Phys.*, B858:63–83, 2012. arXiv:1108.6077, doi:10.1016/j.nuclphysb.2012.01.001.

[66] S. Heinemeyer, W. Hollik, and G. Weiglein. FeynHiggs: A Program for the calculation of the masses of the neutral CP even Higgs bosons in the MSSM. *Comput. Phys. Commun.*, 124:76–89, 2000. arXiv:hep-ph/9812320, doi:10.1016/S0010-4655(99)00364-1.

[67] T. Hahn, S. Heinemeyer, W. Hollik, H. Rzehak, and G. Weiglein. High-Precision Predictions for the Light CP -Even Higgs Boson Mass of the Minimal Supersymmetric Standard Model. *Phys. Rev. Lett.*, 112(14):141801, 2014. arXiv:1312.4937, doi:10.1103/PhysRevLett.112.141801.

[68] Georges Aad et al. Combined Measurement of the Higgs Boson Mass in pp Collisions at $\sqrt{s} = 7$ and 8 TeV with the ATLAS and CMS Experiments. *Phys. Rev. Lett.*, 114:191803, 2015. arXiv:1503.07589, doi:10.1103/PhysRevLett.114.191803.

[69] Georges Aad et al. Measurements of the Higgs boson production and decay rates and coupling strengths using pp collision data at $\sqrt{s} = 7$ and 8 TeV in the ATLAS experiment. *Eur. Phys. J.*, C76(1):6, 2016. arXiv:1507.04548, doi:10.1140/epjc/s10052-015-3769-y.

[70] The ATLAS collaboration. Search for neutral Higgs bosons of the Minimal Supersymmetric Standard Model in pp collisions at $\sqrt{s} = 8$ TeV with the ATLAS detector. 2014.

[71] Vardan Khachatryan et al. Search for neutral MSSM Higgs bosons decaying to a pair of tau leptons in pp collisions. *JHEP*, 10:160, 2014. arXiv:1408.3316, doi:10.1007/JHEP10(2014)160.

[72] The ATLAS collaboration. Constraints on New Phenomena via Higgs Coupling Measurements with the ATLAS Detector. 2014.

[73] First combination of Tevatron and LHC measurements of the top-quark mass. 2014. arXiv:1403.4427.

[74] Motoi Endo, Koichi Hamaguchi, Sho Iwamoto, and Takahiro Yoshinaga. Muon g-2 vs LHC in Supersymmetric Models. *JHEP*, 01:123, 2014. arXiv:1303.4256, doi:10.1007/JHEP01(2014)123.

[75] Gerald Aarons et al. International Linear Collider Reference Design Report Volume 2: Physics at the ILC. 2007. arXiv:0709.1893.

[76] M. Bicer et al. First Look at the Physics Case of TLEP. *JHEP*, 01:164, 2014. arXiv:1308.6176, doi:10.1007/JHEP01(2014)164.

[77] Timothy Cohen, Tobias Golling, Mike Hance, Anna Henrichs, Kiel Howe, Joshua Loyal, Sanjay Padhi, and Jay G. Wacker. SUSY Simplified Models at 14, 33, and 100 TeV Proton Colliders. *JHEP*, 04:117, 2014. arXiv:1311.6480, doi:10.1007/JHEP04(2014)117.

[78] Timothy Cohen, Raffaele Tito D'Agnolo, Mike Hance, Hou Keong Lou, and Jay G. Wacker. Boosting Stop Searches with a 100 TeV Proton Collider. *JHEP*, 11:021, 2014. arXiv:1406.4512, doi:10.1007/JHEP11(2014)021.

[79] Motoi Endo, Koichi Hamaguchi, Teppei Kitahara, and Takahiro Yoshinaga. Probing Bino contribution to muon $g-2$. *JHEP*, 11:013, 2013. arXiv:1309.3065, doi:10.1007/JHEP11(2013)013.

[80] E. Accomando et al. Physics at the CLIC multi-TeV linear collider. In *Proceedings, 11th International Conference on Hadron spectroscopy (Hadron 2005)*, 2004. URL: http://weblib.cern.ch/abstract?CERN-2004-005, arXiv:hep-ph/0412251.

[81] Takeo Moroi and Yasuhiro Okada. Radiative corrections to Higgs masses in the supersymmetric model with an extra family and antifamily. *Mod. Phys. Lett.*, A7:187–200, 1992. doi:10.1142/S0217732392000124.

[82] Takeo Moroi and Yasuhiro Okada. Upper bound of the lightest neutral Higgs mass in extended supersymmetric Standard Models. *Phys. Lett.*, B295:73–78, 1992. doi:10.1016/0370-2693(92)90091-H.

[83] K. S. Babu, Ilia Gogoladze, and Christopher Kolda. Perturbative unification and Higgs boson mass bounds. 2004. arXiv:hep-ph/0410085.

[84] K. S. Babu, Ilia Gogoladze, Mansoor Ur Rehman, and Qaisar Shafi. Higgs Boson Mass, Sparticle Spectrum and Little Hierarchy Problem in Extended MSSM. *Phys. Rev.*, D78:055017, 2008. arXiv:0807.3055, doi:10.1103/PhysRevD.78.055017.

[85] Stephen P. Martin. Extra vector-like matter and the lightest Higgs scalar boson mass in low-energy supersymmetry. *Phys. Rev.*, D81:035004, 2010. arXiv:0910.2732, doi:10.1103/PhysRevD.81.035004.

[86] Peter W. Graham, Ahmed Ismail, Surjeet Rajendran, and Prashant Saraswat. A Little Solution to the Little Hierarchy Problem: A Vector-like Generation. *Phys. Rev.*, D81:055016, 2010. arXiv:0910.3020, doi:10.1103/PhysRevD.81.055016.

[87] Stephen P. Martin. Raising the Higgs mass with Yukawa couplings for isotriplets in vector-like extensions of minimal supersymmetry. *Phys. Rev.*, D82:055019, 2010. arXiv:1006.4186, doi:10.1103/PhysRevD.82.055019.

[88] Motoi Endo, Koichi Hamaguchi, Sho Iwamoto, and Norimi Yokozaki. Higgs Mass and Muon Anomalous Magnetic Moment in Supersymmetric Models with Vector-Like Matters. *Phys. Rev.*, D84:075017, 2011. arXiv:1108.3071, doi:10.1103/PhysRevD.84.075017.

[89] Cyrus Faroughy and K. Grizzard. Raising the Higgs mass in supersymmetry with t-tâĂš mixing. *Phys. Rev.*, D90(3):035024, 2014. arXiv:1405.4116, doi:10.1103/PhysRevD.90.035024.

[90] Sebastian A. R. Ellis, Rohini M. Godbole, Shrihari Gopalakrishna, and James D. Wells. Survey of vector-like fermion extensions of the Standard Model and their phenomenological implications. *JHEP*, 09:130, 2014. arXiv:1404.4398, doi:10.1007/JHEP09(2014)130.

[91] Florian Staub. Automatic Calculation of supersymmetric Renormalization Group Equations and Self Energies. *Comput. Phys. Commun.*, 182:808–833, 2011. arXiv:1002.0840, doi:10.1016/j.cpc.2010.11.030.

[92] Florian Staub. SARAH 4 : A tool for (not only SUSY) model builders. *Comput. Phys. Commun.*, 185:1773–1790, 2014. arXiv:1309.7223, doi:10.1016/j.cpc.2014.02.018.

[93] Mark D. Goodsell, Kilian Nickel, and Florian Staub. Two-Loop Higgs mass calculations in supersymmetric models beyond the MSSM with SARAH and SPheno. *Eur. Phys. J.*, C75(1):32, 2015. arXiv:1411.0675, doi:10.1140/epjc/s10052-014-3247-y.

[94] Stephen P. Martin and Michael T. Vaughn. Two loop renormalization group equations for soft supersymmetry breaking couplings. *Phys. Rev.*, D50:2282, 1994. [Erratum: Phys. Rev.D78,039903(2008)]. arXiv:hep-ph/9311340, doi:10.1103/PhysRevD.50.2282,10.1103/PhysRevD.78.039903.

[95] Sebastian A. R. Ellis and James D. Wells. Visualizing gauge unification with high-scale thresholds. *Phys. Rev.*, D91(7):075016, 2015. arXiv:1502.01362, doi:10.1103/PhysRevD.91.075016.

[96] Michael E. Peskin and Tatsu Takeuchi. A New constraint on a strongly interacting Higgs sector. *Phys. Rev. Lett.*, 65:964–967, 1990. doi:10.1103/PhysRevLett.65.964.

[97] Stephen P. Martin, Kazuhiro Tobe, and James D. Wells. Virtual effects of light gauginos and higgsinos: A Precision electroweak analysis of split supersymmetry. *Phys. Rev.*, D71:073014, 2005. arXiv:hep-ph/0412424, doi:10.1103/PhysRevD.71.073014.

[98] L. Lavoura and Joao P. Silva. The Oblique corrections from vector - like singlet and doublet quarks. *Phys. Rev.*, D47:2046–2057, 1993. doi:10.1103/PhysRevD.47.2046.

[99] M. Baak, J. CÃžth, J. Haller, A. Hoecker, R. Kogler, K. MÃűnig, M. Schott, and J. Stelzer. The global electroweak fit at NNLO and prospects for the LHC and ILC. *Eur. Phys. J.*, C74:3046, 2014. arXiv:1407.3792, doi:10.1140/epjc/s10052-014-3046-5.

[100] M. Baak et al. Working Group Report: Precision Study of Electroweak Interactions. In *Community Summer Study 2013: Snowmass on the Mississippi (CSS2013) Minneapolis, MN, USA, July 29-August 6, 2013*, 2013. URL: http://www.slac.stanford.edu/econf/C1307292/docs/EnergyFrontier/Electroweak-19.pdf, arXiv:1310.6708.

[101] Abdelhak Djouadi. The Anatomy of electro-weak symmetry breaking. II. The Higgs bosons in the minimal supersymmetric model. *Phys. Rept.*, 459:1–241, 2008. arXiv:hep-ph/0503173, doi:10.1016/j.physrep.2007.10.005.

[102] John F. Gunion, Howard E. Haber, Gordon L. Kane, and Sally Dawson. The Higgs Hunter's Guide. *Front. Phys.*, 80:1–448, 2000.

[103] Projected Performance of an Upgraded CMS Detector at the LHC and HL-LHC: Contribution to the Snowmass Process. In *Community Summer Study 2013: Snowmass on the Mississippi (CSS2013) Minneapolis, MN, USA, July 29-August 6, 2013*, 2013. URL: http://inspirehep.net/record/1244669/files/arXiv:1307.7135.pdf, arXiv:1307.7135.

[104] Leandro G. Almeida, Seung J. Lee, Stefan Pokorski, and James D. Wells. Study of the standard model Higgs boson partial widths and branching fractions. *Phys. Rev.*, D89(3):033006, 2014. arXiv:1311.6721, doi:10.1103/PhysRevD.89.033006.

[105] Serguei Chatrchyan et al. Inclusive search for a vector-like T quark with charge $\frac{2}{3}$ in pp collisions at $\sqrt{s}$ = 8 TeV. *Phys. Lett.*, B729:149–171, 2014. arXiv:1311.7667, doi:10.1016/j.physletb.2014.01.006.

[106] Saptaparna Bhattacharya, Jimin George, Ulrich Heintz, Ashish Kumar, Meenakshi Narain, and John Stupak. Prospects for a Heavy Vector-Like Charge 2/3 Quark T search at the LHC with $\sqrt{s} = 14TeV$ and 33 TeV. "A Snowmass 2013 Whitepaper". In *Community Summer Study 2013: Snowmass on the Mississippi (CSS2013) Minneapolis, MN, USA, July 29-August 6, 2013*, 2013. URL: http://inspirehep.net/record/1252064/files/arXiv:1309.0026.pdf, arXiv:1309.0026.

[107] Ammar Abdalgabar, Alan S. Cornell, Aldo Deandrea, and Moritz McGarrie. Large At Without the Desert. *JHEP*, 1407:158, 2014. arXiv:1405.1038, doi:10.1007/JHEP07(2014)158.

[108] Ammar Abdalgabar, Alan S. Cornell, Aldo Deandrea, and Moritz McGarrie. Natural Supersymmetry and Unification in Five Dimensions. 2015. arXiv:1504.07749.

[109] Florian Staub. From Superpotential to Model Files for FeynArts and CalcHep/CompHep. *Comput.Phys.Commun.*, 181:1077–1086, 2010. arXiv:0909.2863, doi:10.1016/j.cpc.2010.01.011.

[110] Florian Staub. SARAH 3.2: Dirac Gauginos, UFO output, and more. *Computer Physics Communications*, 184:pp. 1792–1809, 2013. arXiv:1207.0906, doi:10.1016/j.cpc.2013.02.019.

[111] Arthur Hebecker. 5-D superYang-Mills theory in 4-D superspace, superfield brane operators, and applications to orbifold GUTs. *Nucl.Phys.*, B632:101–113, 2002. arXiv:hep-ph/0112230, doi:10.1016/S0550-3213(02)00253-5.

[112] Eugene A. Mirabelli and Michael E. Peskin. Transmission of supersymmetry breaking from a four-dimensional boundary. *Phys.Rev.*, D58:065002, 1998. arXiv:hep-th/9712214, doi:10.1103/PhysRevD.58.065002.

[113] Moritz McGarrie and Rodolfo Russo. General Gauge Mediation in 5D. *Phys.Rev.*, D82:035001, 2010. arXiv:1004.3305, doi:10.1103/PhysRevD.82.035001.

[114] A. S. Cornell, Aldo Deandrea, Lu-Xin Liu, and Ahmad Tarhini. Scaling of the CKM Matrix in the 5D MSSM. *Phys.Rev.*, D85:056001, 2012. arXiv:1110.1942, doi:10.1103/PhysRevD.85.056001.

[115] Moritz McGarrie. 5D Maximally Supersymmetric Yang-Mills in 4D Superspace: Applications. *JHEP*, 1304:161, 2013. arXiv:1303.4534, doi:10.1007/JHEP04(2013)161.

[116] Gautam Bhattacharyya and Tirtha Sankar Ray. A phenomenological study of 5d supersymmetry. *JHEP*, 1005:040, 2010. arXiv:1003.1276, doi:10.1007/JHEP05(2010)040.

[117] A. Delgado, A. Pomarol, and M. Quiros. Supersymmetry and electroweak breaking from extra dimensions at the TeV scale. *Phys.Rev.*, D60:095008, 1999. arXiv:hep-ph/9812489, doi:10.1103/PhysRevD.60.095008.

[118] Keith R. Dienes, Emilian Dudas, and Tony Gherghetta. Grand unification at intermediate mass scales through extra dimensions. *Nucl.Phys.*, B537:47–108, 1999. arXiv:hep-ph/9806292, doi:10.1016/S0550-3213(98)00669-5.

[119] D. Elazzar Kaplan, Graham D. Kribs, and Martin Schmaltz. Supersymmetry breaking through transparent extra dimensions. *Phys.Rev.*, D62:035010, 2000. arXiv:hep-ph/9911293, doi:10.1103/PhysRevD.62.035010.

[120] Z. Chacko, Markus A. Luty, Ann E. Nelson, and Eduardo Ponton. Gaugino mediated supersymmetry breaking. *JHEP*, 0001:003, 2000. arXiv:hep-ph/9911323.

[121] Moritz McGarrie. Gauge Mediated Supersymmetry Breaking in Five Dimensions. 2011. arXiv:1109.6245.

[122] G.F. Giudice and R. Rattazzi. Theories with gauge mediated supersymmetry breaking. *Phys.Rept.*, 322:419–499, 1999. arXiv:hep-ph/9801271, doi:10.1016/S0370-1573(99)00042-3.

[123] Dario Buttazzo, Giuseppe Degrassi, Pier Paolo Giardino, Gian F. Giudice, Filippo Sala, Alberto Salvio, and Alessandro Strumia. Investigating the near-criticality of the Higgs boson. *JHEP*, 12:089, 2013. arXiv:1307.3536, doi:10.1007/JHEP12(2013)089.

[124] Giuseppe Degrassi, Stefano Di Vita, Joan Elias-Miro, Jose R. Espinosa, Gian F. Giudice, Gino Isidori, and Alessandro Strumia. Higgs mass and vacuum stability in the Standard Model at NNLO. *JHEP*, 08:098, 2012. arXiv:1205.6497, doi:10.1007/JHEP08(2012)098.

[125] J. Ellis, J. R. Espinosa, G. F. Giudice, A. Hoecker, and A. Riotto. The Probable Fate of the Standard Model. *Phys. Lett.*, B679:369–375, 2009. arXiv:0906.0954, doi:10.1016/j.physletb.2009.07.054.

[126] Joan Elias-Miro, Jose R. Espinosa, Gian F. Giudice, Gino Isidori, Antonio Riotto, and Alessandro Strumia. Higgs mass implications on the stability of the electroweak vacuum. *Phys. Lett.*, B709:222–228, 2012. arXiv:1112.3022, doi:10.1016/j.physletb.2012.02.013.

[127] Jose R. Espinosa, Gian F. Giudice, Enrico Morgante, Antonio Riotto, Leonardo Senatore, Alessandro Strumia, and Nikolaos Tetradis. The cosmological Higgstory

of the vacuum instability. *JHEP*, 09:174, 2015. arXiv:1505.04825, doi:10.1007/JHEP09(2015)174.

[128] J. A. Casas, V. Di Clemente, and M. Quiros. The Standard model instability and the scale of new physics. *Nucl. Phys.*, B581:61–72, 2000. arXiv:hep-ph/0002205, doi:10.1016/S0550-3213(00)00199-1.

[129] J. A. Casas, J. R. Espinosa, and M. Quiros. Standard model stability bounds for new physics within LHC reach. *Phys. Lett.*, B382:374–382, 1996. arXiv:hep-ph/9603227, doi:10.1016/0370-2693(96)00682-X.

[130] Vincenzo Branchina and Emanuele Messina. Stability, Higgs Boson Mass and New Physics. *Phys. Rev. Lett.*, 111:241801, 2013. arXiv:1307.5193, doi:10.1103/PhysRevLett.111.241801.

[131] Sidney R. Coleman. The Fate of the False Vacuum. 1. Semiclassical Theory. *Phys. Rev.*, D15:2929–2936, 1977. [Erratum: Phys. Rev.D16,1248(1977)]. doi:10.1103/PhysRevD.15.2929,10.1103/PhysRevD.16.1248.

[132] Curtis G. Callan, Jr. and Sidney R. Coleman. The Fate of the False Vacuum. 2. First Quantum Corrections. *Phys. Rev.*, D16:1762–1768, 1977. doi:10.1103/PhysRevD.16.1762.

[133] Sidney R. Coleman, V. Glaser, and Andre Martin. Action Minima Among Solutions to a Class of Euclidean Scalar Field Equations. *Commun. Math. Phys.*, 58:211, 1978. doi:10.1007/BF01609421.

[134] Ki-Myeong Lee and Erick J. Weinberg. TUNNELING WITHOUT BARRIERS. *Nucl. Phys.*, B267:181, 1986. doi:10.1016/0550-3213(86)90150-1.

[135] Luca Di Luzio and Luminita Mihaila. On the gauge dependence of the Standard Model vacuum instability scale. *JHEP*, 06:079, 2014. arXiv:1404.7450, doi:10.1007/JHEP06(2014)079.

[136] B. Grzadkowski, M. Iskrzynski, M. Misiak, and J. Rosiek. Dimension-Six Terms in the Standard Model Lagrangian. *JHEP*, 10:085, 2010. arXiv:1008.4884, doi:10.1007/JHEP10(2010)085.

[137] Elizabeth E. Jenkins, Aneesh V. Manohar, and Michael Trott. Renormalization Group Evolution of the Standard Model Dimension Six Operators I: Formalism and lambda Dependence. *JHEP*, 10:087, 2013. arXiv:1308.2627, doi:10.1007/JHEP10(2013)087.

[138] Sidney R. Coleman and Frank De Luccia. Gravitational Effects on and of Vacuum Decay. *Phys. Rev.*, D21:3305, 1980. doi:10.1103/PhysRevD.21.3305.

[139] Alan H. Guth and Erick J. Weinberg. Could the Universe Have Recovered from a Slow First Order Phase Transition? *Nucl. Phys.*, B212:321, 1983. doi:10.1016/0550-3213(83)90307-3.

[140] Christophe Grojean, Geraldine Servant, and James D. Wells. First-order electroweak phase transition in the standard model with a low cutoff. *Phys. Rev.*, D71:036001, 2005. arXiv:hep-ph/0407019, doi:10.1103/PhysRevD.71.036001.

[141] Cedric Delaunay, Christophe Grojean, and James D. Wells. Dynamics of Non-renormalizable Electroweak Symmetry Breaking. *JHEP*, 04:029, 2008. arXiv:0711.2511, doi:10.1088/1126-6708/2008/04/029.

[142] Michael Joyce. Electroweak Baryogenesis and the Expansion Rate of the Universe. *Phys. Rev.*, D55:1875–1878, 1997. arXiv:hep-ph/9606223, doi:10.1103/PhysRevD.55.1875.

[143] Michael Joyce and Tomislav Prokopec. Turning around the sphaleron bound: Electroweak baryogenesis in an alternative postinflationary cosmology. *Phys. Rev.*, D57:6022–6049, 1998. arXiv:hep-ph/9709320, doi:10.1103/PhysRevD.57.6022.

[144] M. E. Carrington. The Effective potential at finite temperature in the Standard Model. *Phys. Rev.*, D45:2933–2944, 1992. doi:10.1103/PhysRevD.45.2933.

[145] K. Kajantie, M. Laine, K. Rummukainen, and Mikhail E. Shaposhnikov. Is there a hot electroweak phase transition at m(H) larger or equal to m(W)? *Phys. Rev. Lett.*, 77:2887–2890, 1996. arXiv:hep-ph/9605288, doi:10.1103/PhysRevLett.77.2887.

[146] Physics at a High-Luminosity LHC with ATLAS. 2012.

[147] Florian Goertz, Andreas Papaefstathiou, Li Lin Yang, and Jose Zurita. Higgs Boson self-coupling measurements using ratios of cross sections. *JHEP*, 06:016, 2013. arXiv:1301.3492, doi:10.1007/JHEP06(2013)016.

[148] Vernon Barger, Lisa L. Everett, C. B. Jackson, and Gabe Shaughnessy. Higgs-Pair Production and Measurement of the Triscalar Coupling at LHC(8,14). *Phys. Lett.*, B728:433–436, 2014. arXiv:1311.2931, doi:10.1016/j.physletb.2013.12.013.

[149] Alan J. Barr, Matthew J. Dolan, Christoph Englert, Danilo Enoque Ferreira de Lima, and Michael Spannowsky. Higgs Self-Coupling Measurements at a 100 TeV Hadron Collider. *JHEP*, 02:016, 2015. arXiv:1412.7154, doi:10.1007/JHEP02(2015)016.

[150] Andrei D. Linde. Decay of the False Vacuum at Finite Temperature. *Nucl. Phys.*, B216:421, 1983. [Erratum: Nucl. Phys.B223,544(1983)]. doi:10.1016/0550-3213(83)90293-6.

[151] Andrei D. Linde. Fate of the False Vacuum at Finite Temperature: Theory and Applications. *Phys. Lett.*, B100:37, 1981. doi:10.1016/0370-2693(81)90281-1.

[152] Mariano Quiros. Finite temperature field theory and phase transitions. In *High energy physics and cosmology. Proceedings, Summer School, Trieste, Italy, June 29-July 17, 1998*, pages 187–259, 1999. URL: http://alice.cern.ch/format/showfull?sysnb=0302087, arXiv:hep-ph/9901312.

[153] Ryan Cooke, Max Pettini, Regina A. Jorgenson, Michael T. Murphy, and Charles C. Steidel. Precision measures of the primordial abundance of deuterium. *Astrophys. J.*, 781(1):31, 2014. arXiv:1308.3240, doi:10.1088/0004-637X/781/1/31.

[154] Edward L. Wright. Constraints on Dark Energy from Supernovae, Gamma Ray Bursts, Acoustic Oscillations, Nucleosynthesis and Large Scale Structure and the Hubble constant. *Astrophys. J.*, 664:633–639, 2007. arXiv:astro-ph/0701584, doi:10.1086/519274.

[155] Vimal Simha and Gary Steigman. Constraining The Early-Universe Baryon Density And Expansion Rate. *JCAP*, 0806:016, 2008. arXiv:0803.3465, doi:10.1088/1475-7516/2008/06/016.

[156] Tanja Rindler-Daller and Paul R. Shapiro. Complex scalar field dark matter on galactic scales. *Mod. Phys. Lett.*, A29(2):1430002, 2014. arXiv:1312.1734, doi:10.1142/S021773231430002X.

[157] Bohua Li, Tanja Rindler-Daller, and Paul R. Shapiro. Cosmological Constraints on Bose-Einstein-Condensed Scalar Field Dark Matter. *Phys. Rev.*, D89:083536, 2014. arXiv:1310.6061, doi:10.1103/PhysRevD.89.083536.

[158] Frans R. Klinkhamer and N. S. Manton. A Saddle Point Solution in the Weinberg-Salam Theory. *Phys. Rev.*, D30:2212, 1984. doi:10.1103/PhysRevD.30.2212.